LEVEL

12

AD A089066

QUANTITATIVE SCHLIEREN ANALYSIS OF ACOUSTIC INTERACTION WITH SUBMERGED PLATES

Roger Thomas Richards

Technical Memorandum
File No. TM 80-139
June 24, 1980
Contract No. N00024-79-C-6043

Copy No. 7

The Pennsylvania State University
Intercollege Research Programs and Facilities
APPLIED RESEARCH LABORATORY
Post Office Box 30
State College, PA 16801

APPROVED FOR PUBLIC RELEASE
DISTRIBUTION UNLIMITED

NAVY DEPARTMENT

NAVAL SEA SYSTEMS COMMAND

UNCLASSIFIED

SECURITY CLASSIFICATION OF THIS PAGE (When Data Entered) (9) Technical memo

REPORT DOCUMENTATION PAGE

READ INSTRUCTIONS BEFORE COMPLETING FORM

1. REPORT NUMBER: TM 80-139	2. GOVT ACCESSION NO.: AD-A089 066
3. RECIPIENT'S CATALOG NUMBER	
4. TITLE (and Subtitle): QUANTITATIVE SCHLIEREN ANALYSIS OF ACOUSTIC INTERACTION WITH SUBMERGED PLATES	5. TYPE OF REPORT & PERIOD COVERED: PhD Thesis, August 1980
	6. PERFORMING ORG. REPORT NUMBER: TM 80-139
7. AUTHOR(s): Roger Thomas Richards (10) (15)	8. CONTRACT OR GRANT NUMBER(s): N00024-79-C-6043
9. PERFORMING ORGANIZATION NAME AND ADDRESS: The Pennsylvania State University, Applied Research Laboratory, P. O. Box 30, State College, PA 16801	10. PROGRAM ELEMENT, PROJECT, TASK AREA & WORK UNIT NUMBERS: (11) 24 Jun 80
11. CONTROLLING OFFICE NAME AND ADDRESS: Naval Sea Systems Command, Department of the Navy, Washington, DC 20362 (12) 1584	12. REPORT DATE: June 24, 1980 (13) 11 July
	13. NUMBER OF PAGES: 153 pages & Figures
14. MONITORING AGENCY NAME & ADDRESS (if different from Controlling Office): (14) NRL/PSH/TM-80-139	15. SECURITY CLASS. (of this report): Unclassified, Unlimited
	15a. DECLASSIFICATION/DOWNGRADING SCHEDULE

16. DISTRIBUTION STATEMENT (of this Report)

Approved for public release, distribution unlimited, per Naval Sea Systems Command - July 11, 1980.

17. DISTRIBUTION STATEMENT (of the abstract entered in Block 20, if different from Report)

18. SUPPLEMENTARY NOTES

19. KEY WORDS (Continue on reverse side if necessary and identify by block number)

underwater sound, transmission, radiation, plates, schlieren, thesis

20. ABSTRACT (Continue on reverse side if necessary and identify by block number)

The transmission and radiation of sound from submerged plates are investigated by means of a quantitative Schlieren method which produces accurate visual representations of sound fields. The method is shown to have significant advantages over the usual time-consuming, point-by-point scans of acoustic fields. Previous investigations have shown the feasibility of quantizing Schlieren data, and this investigation demonstrates a dramatic improvement in the accuracy of that data, reducing the standard error to

DD FORM 1 JAN 73 1473 EDITION OF 1 NOV 65 IS OBSOLETE S/N 0102-LF-014-6601

391007 UNCLASSIFIED

SECURITY CLASSIFICATION OF THIS PAGE (When Data Entered)

20. ABSTRACT (continued)

under one decibel which places the accuracy of the method on equal footing with other acoustic measurement systems. The further addition of stroboscopic techniques enabled the resolution of individual acoustic waves and permitted the differentiation between standing waves and progressive waves. The low frequency resolution of the classical Schlieren system was also improved by nearly two orders of magnitude; sound waves as low as 27 kHz were easily visualized. These improvements in the quantitative Schlieren system are demonstrated by a thorough study of transmission of sound through submerged metal plates over a frequency range extending from below to over one hundred times the classical coincidence frequency. Recent theoretical descriptions of the lowest order symmetrical Lamb mode are confirmed, and cancellation of modal pairs of Lamb waves with increasing frequency is observed.

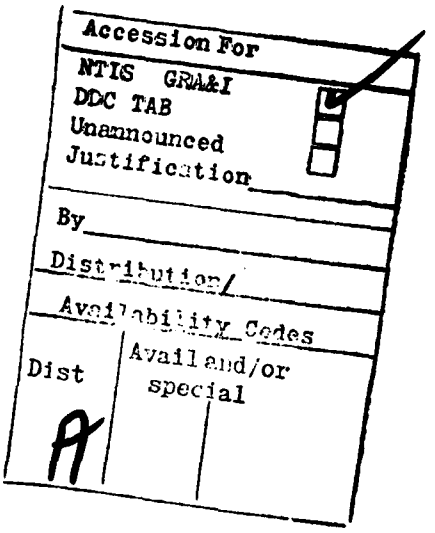

ABSTRACT

The transmission and radiation of sound from submerged plates are investigated by means of a quantitative schlieren method which produces accurate visual representations of sound fields. The method is shown to have significant advantages over the usual time-consuming, point-by-point scans of acoustic fields. Previous investigations have shown the feasibility of quantizing schlieren data, and this investigation demonstrates a dramatic improvement in the accuracy of that data, reducing the standard error to under one decibel which places the accuracy of the method on equal footing with other acoustic measurement systems. The further addition of stroboscopic techniques enabled the resolution of individual acoustic waves and permitted the differentiation between standing waves and progressive waves. The low frequency resolution of the classical schlieren system was also improved by nearly two orders of magnitude; sound waves as low as 27 kHz were easily visualized. These improvements in the quantitative schlieren system are demonstrated by a thorough study of transmission of sound through submerged metal plates over a frequency range extending from below to over one hundred times the classical coincidence frequency. Recent theoretical descriptions of the lowest order symmetrical Lamb wave are confirmed, and cancellation of modal pairs of Lamb waves with increasing frequency is observed.

TABLE OF CONTENTS

LIST OF TABLES

LIST OF FIGURES

CHAPTER 1

BACKGROUND

1.1 Introduction

The interaction of sound with physical structures is a topic of major concern in acoustics. Specific items of interest are the diffraction of sound around edges and through apertures, the transmission and reradiation of sound by jointed and welded panels, and the radiation of sound from plates and shells. Such phenomena are very complex because of the generation of free and forced Lamb and Rayleigh waves and their subsequent radiation into the surrounding medium. A basic understanding of these phenomena is necessary in order to more accurately predict the acoustic qualities of auditoriums, the noise levels transmitted between living areas, or the noise radiated by machinery in the work environment.

In previous work, the evaluation of such intricate sound fields had to be based on much guesswork. In this thesis, a stroboscopic illumination of the sound field by periodically interrupting a laser beam has made it possible to differentiate between standing and progressive waves,

and to measure their wave lengths with great accuracy. Interpretation and analysis of the various phenomena that appeared through use of this schlieren method was thus possible.

In addition to demonstrating the power of the stroboscopic schlieren technique in the analysis of several interesting, complex acoustic fields, much of the effort of this dissertation was concentrated on the investigation of the sound transmission of simple plates and the various types of waves, longitudinal waves, forced vibrations, transient waves, etc., that are associated with this transmission. The mathematical treatment of sound radiation by a vibrating plate and sound reflection from a plate is quite similar and the results readily applicable to either case. Although the literature in the last few years reflects considerable interest in theoretical treatments of the problem, very little experimental effort has been expended. This investigation is intended to fill part of that gap.

The experimental approach is based on the schlieren technique. This method has in the past been limited to acoustic frequencies near 1 MHz and above. Since this range is far above frequencies of normal, practical engineering interest, an attempt was made to construct a schlieren system which would be capable of imaging sound fields of considerably lower frequencies. The result was an instrument which was capable of producing clear, sharp

images of acoustic waves at frequencies as low as 27 kHz, or nearly two orders of magnitude below the frequency range commonly used. Futhermore, it was found that, by combining stroboscopic techniques with the schlieren method, numerous additional measurements could be obtained on progressive fields which were previously impossible.

A major obstacle to the use of a schlieren system in such an investigation was the previous unreliability of quantitative data obtained with the method. One of the most striking achievements of this project was the demonstration of the extreme accuracy and repeatability of the resulting data. In most cases, tolerances as close as 1 dB were easily maintained. This, combined with the other obvious advantages of the schlieren method, e.g., a full two-dimensional representation of a sound field with no inherent disturbance of the field by the measurement process as opposed to the usual point-by-point probing techniques should offer great encouragement for its future use.

1.2 Objectives

The standard schlieren method reproduces sound intensity as white and dark shades in the schlieren photographs, but does not give any information about the type of waves that give rise to the sound field. An exact analysis of these various waves has been one of the great difficulties with previous schlieren investigations; thus, the major

task of this research was the development of stroboscopic and highly accurate procedures for analyzing complex sound fields. The second basic objective of this research was to obtain experimental confirmation of recent theoretical treatments of the acoustic radiation and transmission through submerged plates. Furthermore, it was intended that previous experimental confirmations of the dispersion relations would be extended to much higher frequency parameters. Analysis of the latter produced some surprising results regarding the appearance of the cancellation of modal pairs. Since the theoretical predictions apply to ideal, infinite plates, a secondary objective was to obtain experimental results showing the perturbations caused by nonidealized plates, e.g., the effects of the plate edges and of discontinuities such as ribs and weld joints. A prerequisite to this was the improvment of accuracy and low-frequency resolution of the quantitative schlieren method as well as the addition and perfection of the stroboscopic techniques necessary for the analysis of progressive-wave fields.

1.3 Sound Interaction with Plates

1.3.1 Transmission at Oblique Angles

The plates to be discussed herein will be treated as isotropic elastic material bounded by two infinite parallel planes and submerged in an infinite fluid medium. The

original theoretical treatment of such infinite plates was by Rayleigh [1] and Lamb [2, 3], the general results of which are now referred to as the "classical plate" theory. The latter paper [3] discussed the infinite set of propagation modes which are possible for waves traveling in the plate at high frequencies. These modes are usually referred to as either "free plate waves" or "Lamb waves". Earlier, Rayleigh [1] had predicted the existence of "Rayleigh waves" at the surface of a semi-infinite solid which, in the context of the present investigation, can be thought of as an infinitely thick plate.

With the exception of Knott's study [4] in 1899 on the reflection of elastic waves, little was done concerning sound interaction with plates until 1934, at which time three groups began reporting on various series of relevant investigations. One group headed by Lindsay [5, 6, 7] first developed a theoretical description of sound transmission through stratified layers of solids and fluids. Then, Smyth and Lindsay [8] tested the theory by means of an experimental investigation of sound transmission through arrays of multiple plates using a torsional disk to measure the amplitude of the transmitted sound. A second group, headed by Schaefer and Bergmann [9, 10, 11], developed a method of measuring the velocities of the longitudinal and shear waves in transparent solids by means of a light diffraction technique. They also attempted to extend the method to opaque materials by reflecting the light beam off

the surface of the solid [10]. The third group, headed by Walti [12, 13], developed a method of measuring elastic constants by determining the sound velocities in the solids from the character of the transmission data. They used thin wedges of material and found the dispersion curve by using the diffraction pattern produced by a beam of light passing through the transmitted sound field.

A landmark experiment by Sanders [14] in 1939 also used an optical method to find the angular locations of the peaks in the transmission curves (from which the sound velocities can be determined) for brass and nickel at frequencies up to about six times the classical coincidence frequencies of the plates. In the mid-nineteen forties, Osborne and Hart [15, 16] showed the existence of a precursor in the received signal caused by the higher sound velocity in the plate; detonator caps were used to produce a sharp acoustic pulse which was then reflected off a large, submerged steel plate. At the same time, Reissner [17, 18] was making substantial improvements in the theory of plates with his attempts to include the effects of shear deformations in the classical derivation.

With the development of electronic computers, Firestone [19] was, in 1948, able to solve the transcendental equations which describe the dependency of the phase velocities of the various Lamb waves on frequency, i.e., the dispersion curves. The comparison with experimental data was good up to frequencies of the order of fifty times

the classical coincidence frequency of the plate, which included the first eight to nine Lamb modes. The same year, Fay [20] predicted and his associate, Finney [21], measured backscatter (i.e., acoustic energy radiated back towards the sound source along the angle of incidence) from submerged steel plates for frequencies up to thirteen times the coincidence frequency of the plate. This same laboratory then took the next step beyond simply attempting to determine the angular locations of the peaks in the transmission curve and produced [22] some of the first, and still most detailed, experimental curves of sound transmission vs angle of incidence for steel plates in water. Curves were presented for very closely spaced frequency intervals covering the range from 2.7 to 50 times the classical coincidence frequency. At about the same time, another group, Schneider and Burton [23], produced several plots of transmission vs angle for aluminum plates in water scattered rather sparsely in the frequency range from eighteen to seventy-one times the coincidence frequency; this served as a validation of a method they then used to determine the elastic constants of several resins. They also succeeded in obtaining schlieren photographs of sound transmission through aluminum plates at thirty-five times the coincidence frequency [24] but were unable to obtain any quantitative data with the latter method and thus did little more than provide a sequence of photographs and a confirmation of the angular locations of the radiation from a couple of the Lamb waves.

In 1950, Schoch [25] brought together all of the previous work on sound interaction with plates in a superbly detailed tutorial paper. Immediately thereafter, Mindlin [26] developed the theoretical description of plate motion now named after him by successfully including the effects of rotary inertia and shear in the description of the flexural motion of plates. He and his co-workers (Kane and Mindlin [27], and Mindlin and Medick [28]) then extended the theoretical description to include extensional vibrations. The various parts were brought together by Mindlin [29] in 1960.

Experimental work began tapering off during this time period. However, in 1952, Makinson [30] presented several very detailed dispersion curves using the method developed by Bär and Walti [12], but made no attempt to solve the transcendental equations needed for a theoretical comparison as Firestone [19] had done for the case of aluminum plates. In the late 1950's, Liamshev and Rudakov [31, 32] were able to obtain several angular plots for the sound reflected from or radiated by various types of submerged metal plates. This was accomplished by means of a quartz transducer and barium titanate vibrators. Worlton [33] calculated the dispersion curves for the first eighteen to twenty Lamb modes in aluminum and in zirconium. He then was able to experimentally determine several scattered points which indicated reasonably good confirmation of these curves for aluminum. There apparently have been very

few attempts during the last twenty years to experimentally confirm the dispersion curves in other substances or to report detailed plots of transmission ratios at oblique angles.

The theoretical efforts have not slackened; in fact, they seem to have gained momentum in the last few years. In 1959, Tamm and Weis [34] gained some interesting insight into the behavior of the dispersion curves at very high frequencies by calculating a set of curves for an extremely high Poisson's ratio of 0.49 (the theoretical maximum is 0.50). In 1966, Feit [35, 36] was able to calculate the far-field radiation pattern of a vibrating plate based on the Mindlin plate equations. Then, in 1975, Stepanishen [37] investigated the effects of shear and rotary inertia on, specifically, the transmission of sound through plates (also note the resulting comments by Young [38] and Stepanishen's subsequent reply [39]). Stuart [40, 41] then analyzed the effects of fluid loading on the radiated field by using a technique based on leaky wave poles. One result of this work is the possible indication of additional real roots in limited cases dependent on the occurrence of certain combinations of parameters. The corresponding physical explanation for this possibility has given rise in this past year to several other papers with Crighton [42] and particularly, Strawderman et al. [43], insisting that the additional real roots have no physical basis, but with Pierucci and Graham [44] offering support for their

existence. Most recently, the Mindlin plate theory has been applied to the problem of composite plates by Rudgers [45], and to the problem of acoustic backscattering from plates by Rumerman [46].

The following treatises should be consulted for more detailed summaries of the previous work on the radiation and reflection of sound waves from plates: Ewing et al. [47], Brekhovskikh [48], Viktorov [49], Junger and Feit [50], and Graff [51].

1.3.2 Effects of Bounded Beams

Götz [52] was able to obtain, in 1943, several transmission curves as a function of angle by scanning the transmitted acoustic field with a hydrophone. Furthermore, when scanning near to, and parallel to, the back surface of the plate, he found a pronounced lateral shift in the location of the transmitted beam when the angle of incidence was near one of the critical angles of the Lamb modes. Schoch [53] succeeded in explaining the phenomenon so convincingly that it was not until twenty years later that Neubauer [54] was able to obtain experimental data of sufficient range and accuracy to turn up discrepancies in Schoch's theory. Neubauer's work prompted Bertoni and Tamir [55] to improve on Schoch's treatment by basing the predictions of the magnitude of the beam displacement on the intensity across the width of the beam as well as its frequency. Additional experimental evidence was obtained

by Plona [56, 57] and some additional theoretical work was done by Pitts [58, 59, 60] while both were at Georgetown University.

First, Tolstoy and Usdin [61] in 1957 and then Viktorov [49] in 1967 discussed the possibility of the phase velocity and the group velocity having opposite signs within certain very narrow frequency ranges. The lowest frequency at which this might occur is at the onset of the second symmetrical plate mode, i.e., the S_1 Lamb wave. The first hint of an experimental confirmation of this rather surprising prediction was presented by Negishi [62] in a paper presented at a recent joint meeting of the Acoustical Society of America and the Acoustical Society of Japan.

CHAPTER 2

THEORETICAL FOUNDATIONS

2.1 Scale Models

The building and testing of scale models before the construction of a full-size prototype is a common practice in many branches of engineering. In fact, in such cases as the testing of aircraft designs in wind tunnels or the testing of harbor and estuary scale models are used universally. The principal motivation for such model studies is the economics involved in investigating the effects of changes in various parameters in the design of the full-size prototypes for structures which are too complex to be treated analytically. The relationships used to predict the behavior of the prototype from the results of the model studies are based on the principles of dimensional analysis. These were first drawn together in 1915 by Lord Rayleigh [63], although some of the main concepts had been used previous to that time by Rayleigh and others.

Dimensional analysis is used with such frequency as to be nearly second nature to most engineers and physicists. Consequently, the degree of physical intuition needed to

properly choose the various physical parameters which need to be included in the dimensional equation or which need to be scaled and those which can simply be ignored, is generally overlooked. Bridgman [64], for example, discusses the problem of deducing the time of oscillation of a small drop of liquid. After arguing for the inclusion or exclusion of various parameters such as surface tension, density, radius, viscosity, etc., he concludes that: "The untutored savage in the bushes would probably not be able to apply the methods of dimensional analysis to this problem and obtain results which would satisfy us." This reliance on physical intuition can complicate the defense of one's final choice of parameters to be included in the scaling equations.

The common practice with acoustical scale modeling in general and in schlieren systems specifically is to scale each of the three linear dimensions down by the same factor, build the model of the same material as the full-size prototype, and submerge it in the same acoustic medium. This implies that such crucial parameters as sound velocity, density, elastic moduli, etc., will not be scaled down in parallel with the geometric size. The problem is then to either defend this technique or to find exactly what effect this distortion will have on the results of the model investigation.

Beginning with a simple point mass compliance system the equation of motion is

$$M\ddot{\xi} + R\dot{\xi} + \xi/K = F, \tag{1}$$

where M is the mass, R the resistance, K the compliance, F the driving force, and ξ the displacement. This can also be written as

$$\ddot{\xi} + 2\,\delta\dot{\xi} + \omega_o^2\xi = F/M, \tag{2}$$

where

$$\delta = R/2M \text{ is the damping} \tag{3}$$

and

$$\omega_o = 1/\sqrt{MK} \text{ the natural frequency.} \tag{4}$$

If the system is scaled by changing the geometrical dimensions by a factor a, i.e., $L \rightarrow aL$, then each term in the equation of motion must scale in a similar manner if the equation is to hold for all sizes of models. The steady-state response of the system can be found with no loss of generality by assuming a forcing function of the form

$$F = f\exp(j\omega t). \tag{5}$$

Equation (2) reduces to

$$[1 - 2j\delta/\omega - \omega_o^2/\omega^2] = f/(-\omega^2 M). \tag{6}$$

This implies that the damping and the frequency parameters must scale in a similar manner

$$\delta/\omega \rightarrow \delta/\omega \tag{7}$$

and that the right-hand side must scale as a length, i.e.,

$$f/\omega^2 M \rightarrow af/\omega^2 M. \tag{8}$$

Furthermore, if the phase relations are to be preserved, then Equation (5) implies that

$$\omega t \rightarrow \omega t \tag{9}$$

must be invariant under a change in scale.

The above treatment assumed that the linear strain, i.e., the change in displacement per unit length, is invariant under a change in scale. It follows from this same assumption that if the model is constructed of the same material as the full-size prototype, then by Hooke's Law, the stresses will also be invariant. Thus, the forces must scale as lengths squared:

$$F \rightarrow a^2 F. \tag{10}$$

Furthermore, if the model is indeed to be constructed of the same material, then the mass must scale as a length cubed,

$$M \rightarrow a^3 M, \tag{11}$$

since, obviously, the volume scales as a length cubed. Combining relations (10) and (11) yields

$$F/M \rightarrow F/aM \tag{12}$$

which, when compared with Equation (2), shows that acceleration scales as the inverse of a length, i.e.,

$$\ddot{\xi} \rightarrow \ddot{\xi}/a \tag{13}$$

and also that

$$\omega_o \rightarrow \omega_o/a. \tag{14}$$

Comparing the latter relations with Equation (9) yields

$$t \rightarrow at. \tag{15}$$

Consequently, the effect of scaling on any parameter can be found from only three of these relations: the mechanical dimensions of length, mass, and time. Summarizing these from above, one sees that if

$$L \rightarrow aL,$$

$$\text{then} \quad T \rightarrow aT \tag{16}$$

$$\text{and} \quad M \rightarrow a^3M.$$

These relationships now need be applied only to the dimensional equation of the parameter of interest. The more commonly needed parameters in acoustics are summarized in Table 1.

TABLE 1

Summary of Scaling Relations

Prototype		Model
acceleration	ξ	ξ/a
compliance	K	K/a
damping	δ	δ/a
density	ρ	ρ
displacement	ξ	$a\xi$
elastic moduli	Y, G, B	Y, G, B
energy	E	a^3E
force	F	a^2F
frequency	ω	ω/a
impedance, characteristic	ρc	ρc
intensity	I	I
mass	M	a^3M
Poisson's Ratio	ν	ν
power	W	a^2W
pressure	p	p
resistance, radiation	R	a^2R
torque	τ	$a^3\tau$
velocity	c	c
wave number	k	k/a

2.2 Collimated Acoustic Beams

The common theoretical treatments of sound interaction with plates presumes the use of an acoustic plane wave. Obviously, infinite plane waves do not exist in the laboratory. The most congenial experimental situation which one can hope to obtain would be with the use of a collimated acoustic beam. In general, however, acoustic beams are not well collimated; they spread as they travel down range with a characteristic angle known as the beam width. This angle is dependent on the ratio of the lateral dimensions of the transducer to the acoustic wavelength and can be made "arbitrarily" small by increasing the diameter of the transducer. Unfortunately, when one is working in a small test tank, one cannot arbitrarily increase the size of the transducer without quickly reaching the point of diminishing returns.

Figure 1 shows the criteria which need to be met. The figure is a full-scale schematic representing a typical schlieren photograph depicting an acoustic beam reflected from the surface of a plate. The cross section of the optical beam is five inches in diameter, and the acoustic beam, which enters from the upper right, is depicted as having a width of 2.5 inches. In order to determine the reflection coefficient of the plate, one must, of course, be able to resolve the incident and reflected beams. As can be seen, this would become impossible if the diameter

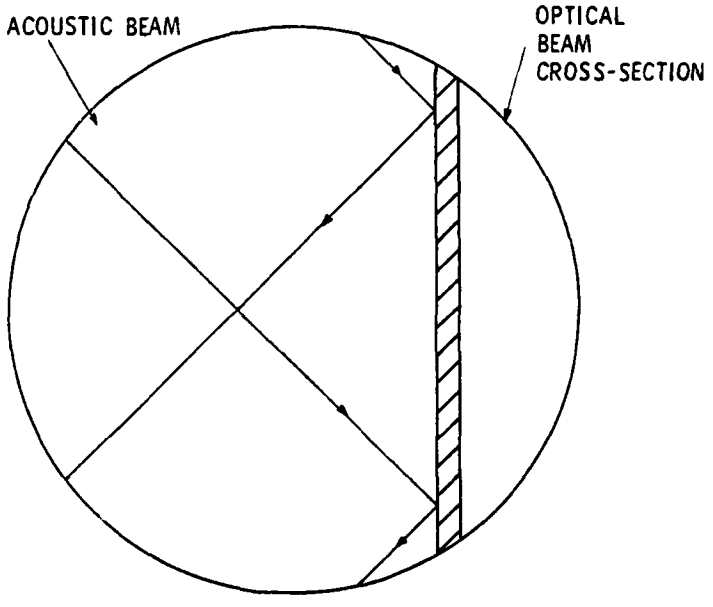

FIGURE 1. Acoustic beam reflection from a plate.

of the acoustic beam was much greater than that shown in this figure. The second point which needs to be made is that, if the beam is spreading, then the on-axis intensity of the reflected beam cannot be directly compared to the on-axis intensity of the incident beam. The net result of these observations is that one ideally would like to have an acoustic beam which is no larger across than about half the diameter of the optical beam and collimated over a range of no less than four times its own diameter. In the instant case, this requires an acoustic beam 2.5 inches in diameter and 10 inches long.

The fact that one of the major goals of this research is to demonstrate the feasibility of using the schlieren technique at frequencies an order of magnitude lower than frequencies traditionally used with schlieren systems somewhat complicates the task. In order to achieve the same angular beam width at a frequency ten times lower one must construct a transducer with a diameter ten times larger. An examination of the near field of a vibrating piston, as shown in Figure 2, indicates that the problem can be resolved. The figure is a typical textbook illustration [65] showing the near field and the transition to the far-field pattern of the piston. At the face of the piston, the extreme near field is greatly complicated by the occurrence of a series of peaks and nulls within the cylindrical beam. However, in the remaining portion of the near field between the last on-axis peak in the extreme

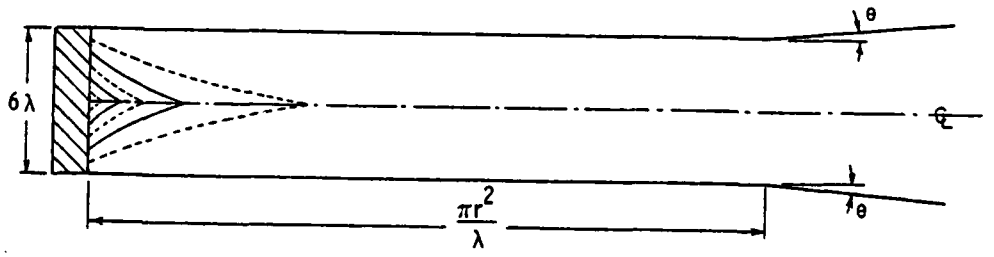

FIGURE 2. The near field of a piston vibrator.

near field and the transition zone to the far-field region, the beam is relatively well-collimated and well-behaved.

The transition zone between the near and far fields occurs at the intersection of the cylinder whose diameter is given by the diameter of the piston and a cone of half-angle θ emanating from the center of the piston face [65]. One can thus see the trade-off involved: if the diameter of the piston is made smaller (and thus the diameter of the cylindrical beam), θ will increase and the transition zone will occur closer to the piston. Consequently, the useful range of the transducer is reduced. The minimum beam diameter, d_m, can be defined as the cord which subtends the angle 2θ at a range, R:

$$d_m/2 = R \tan\theta. \tag{17}$$

If the angular beam width is assumed to be measured between the 3 dB down points (several other criteria are also in common use), then the usual expression employed for the beam half-angle is:

$$\theta = 30^{\circ} \lambda/d. \tag{18}$$

Substituting this relation into Equation (17) together with the fact that here the minimum range which can be tolerated appears to be about 12 inches, one obtains the following transcendental equation:

$$d_m = 24 \tan(31416/fd_m) \quad \text{(in.)} \tag{19}$$

The left- and right-hand members are graphed in Figure 3, and the resulting solution for d_m is shown in Figure 4. It can be readily seen from Figure 4 that, although there are no problems when working in the frequency range generally used with schlieren systems, i.e., about 1 MHz and above, the criteria deduced from Figure 1 cannot be achieved for frequencies below about 150 kHz. As will be seen in Chapter 4, this is the most serious limitation on the low frequency capabilities of the schlieren system in the form in which it was implemented.

2.3 Plate Theory

2.3.1 Dispersion Relations

The problem to be treated consists basically of an infinite plane acoustic wave incident at an oblique angle onto an infinite elastic plate submerged in a fluid. It will be assumed that the plate is homogeneous, isotropic, and bounded by parallel planes. At an arbitrary angle, the acoustic energy will, in general, be partially reflected and partially transmitted. The percentage which is transmitted can be determined experimentally with relative ease using the methods described in Chapter 3; hence, that quantity (as a function of angle of incidence and of frequency) will be used in the theoretical comparisons.

Figure 5 shows the geometry of the problem under consideration. For a plate of sufficient thickness (i.e.,

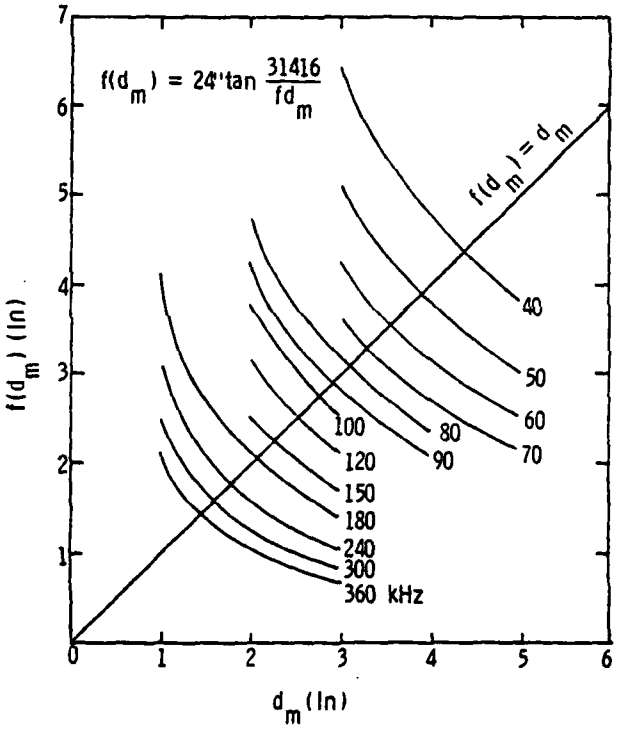

FIGURE 3. A graphical solution of Equation (19).

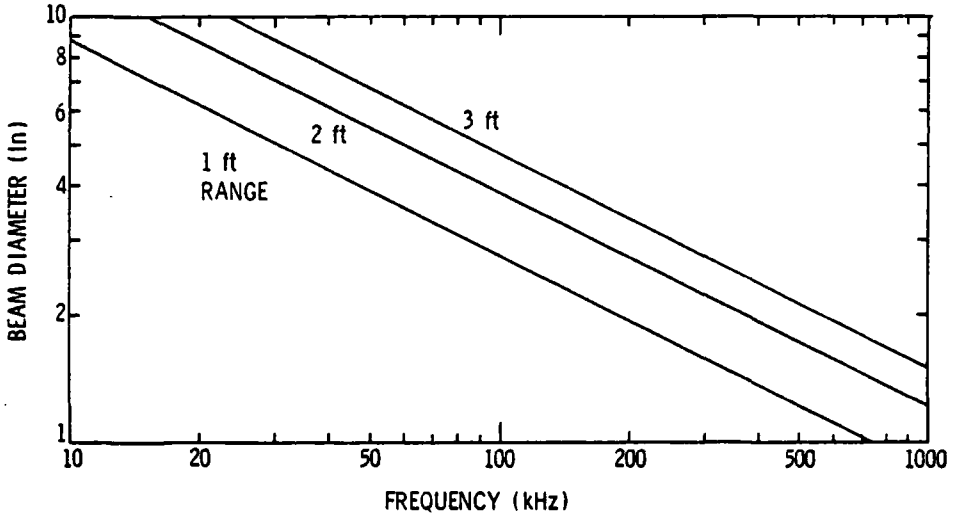

FIGURE 4. The minimum acoustic beam diameter which can be achieved for a given frequency.

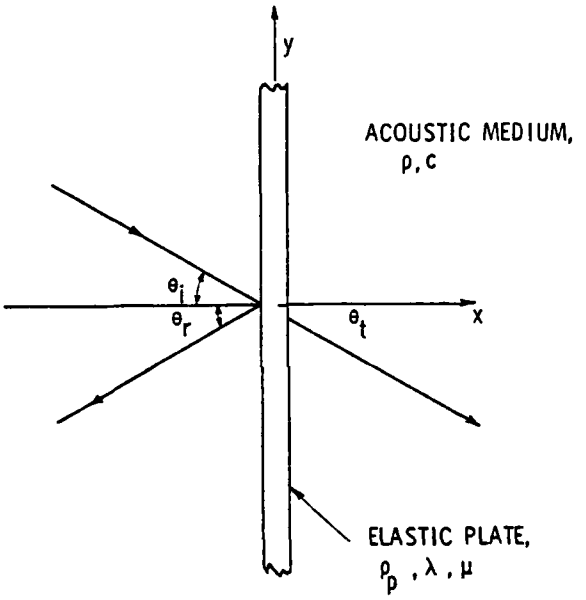

FIGURE 5. Definition of the problem

several wavelengths) several different modes of vibration can be sustained. Each of these modes has a characteristic phase velocity for a given frequency. Hence, as the angle of incidence is increased from normal incidence, 0°, to grazing incidence, 90°, the projection of these phase velocities will, at specific angles, coincide with the velocity vector of the incident wave. At these coincidence angles the transmission ratio (transmitted intensity relative to incident intensity) will show a sharp rise approaching a value of unity, i.e., total transmission, or equivalently, zero reflection. The dispersion relations or formulae relating the phase velocities to the frequency which describe these plate modes were first derived by Rayleigh [1] and Lamb [3] for a plate in vacuo.

By assuming that both the incident plane wave and the plate are infinite in extent, the problem reduces to one of only two dimensions. The equations of motion for the plate then (omitting a constant time factor $\exp[-j\omega t]$) reduce to:

$$\frac{\partial^2 \phi}{\partial x^2} + \frac{\partial^2 \phi}{\partial y^2} + k_l^2 \phi = 0, \tag{20}$$

$$\frac{\partial^2 \psi}{\partial x^2} + \frac{\partial^2 \psi}{\partial y^2} + k_t^2 \psi = 0, \tag{21}$$

where the wave numbers k_l and k_t are for longitudinal and the transverse waves, respectively. They are given by

$$k_l^2 = \omega^2 \rho_p / (\lambda + 2\mu) \tag{22}$$

$$k_t^2 = \omega^2 \rho_p / \mu, \tag{23}$$

where λ and μ are the Lamè constants, ρ_p is the density of the plate, and ω is the circular frequency. The particle velocity can be found from the longitudinal and shear wave potentials ϕ and ψ, respectively, by means of the relationship

$$v = \nabla \phi + \nabla \times \psi . \tag{24}$$

At the boundaries of the plate, i.e., at $x = \pm h/2$, the stresses must be zero. These boundary conditions can be substituted into equations (20) and (21) together with the following representations for the solution:

$$= A \, ch\{(k^2 - k_l^2)^{1/2} x\} \, e^{jky} + B \, sh\{(k^2 - k_l^2)^{1/2} x\} \, e^{jky} \tag{25}$$

and

$$= C \, sh\{(k^2 - k_t^2)^{1/2} x\} \, e^{jky} + D \, ch\{(k^2 - k_t^2)^{1/2} x\} \, e^{jky}, \tag{26}$$

where A, B, C, and D are arbitrary constants, and sh and ch represent the hyperbolic sine and cosine functions, respectively. Some minor algebraic manipulations yield the eigenvalue equation

$$\left[\frac{\tanh\{(k^2-k_t^2)^{1/2} h/2\}}{\tanh\{(k^2-k_l^2)^{1/2} h/2\}}\right] = \left[\frac{4k^2(k^2-k_l^2)^{1/2} \, (k^2-k_t^2)^{1/2}}{(2k^2-k_l^2)^2}\right] \pm 1 \tag{27}$$

where the solution arising from the longitudinal mode is given by the minus sign in the exponent and that arising from the transverse mode is given by the plus sign. Solutions of this transcendental equation were very difficult to obtain until the advent of electronic computers. It was thus not until 1948 that Firestone [19] was able to obtain a sufficiently complete numerical solution which he then was able to compare with experimental results. His data on the location of the transmission peaks for an aluminum plate submerged in xylene offered confirmation for the first ten modes and for frequencies up to approximately fifty times the classical coincidence frequency of the plate.

2.3.2 Transmission Through a Mindlin Plate

The angular location of the peaks in the transmission curve is, however, only part of the description. Also of considerable interest is the magnitude and width of the peaks, as well as, for that matter, the behavior between the peaks. The classical derivations of the relevant equations omit the effects of shear and rotary inertia. Consequently, the equations are valid only for thin plates (i.e., thin compared with the wavelength). The range of validity is thus limited to frequencies near or below the classical coincidence frequency. At these frequencies, the higher Lamb modes cannot be excited and the phenomenon of multiple peaks in the transmission curves discussed above

does not occur. In order to extend the range of validity to higher frequencies, it is necessary to include the effects of shear and rotary inertia as was done by Mindlin [26]. The equations needed for direct comparison with experiment can be found most quickly by following the work of Stuart [40, 41].

Assuming an $\exp(-j\omega t)$ time dependence, the Mindlin plate equation reduces to:

$$\{[\nabla^2 + mS\omega^2/D][\nabla^2 + mI\omega^2/D] - m\omega^2/D\}\, u(x) = 1/D\,[1 - S\nabla^2 - mSI\omega^2/D]\, q(x), \quad (28)$$

where $m = \rho_p h$, the density per unit area of the plate,

ρ_p = plate density,

h = plate thickness,

$D = E h^3 /12(1 - \nu^2)$,

E = Young's Modulus,

ν = Poisson's Ratio,

$S = h^2 /6\ell^2 (1 - \nu)$,

ℓ^2 = Mindlin's shear correction factor ($\sim 0.76 + 0.3\nu$),

$I = h^2 /12$,

$u(x)$ = the transverse displacement

and $q(x)$ = the distributed load.

Note that if the shear, S, and the rotary inertia, I, are set equal to zero, this equation reduces to the classical plate equation.

Taking the Fourier transform in space and expressing the result in a nondimensional form yields

$$m\omega^2[\Omega^2(K^2 - K_I^2)(K^2 - K_S^2) - 1]\, U(K) =$$

$$= [1 + \Omega^2 K_S^2(K^2 - K_I^2)]\, Q(K), \qquad (29)$$

where the following normalizations have been used:

$$\Omega = \omega/\omega_c,$$

$$\omega_c = \sqrt{12}\ c^2/h\, c_p, \text{ the classical coincidence frequency,}$$

$$K = \kappa/k = \sin\theta,$$

$$K_S = \kappa_S/k = c/c_s,$$

$$c_s = \sqrt{\ell^2 G/\ _p} = \sqrt{\ell^2 c_p^{\,2}(1 - \nu)/2},$$

$$G = \text{the shear modulus},$$

$$K_I = \kappa_I/k = c/c_p,$$

$$c_p = \sqrt{E\ /(1 - \nu^2)\rho_p}$$

and c = sound velocity in the surrounding medium. The velocities c_s and c_p are those of the shear wave and of the dilitational wave in the plate, respectively. The parameters U and Q are the transforms of the displacement, u, and of the loading, q, respectively, and are given by:

$$U = \int_{-\infty}^{\infty} u(x)\ e^{j\kappa x}\, dx, \qquad (30)$$

and

$$Q = \int_{-\infty}^{\infty} q(x)\ e^{j\kappa x}\, dx. \qquad (31)$$

The impedance of the plate can now be found from the ratio of the transformed net force, Q, to the transformed velocity, $-j\omega U$, as obtained from Equation (29), i.e.,

$$Z_p/\rho c = - \frac{-j\mu\,\Omega[\Omega^2(K^2 - K_S{}^2)(K^2 - K_I{}^2) - 1]}{[1 + K_S{}^2\,\Omega^2(K^2 - K_I{}^2)]} \,. \qquad (32)$$

The acoustic impedance at the surface of the plate is found in a similar manner. Thus,

$$Z_a/\rho c = j/(K^2 - 1)^{1/2} = 1/\cos\,\theta. \qquad (33)$$

The acoustic transfer function given by

$$T = 2\,Z_a/(2\,Z_a + Z_p) \qquad (34)$$

can now be evaluated by means of Equations (32) and (33) and used to predict the transmission ratio of a plate submerged in a fluid as a function of the angle of incidence, θ, and the frequency, ω, of the incident beam.

2.3.3 The Longitudinal Plate Wave:

An Augmented Mindlin Equation

The equations derived in the previous section, which were based on the Mindlin plate theory, do not describe the full phenomenon. In fact, as Stuart [40] states, they represent only the effect of the first, and partially of the second, antisymmetrical mode of the plate. Because both of these modes occur only for those frequencies above the classical coincidence frequency, the most serious omission is that of the first symmetrical mode, i.e., the first longitudinal mode, of the plate. This mode can produce a peak in the transmission curve even at

frequencies below the coincidence frequency. For low frequencies, an augmented Mindlin equation can be obtained with relative ease.

Beginning with the longitudinal equation of motion from Liamshev [31]:

$$[-\nabla^2 + \frac{m}{D}I\frac{\partial^2}{\partial t^2}]\ u_1(x) =$$

$$= \frac{h}{2E}[\nabla^2 + \frac{m}{D}I(\nu^2 - 1)\frac{\partial^2}{\partial t^2}]\ q_1(x). \qquad (35)$$

Previously, u(x) and q(x) included only the antisymmetrical components; here, $u_1(x)$ represents the symmetrical displacement of the plate surface produced by the longitudinal wave, and $q_1(x)$ represents the symmetrical loading on the plate. This equation is valid only at low frequencies, but, as will be seen later, its range of validity is very much in line with that of the results derived for antisymmetrical waves.

Proceeding as before, the Fourier Transformation of Equation (35) is

$$(K^2 - K_I^2)\ U_1 = \frac{(1 - \nu^2)}{2E}\ h(K^2 - \ell^2 K_I^2)\ Q_1. \qquad (36)$$

The corresponding impedance is then given by

$$Z_1/\rho c = \frac{j\beta}{\Omega}(K^2 - K_I^2)/(K^2 - \ell^2 K_I^2), \qquad (37)$$

where $\beta = 2\ \ell^2/(k_c h K_I)^2$.

This derivation serves to correct several typographical errors which occurred in Stuart and Jensen [66]. The

results now appear to be consistent with those published by Liamshev [32] but disagree with the recent work of Dym et al. [67] by the equivalent of a factor of two in Z_1.

The transmission ratio is thus given by

$$T = 2\ Z_a/(2\ Z_a + Z_p) + Z_a(Z_a + Z_1). \tag{38}$$

As will be seen in Chapter 5, this composite equation will accurately predict the transmission of a sound wave through a submerged plate at oblique angles for frequencies up to nearly ten times the classical coincidence frequency of the plate.

2.4 Bounded Beams

The theory developed in the preceding section applies to infinitely wide plane waves and predicts quite accurately the far-field sound pressure level versus angle of incidence. It does not, however, predict the lateral shift or the feathering exhibited by acoustic beams having a finite width. These phenomenon can be treated by introducing a Taylor series expansion in the development of the reflection (or transmission) coeffecient.

First, the reflection coeffecient can be written in the form

$$\bar{R}(\kappa_x) = R(\kappa_x)\ e^{j\phi(\kappa_x)}. \tag{39}$$

The reflected pressure can then be expressed by the transform

$$p_r(x,0) = \int_{-\infty}^{\infty} F(\kappa_x) e^{j\kappa_x x} R(\kappa_x) e^{j\phi(\kappa_x)} d\kappa_x. \quad (40)$$

Considering a bundle of plane waves travelling in slightly different directions relative to the axis of the main beam, a Taylor series expansion around κ_i is equivalent to physically summing many plane waves around κ_i, each travelling in a slightly different direction. The resultant is a bounded acoustic beam travelling in the κ_i direction. The expansion takes the form

$$F(\kappa_x) = F(\kappa_i) + (\kappa_x - \kappa_i)F'(\kappa_i) \quad (41)$$

$$= A + B\kappa_x. \quad (42)$$

The reflection coeffecient becomes

$$R(\kappa_x) = R(\kappa_i)+(\kappa_x-\kappa_i)R'(\kappa_i)\exp\{j[\phi(\kappa_x)+(\kappa_x-\kappa_i)\phi'(\kappa_i)]\}+\ldots \quad (43)$$

$$= (R_1 + R_2\kappa_x)e^{j\phi(\kappa_i)} \exp\{j(\kappa_x-\kappa_i)\phi'(\kappa_i)+\ldots\}. \quad (44)$$

If the κ_x dependence of F and R is neglected relative to that of the exponent, then the reflection coefficient simply becomes

$$R(\kappa_x) = R(\kappa_i)\exp\{j[(\kappa_x-\kappa_i)\phi'(\kappa_i)+\ldots]\} \quad (45)$$

and the Fourier integeral for the pressure reduces to

$$p_r = \int_{-\infty}^{\infty} F(\kappa_i) e^{j\kappa_i x} R(\kappa_i) \exp\{(\kappa_x-\kappa_i)\phi'\} e^{j\kappa_x x} d\kappa_i \quad (46)$$

$$= \int_{-\infty}^{\infty} F(\kappa_i) R(\kappa_i)\, e^{-j\kappa_i\phi'}\, e^{\kappa_x(x-\phi')} d\kappa_i \quad (47)$$

$$= R(\kappa_i)p_i(x-\phi'). \tag{48}$$

Thus, the reflected and transmitted beams are shifted in the positive x direction by

$$\Delta x = \phi' . \tag{49}$$

This same mathematical treatment is frequently used in the computation of transients for filter designs.

The preceding computation assumes that $\kappa_x \sim \kappa_i$, so that $F(\kappa_x) = F(\kappa_i)$ and $R(\kappa_x) = R(\kappa_i)$, and thus considers only a narrow angular region. If this assumption does not apply, it may be necessary to decompose R and F into several κ_x groups and perform the integration for each group separately.

The critical asumption is in the Taylor series development, i.e., that the phase angle is given by

$$\phi(\kappa_x) = \phi(\kappa_i) + (\kappa_x-\kappa_i)\phi'(\kappa_i) + \ldots \tag{50}$$

This implies that the contributing wavenumber range $(\kappa_x-\kappa_i)$ must be small, since $\phi'(\kappa_i)$ may change quite rapidly for large values of $(\kappa_x-\kappa_i)$. Hence, the angular spectrum of the incident beam must be narrow, since the contributing wavenumber range for a beam of width a is of order

$$\kappa_x - \kappa_i \sim \pi/a. \tag{51}$$

The width of the beam must then be large compared to $\phi'(\kappa_i)$ which is equal to the magnitude of the beam shift, since the Taylor series will converge if

$$(\kappa_x-\kappa_i)^n\phi^n(\kappa_i) \ll 1, \tag{52}$$

or to a first order approximation if

$$(\kappa_x-\kappa_i) \ll 1/\phi'(\kappa_i). \tag{53}$$

2.5 Transmission of Bounded Beams

If the amplitude of the incident wave is constant, and its trace velocity is such that $k \sin\theta_o$ is equal to the wavenumber, κ_n, of a free plate wave, i.e., a Lamb wave, then only this wave will be excited and other wave components can be neglected. Under non-ideal conditions, other waves may be excited; most frequently, these waves arise because of the finite width of the beam and because of inhomogeneities in the velocity distribution of the incident beam.

If the half-width of the acoustic beam is a, then in the interval $-a < x < a$, the forced excitation creates two plate waves travelling in opposite directions (see Figure 6). The wave propagating in the same direction as the incident wave, i.e. whose κ_n has the same sign, will have a significantly greater magnitude. Assuming that κ_i is positive, then

$$p = D(\kappa)[e^{j\kappa_o x} - e^{-\kappa''(x+a)}\, e^{j\kappa_n(x+a)}]. \tag{54}$$

The two waves interfere because of the phase difference. At the left edge, the interference is destructive and the

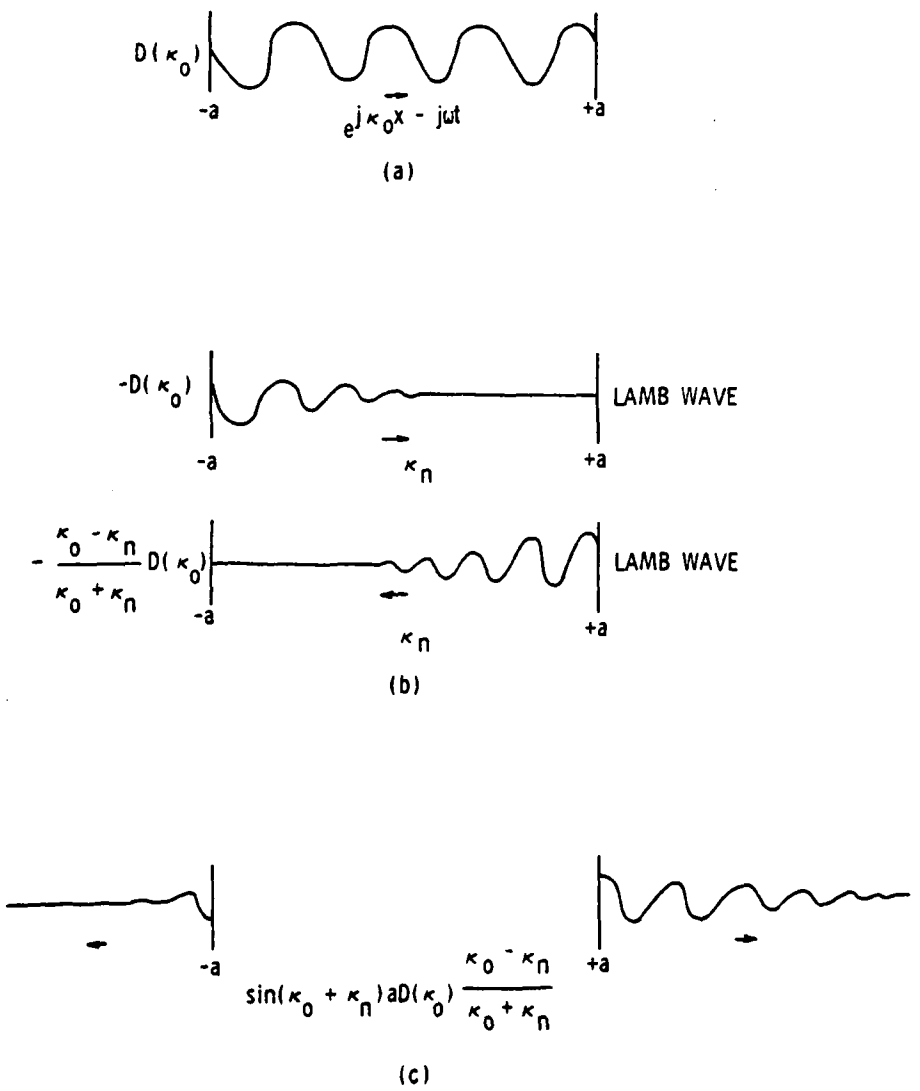

FIGURE 6. Plate wave excited by a bounded beam.

net result is zero. At the right, the interference is constructive and grows exponentially toward the value $D(\kappa_o)$. The plate wave must travel a distance approximately equal to the excitation distance before reaching full amplitude; thus, if the beam width is small compared to $1/\kappa_o''$, the transmitted wave may be considerably smaller than the predition for a beam of infinite width. This excitation distance is given by

$$\omega\eta/2 = (2r/\omega m)(\omega/2) = r/m = \rho_o c_o/\rho_p h \tag{55}$$

$$\kappa_n'' = \omega\eta/ec_p = \rho_o c_o/\rho_p c_p h \tag{56}$$

For the case of an aluminum plate in water, κ_n'' becomes:

$$\kappa_n'' \sim h/10 \tag{57}$$

and

$$x_{ext} = 1/\kappa_n'' \sim 10h. \tag{58}$$

For a longitudinal plate vibration, the tranverse vibration is approximately equal to $\eta\dot{\xi}$ ($\dot{\xi}$ being the longitudinal velocity component) and the excitation distance is approximately $1/\eta^2$ times as great, i.e.,

$$x_{ext} \sim 100h. \tag{59}$$

Thus, for longitudinal waves, the excitation distance is significantly greater than for transverse vibrations.

CHAPTER 3

EXPERIMENTAL APPARATUS

3.1 Introduction

The data were obtained with a quantitative schlieren system. A general schematic of the system is shown in Figure 7, and schematics of the electronic layouts are shown in Figures 8 and 9. The geometrical configuration depicted in Figure 7 originated with Toepler's work in the 1860's [68-72]. Although several other configurations have been developed since then, this is still one of the most successful of the choices available. The only changes from Toepler's original design are direct substitutions of modern technology. A laser, for example, was substituted for the spark gap, which Toepler used for a light source, since the major requirement was simply high intensity. The only other significant change, assuming that modern electronics can pass without mention, was the substitution of a closed circuit TV camera at the exact position Toepler described as the location at which the experimenter should place his eye. Actually, there are also other ways in which the schlieren image could be observed. These include

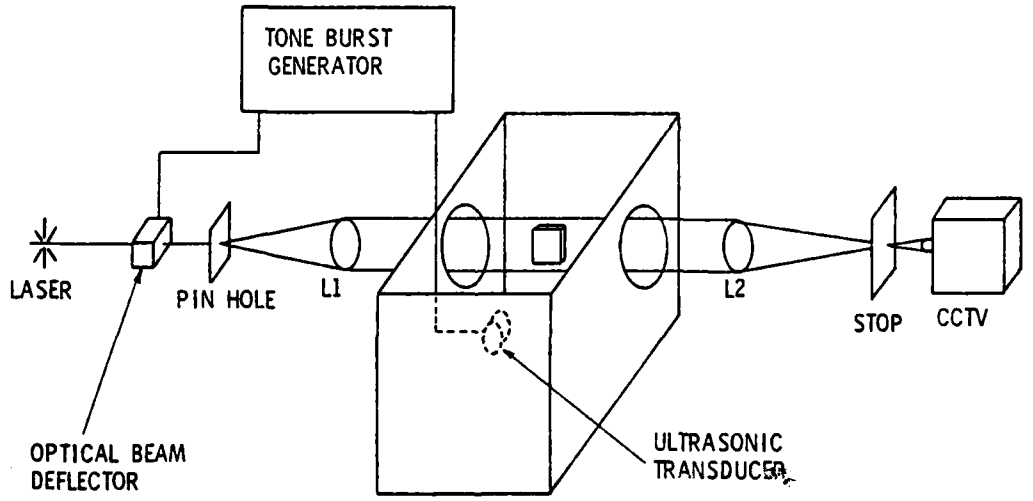

FIGURE 7. The schlieren experimental system.

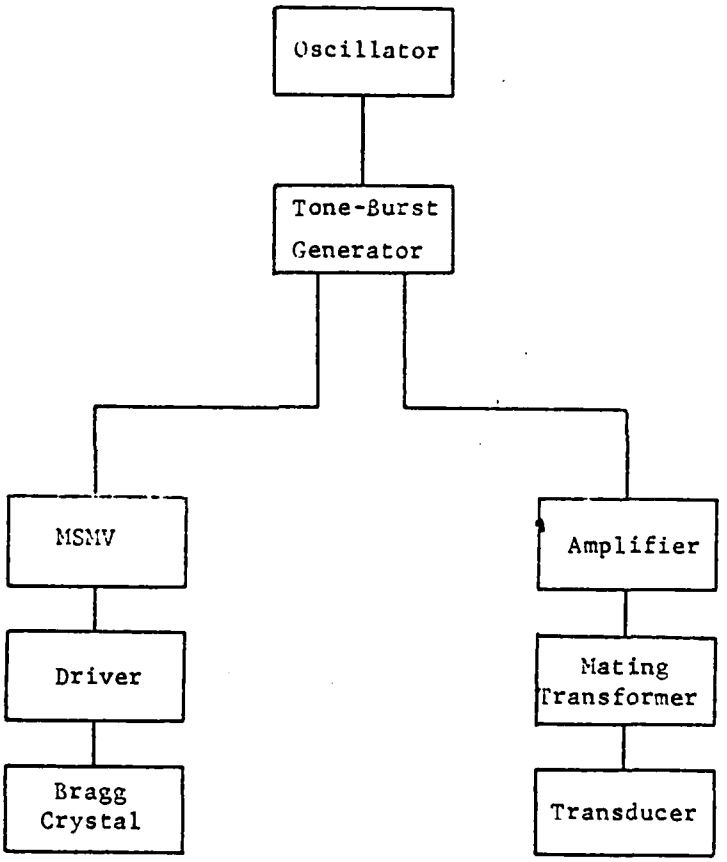

FIGURE 8. Layout of the acoustic subsystem.

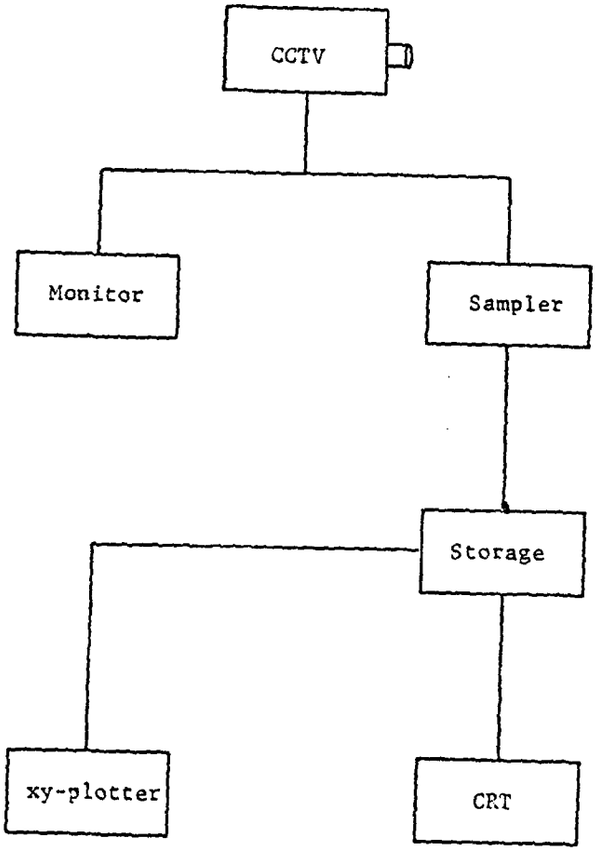

FIGURE 9. Layout of the data acquisition system.

placing a ground glass screen or a photographic plate at this same location. The photographs presented both by Toepler in the 1860's and those presented herein were obtained in this manner.

The use of a vidicon, however, opened up the possibility of obtaining quantitative data. Earlier attempts to quantize schlieren data were limited to densitometer analyses of schlieren photographs, which were not overly successful. In recent years, considerable technology has evolved for processing video signals, which gives rise to an alternative approach. Briefly, it consists of sampling the voltages at equidistant points along each horizontal line of the video scan, storing the resulting data points (which represent brightness), and then plotting the sequential list. This produces a plot corresponding to optical intensity along a vertical line down the TV screen. Since optical intensity can be directly related to acoustic pressure amplitude in a schlieren image, this plot also corresponds to the amplitude of the acoustic field along this vertical slice.

3.1.1 Optical System

The details of the optical system can be understood most easily by following the path taken by the laser beam as it passes through the apparatus, i.e., left to right as shown in Figure 7. The light source was a Spectra Physics Model 125 laser, which generated a continuous 50 mW beam of

632.8 nm light. This beam was strobed by means of an Isomet Model 1205 Acousto-Optic Modulator. The Modulator, basically a Bragg crystal deflector, was driven with a Dranetz Tone Burst-Timing Generator (Series 206). This also supplied the acoustic pulse to the transducer and thus permitted a precise adjustment of the time delay between the optical strobe and the acoustic pulse. The net result was that the acoustic pulse could be photographed at numerous discrete points, and thus its path across the field of view could be determined even when the pulse reflected back from complex structures scattering out in many directions. An electronic interface was designed and constructed for the purpose of mating the Tone Burst Generator to the Acousto-Optical Modulator, which were originally incompatible with one another. By incorporating a monostable multivibrator in this interface, it was possible to improve the strobe speed from 10 μs to 100 ns. The speed was continuously adjustable from 100 ns to 100 μs. Normally, the duty cycle was set between 2 - 5 kHz. Even at these speeds, there was sufficient light passing through the system to require the use of neutral density filters in order not to oversaturate the TV camera. The 100 ns strobe speed allowed the acoustic pulse only enough time to travel 0.006 in. through the water, which obviously produced no observable smearing of the resulting photographs. This was a considerable improvement over the original 10 μs strobe speed, which would have permitted a skid of over half an inch.

Having travelled through the Acousto-Optical Modulator, the laser beam passed into a Space-Optics Research Labs optical beam expander. This consisted of little more than a pin hole and the necessary optics for isolating and collimating the light in the zeroth diffraction order created by the pin hole. The resulting 5 in. diameter beam then passed into the test tank.

The tank was constructed from 1/2 and 3/4 in. sheets of Lexan, with a width and height of 2 ft and a length of 4 ft 3 in. Waterproofing was accomplished by means of the same silicone rubber sealant used in commercial aquariums. Aluminum angle bracing was added to the long sides to reduce the bowing produced by the weight of the water. The clear Lexan greatly eased the problems of positioning the transducers and various test samples, but it was not, of course, of sufficient optical quality to consider passing the expanded laser beam through it. Consequently, 10 in. diameter holes were cut out of the two long sides and replaced with 1/10 wave optical glass windows. The use of optical glass seems, in retrospect, to be unnecessary. Due to several serious reams in the original pair of optical glass windows, they were returned to the manufacture for exchange, and the apparatus was used for several months with ordinary float-glass windows. The results were sufficiently satisfactory that it appears the best procedure would have been simply procuring a half-dozen pieces of float glass and using the pair which performed best.

A pair of sliding cross rails were added to the top of the tank for use in positioning the transducer and the test samples. A small low-geared motor was used to raise and lower the projection angle of the transducer. Angular scales, which were inscribed at each degree, were included for determining the pitch angle of the transducer and the yaw angle of the test sample. The reproducibility was easily within 1/4 degree when the backlash in the gears was correctly countered.

Upon leaving the test tank, the optical beam passed through a 30 in. focal length Space Optics Research Lab lens; this focused the beam onto a slide glass cover resulting in a spot approximately 1/2 mm in diameter. An opaque stop, which was as nearly as possible the same size and shape as the spot of light, was placed at this focal point. The zeroth diffraction order was thus completely blocked out and only higher diffraction orders produced by the acoustic disturbances in the water, if any, passed into the TV camera.

3.1.2 Spatial Filtering

The size of the optical stop is critical. It must be large enough to block out all of the light passing through the quiescent system; otherwise, the background level is increased and the dynamic range of the system is degraded. Therefore, the stop must be at least as large as the circle of least confusion; the question is how much larger - if

larger at all. From the original series of papers by Raman and Nath [73 - 79], it is quite well known that the relative intensity of each diffraction order is given by the square of the Bessel Function, $J_n^2(v)$, where n is the order number and v is the Raman-Nath parameter,

$$v = k\mu L, \tag{60}$$

where μ is the index of refraction in the medium and L is the width of the sound beam. If the zeroth order is filtered out and all remaining orders passed through, the resulting intensity is then given by

$$I = 2 \sum_{n=1}^{\infty} J_n^2(v). \tag{61}$$

This is shown graphically in Figure 10. Also shown are the corresponding curves for larger stops, and specifically for a stop which blocks both the zeroth and the first order and one which blocks the zeroth, the first and the second order.

A line which approximates the background level found with the actual experimental system is also included. This background is mainly due to the ambient room light, but also includes stray light from scattering phenomenon, etc. The background was minimized by collecting all data at night when the overhead work area lights could be extinguished.

The dynamic range to be expected from the system can be estimated from the point at which the intensity rises

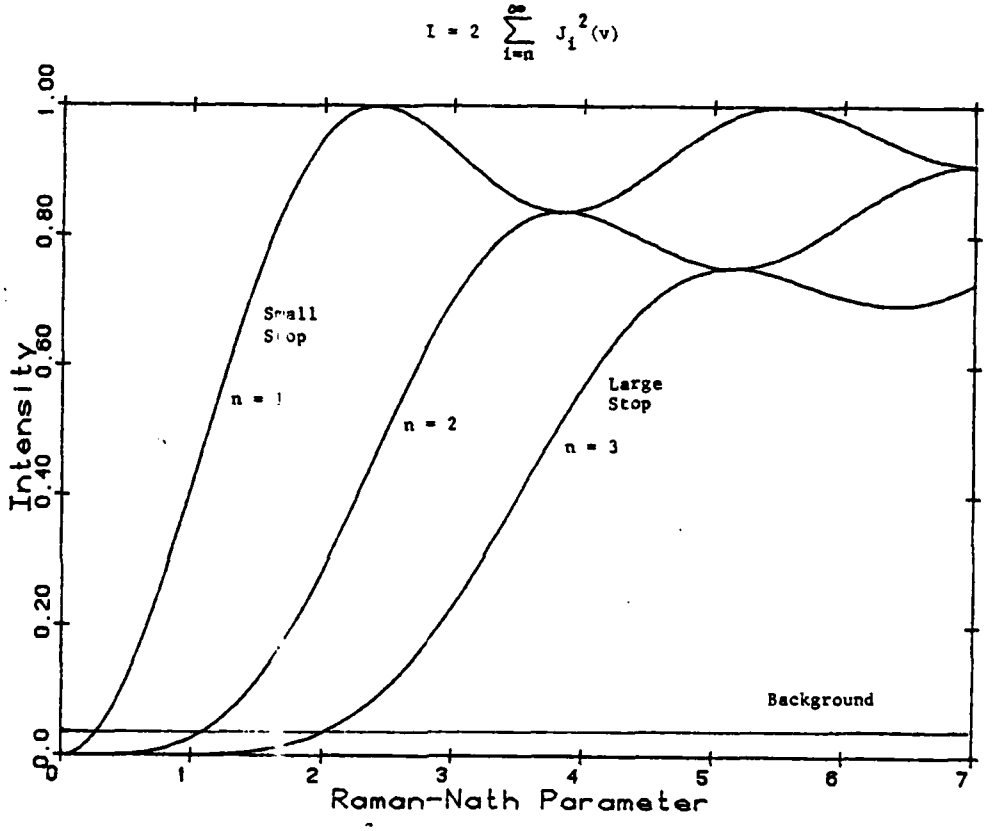

FIGURE 10. The resulting effect on optical intensity for spatial filters of various sizes. n=1 blocks only the zeroth order; n=2 blocks the zeroth and first orders; and n=3 blocks the zeroth, first and second orders [cf. 80].

above the background and the point at which the curve becomes multivalued. If only the zeroth order is stopped, the dynamic range is thus seen to be about 20 dB; stopping the first order in addition to the zeroth order reduces this to 11 dB; and increasing the stop size further to include the second diffraction order further reduces the dynamic range to 8 dB. The conclusion seems to be that the preferable choice is to stop only the zeroth order. Experimentally, this is by far the most convenient choice, since the size of the circle of least confusion is independent of the acoustic frequency, while the distance between the diffraction orders is directly related to the frequency. Thus if one wished to block both the zeroth and first orders different-sized stops would be needed for each frequency of interest. If only the zeroth order is to be blocked, only one size stop is needed.

The actual stop was mounted in a ring with a finite diameter, which means that not all of the infinite set of diffraction orders was passed through to the video camera. Figure 11 shows, for the first time, the effect of transmitting only a few diffraction orders, i.e., of prematurely truncating the series given in Equation (61). It can be clearly seen that surprisingly few terms need to be included in order to approximate the useful portion of the curve. Four diffraction orders are sufficient to duplicate the part of the curve lying between $v = 0$ and $v = 2.405$, which covers all intensities between $I = 0$ and $I = 1$,

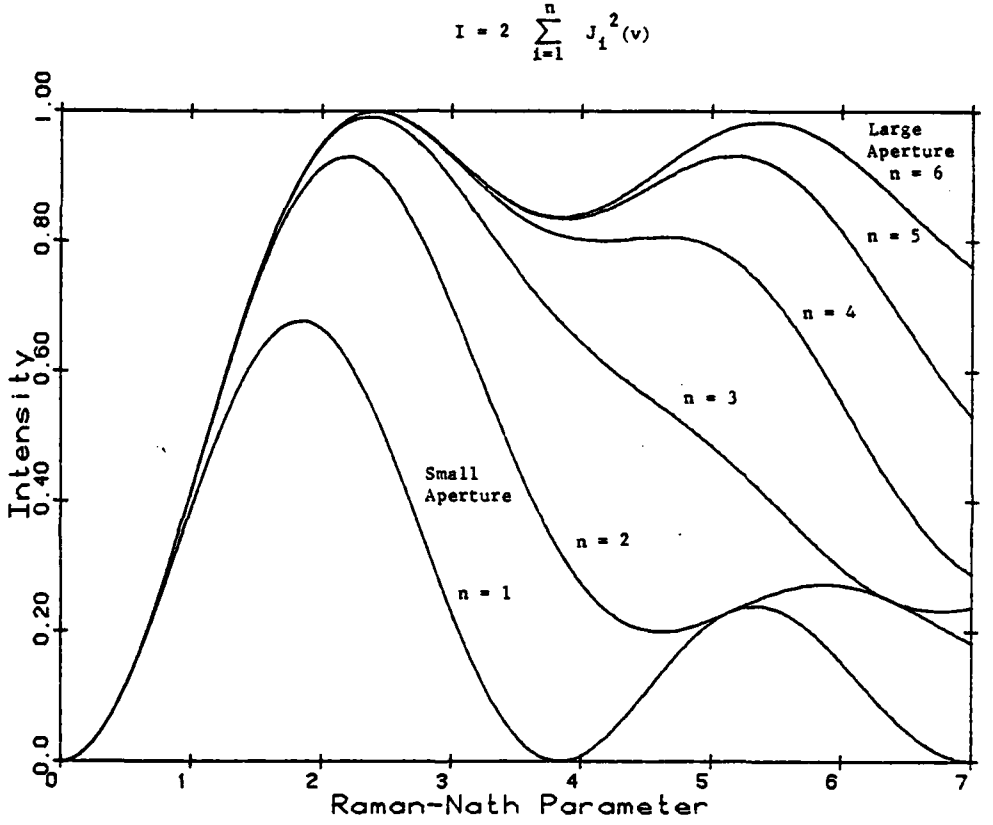

FIGURE 11. The effect on optical intensity is shown for concentric rings of various sizes.

respectively. The size of the holder ring was far too large to have any detrimental effect on the schlieren image, even at the highest frequencies used. An interesting possiblity would be an attempt to use this fact to filter out the higher harmonics of the acoustic transducer by adjusting the diameter of a concentric ring surrounding the stop. The higher harmonics are especially prevalent in photographs taken at extremely low frequencies, since the sensitivity of the schlieren system is highly dependent on the acoustic frequency.

3.1.3 The Acoustic System

The acoustic system interfaced with the optical system as shown in Figure 8. This portion of the experimental equipment was indicated in the general figure (Figure 6) simply as a tone-burst generator. In reality, a Hewlett Packard Model 606B Signal Generator was used to produce a continuous sine wave signal for the frequency range above 50 kHz and a GenRad Type 1162A Frequency Synthesizer was used for lower frequencies. The Tone-Burst Generator, which was described in Section 3.1.1, then gated this signal into a series of short (generally 10 μs) pulses and simultaneously produced the timing signals used to strobe the laser beam. The acoustic pulses were amplified with a Model 240L ENI Class A RF power amplifier and matched to the transducers by means of an ENI Model 240-2T transformer.

The acoustic transducers (see Table 2) were, for the most part, constructed from single thickness-mode discs of PZT-4 ceramic. The discs were mounted in cylindrical aluminum housings with air backing by use of silicone rubber sealant. The design criteria developed in Section 2.2 were used and proved to be quite successful. The resulting transducers were quite well collimated in the range of 3-12 in. One additional transducer, shown in Figure 12, was constructed for use at frequencies below 30 kHz using the traditional tonpilz design.

3.1.4 Data Acquisition

The data acquisition system layout is shown in Figure 9. Briefly, the data were obtained by electronically sampling the horizontal lines on a standard television raster. The starting point of each line was identified by means of the blanking pulse and then, after a given delay time, the voltage was stored and the next line sampled. The resulting set of sequential stored values corresponded to the voltage curve plotted along a vertical slice down the screen. This vertical sample line could be adjusted to any required location by simply adjusting the given delay time. The stored data was either displayed in real time on an oscilloscope was plotted by means of an x-y plotter.

Two calibrations were necessary. First, the response characteristics of the vidicon tube had to be found. Normally, this would have to be repeated for a large number

TABLE 2

TRANSDUCERS

Ident.	Resonance	Diameter
AL180A	195 kHz	2.0 in.
AL180B	190	2.0
AL180C	189	2.0
AL340A	353	1.5
AL680A	692	1.0
AL680B	688	1.0
BR-1	362	1.0
AL-27	27	1.5 in. sq.

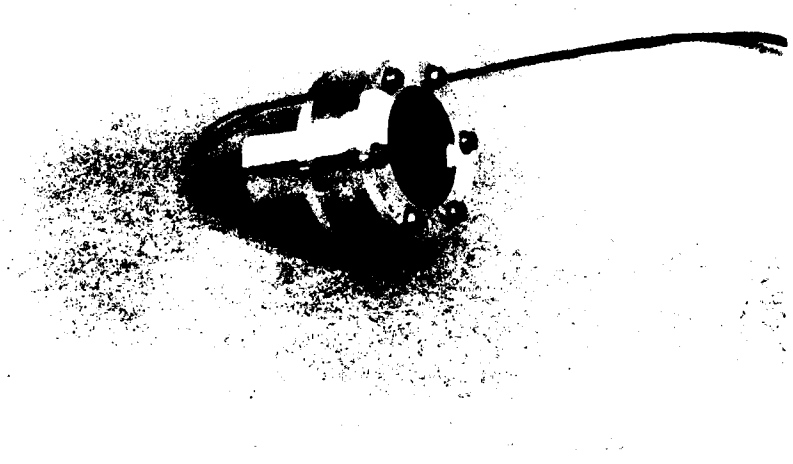

FIGURE 12. Tonpilz transducer resonant at 27 kHz.

of locations across the face of the tube, since the response falls off quite noticeably near the edges. Because of the experimental techniques described in Section 5.3, this was generally avoided and only the response curve for the center point of the tube was necessary. This was determined by turning off the acoustic system, which has nothing to do with this particular calibration, and recording the voltage sample level for the laser beam masked by a large range of neutral density filters. This produced the characteristic curve shown in Figure 13.

The second calibration gives the correlation between the acoustic pressure and the optical intensity. This was performed by placing an acoustic beam across the center of the field of view and taking data scans for a wide range of transducer drive voltages. The actual voltage at the input terminals of the transducer was used to avoid the possibility of nonlinearities arising from the amplifier circuits. This still assumes that the transducer itself was linear, which is generally not an unreasonable assumption. The resulting calibration curve is shown in Figure 14. This data collection system is described more fully by Stanic [81].

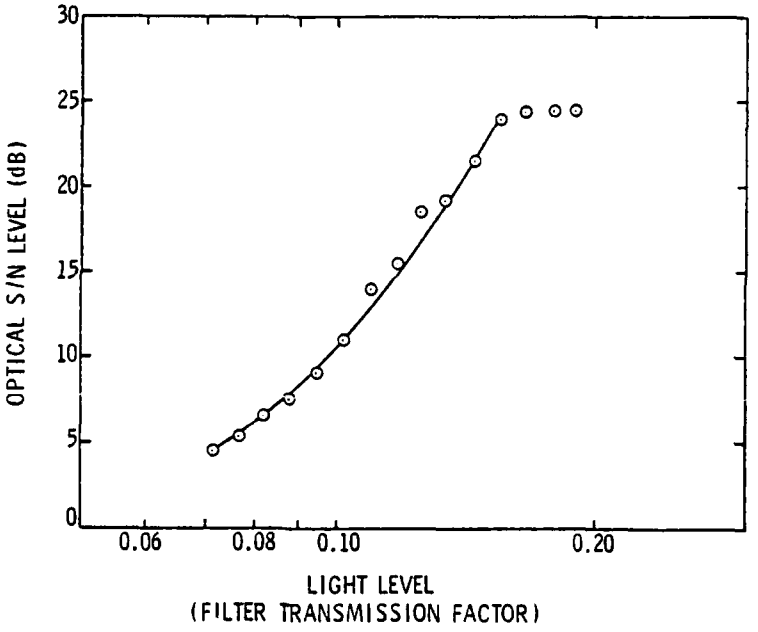

FIGURE 13. Response characteristic curve of vidicon tube.

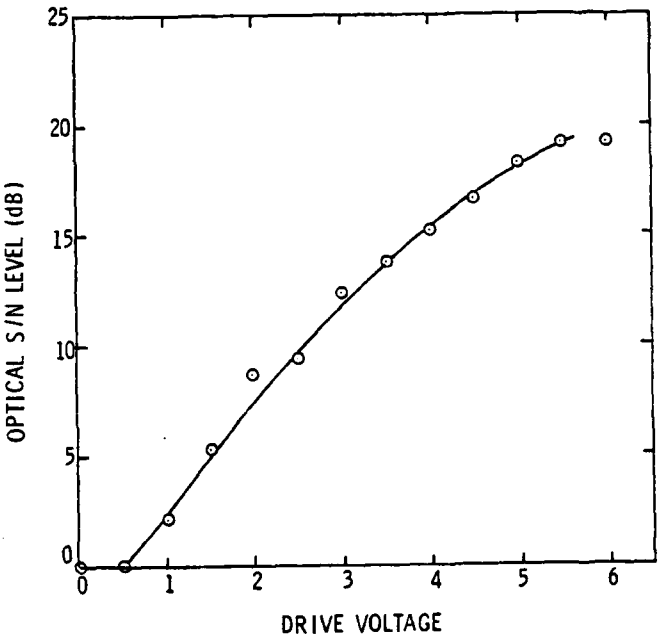

FIGURE 14. Schlieren system calibration curve.

CHAPTER 4

QUALITATIVE OBSERVATIONS

4.1 Low Frequency Schlieren

Schlieren systems have long been used for qualitative studies of sound fields. The quantitative data presented in Chapter 5 demonstrate clearly that schlieren systems can now be used to obtain very accurate quantitative descriptions of acoustic fields. Such quantitative data, however, only supplements the more traditional schlieren photographs; it cannot, and is not intended to, supplant the photographic representations which yield excellent overviews by means of their full two-dimensional depictions of acoustic fields. The quantitative data curves on the other hand are intended to collect the amplitudes of single points on the photographs and show the change in that amplitude as a function of the various parameters such as angle of incidence or frequency. It should be noted that the observations presented in this chapter resulted from over 1000 hours of viewing real-time schlieren images; the photographs presented herein were culled from the full collection for their representativeness and for their reproducibility.

One of the most striking achievements of this research was the demonstration of the schlieren effect at frequencies nearly two orders of magnitude lower than those traditionally used with the schlieren technique. Figure 15 shows a very clear, sharp photograph of an acoustic field at 27 kHz. The lowest limit achieved by earlier investigators was 50 percent higher than this frequency [82].

4.2 Transmission Through Flat Plates

Figure 16 depicts the acoustic transmission through a 0.032 in. thick aluminum plate at a frequency 7.7 times the classical coincidence frequency of the plate. This corresponds to the same conditions as for Figure 36. The incident beam in these photographs, and those to follow, enters from the upper left, and is partially transmitted into the lower right quadrant and partially reflected into the lower left. Figure 16(a) shows the transmission at the critical angle for the A_0 Lamb mode, and Figure 16(b) shows the S_0 Lamb mode. Two observations should be noted, both of which are more clearly shown in Figure 16(b). First, the reflected beam shows the characteristic dark band, which has been interpreted [55] as the overlap of the specularly reflected beam and the reradiated field from the Lamb wave, which are 180° out of phase and thus cancel each other. Second, by lining up the upper edges of the incident and transmitted beams, one can see an obvious downward shift in the location of the transmitted beam from that which would

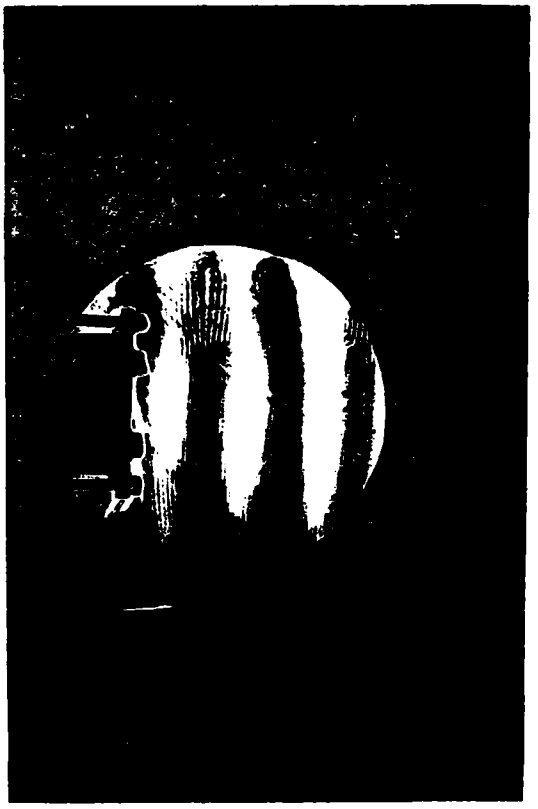

FIGURE 15. Schlieren visualization of a 27 kHz acoustic field.

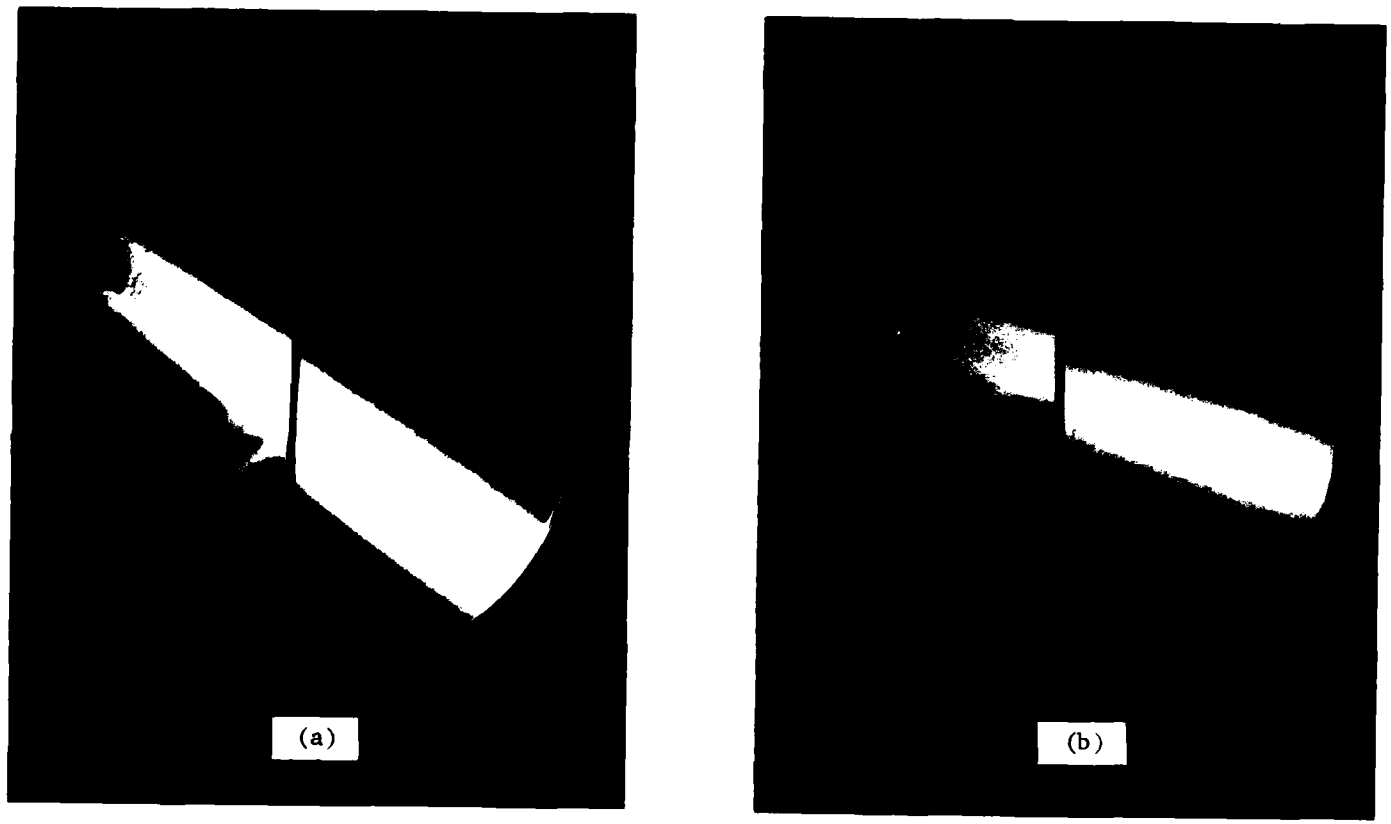

FIGURE 16. Transmission of an acoustic beam through a 0.032 in. thick aluminum plate at a frequency of 2.125 MHz, which is 7.78 times the classical coincidence frequency of the plate. Transducer AL680B which has a beam width of 1.0 in. was used. (a) The A_0 Lamb mode is excited at an angle of incidence of 33.5^{o}. (b) The S_0 Lamb mode is excited at an angle of incidence of 17.5^{o}.

be normally expected. This shift was first explained by Schoch [53]. Very precise experimental measurements by Neubauer [54] exposed flaws in Schoch's theory due to his assumption of a flat intesity distribution across the beam and to the inapplicability of the theory to narrow acoustic beam widths. By interpreting the shifted beam as a reradiated beam produced by the Lamb wave travelling down the plate, Bertoni and Tamir [55] obtained very satisfactory agreement with Neubauer's measurements.

Figure 16 was obtained by using a continuous acoustic beam, while Figure 17 was obtained by using a short 10 μs pulse. Figure 17 shows the reradiation from the A_1 Lamb wave for the same condition as Figure 16. The photograph was taken approximately 30 μs after the incident pulse contacted the plate; as the Lamb wave travelled down the plate, it reradiated energy into the surrounding medium. This gradual loss of energy in the plate wave is shown by the corresponding loss in intensity of the reradiated pulse. Note that the upper portion of the pulse is thus much brighter than the lower portion.

A small pulse of acoustic energy incident at an oblique angle on an infinite plate normally reflects back as a compact pulse package retaining its original shape. However, as was shown in Figure 17, if a Lamb mode is excited, the shape of the pulse can be greatly elongated. A distortion in the shape of the pulse can occur, even for normally incident pulses as is shown in the sequence of

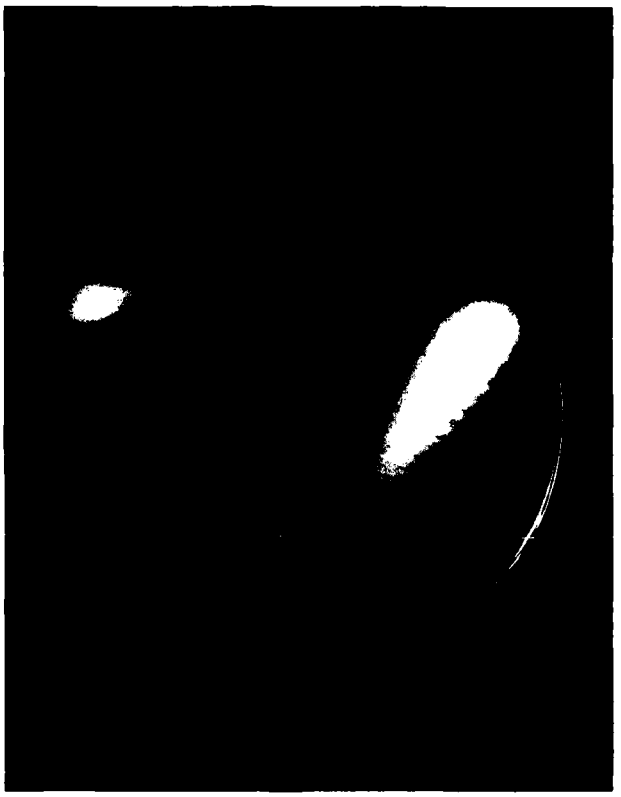

FIGURE 17. Transmission of a 10 μs acoustic pulse through a 0.032 in. thick aluminum plate at a frequency of 2.125 MHz, which is 7.78 times the classical coincidence frequency of the plate. Transducer AL680B which has a beam width of 1.0 in. was used. The A_1 Lamb mode is excited at an angle of incidence of 6.5^{o}.

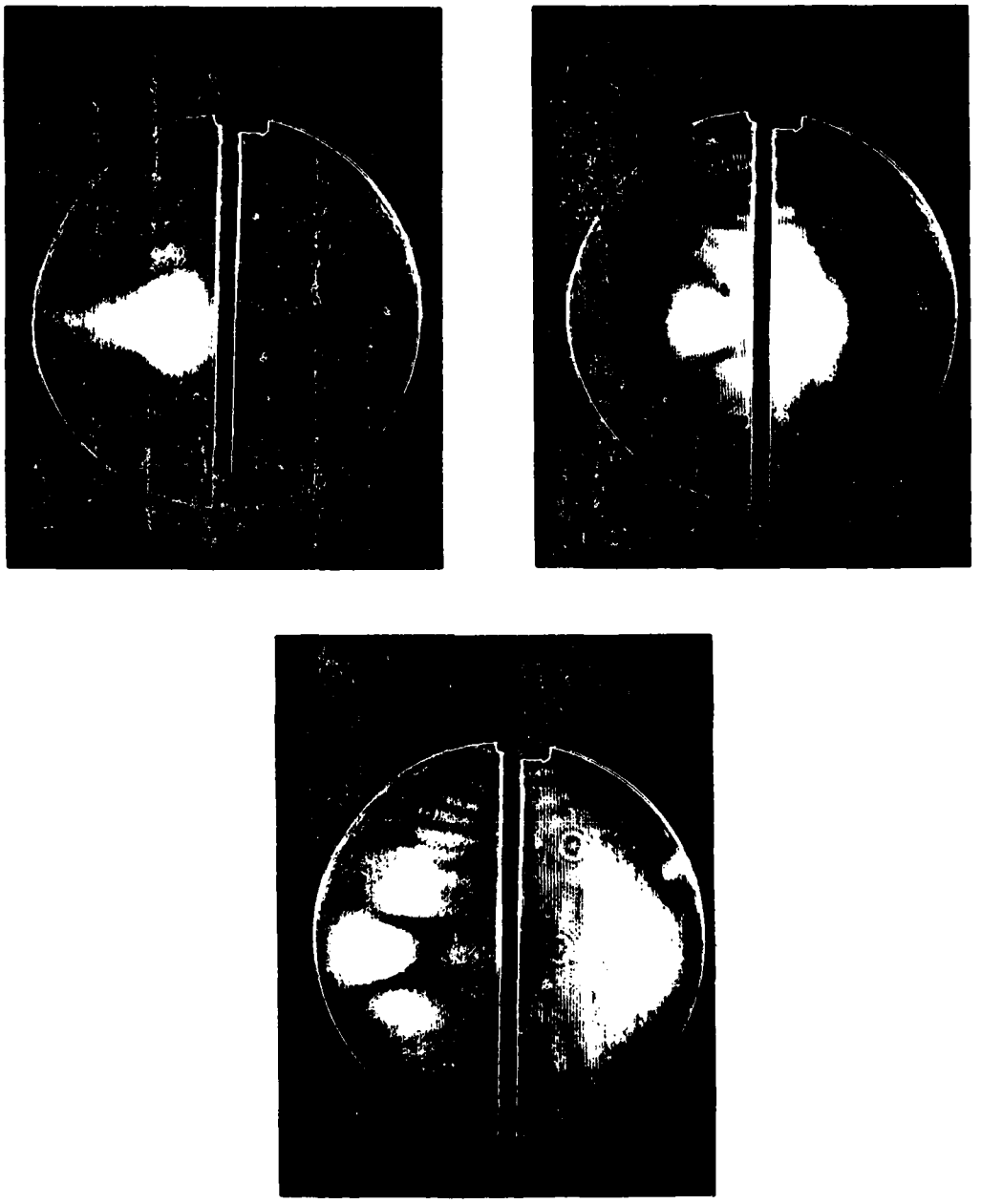

FIGURE 18. Transmission of a 10 μs acoustic pulse through a 0.501 in. thick aluminum plate at a frequency of 680 kHz, which is 14.9 times the classical coincidence frequency of the plate. At normal incidence this excites the S_1 Lamb mode. Transducer AL680A which has a beam width of 1.0 in. was used.

photographs reproduced in Figure 18, which shows the initial emergence of the S_1 Lamb mode at 0^o.

4.3 Edge Effects

As has been seen, when an incident wave strikes an infinite plate, or one of sufficient size that the edges are many wavelengths away, then there are beams transmitted and reflected (or reradiated) in only two directions. Near the edge of a finite plate, however, the Lamb wave will be reflected from the plate edge and travel back up the plate. This can set up a strong standing wave in the plate, which will then greatly complicate the resulting radiation pattern. This is demonstrated in Figure 19. In this photograph, the S_0 Lamb mode has been excited and the superposition of the fields reradiated by the Lamb wave travelling in opposite directions in the plate shows a clear standing wave pattern in the surrounding medium with the wave fronts perpendicular to the plate. It is not uncommon to see standing-wave patterns near a plate due to the superposition of the incident and the specularly reflected wave, but, in that case, the wave fronts are necessarily parallel to the plate, not perpendicular. Furthermore, they appear only on one side of the plate.

As was noted above, one normally sees only two beams emerging from the plate. When a Lamb mode is excited, the situation becomes more complex because there is now a radiation field superimposed on top of the specular field.

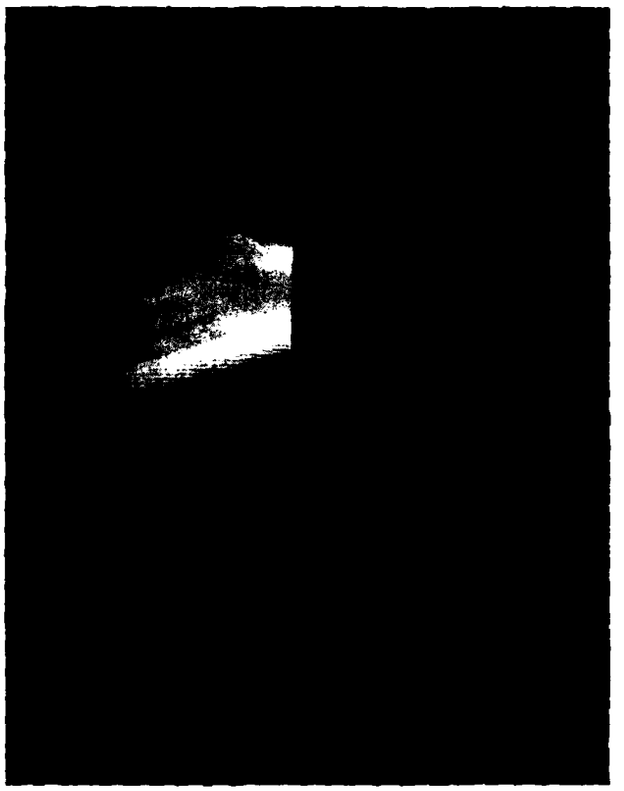

FIGURE 19. Transmission of an acoustic beam through a 0.023 in. thick steel plate at a frequency of 2.125 MHz, which is 5.26 times the classical coincidence frequency of the plate. The S_0 Lamb wave is excited at an angle of incidence of 17.5°; the edge of the plate causes the formation of a standing wave pattern in the surrounding medium. Transducer AL680B which has a beam width of 1.0 in. was used.

For an infinite plate, there is little energy radiated into the upper quadrants but, near the edge of a finite plate, this is not true. In Figure 20, the incident beam has been moved even closer to the edge than was the case for Figure 19. Figure 20(a) shows a beam being radiated quite strongly into the upper right quadrant. By changing from a continuous beam to a pulse, as in Figure 20(b), it can be further seen that there is also a strong beam being radiated directly back along the path of the incident beam toward the transducer. The same phenomenon can be seen again in Figure 21 for a much lower frequency. Backscattering does not occur near the center of the sample plates with nearly as great an intensity as near the edges, which can be seen by comparing these last two figures with Figure 22. This figure shows a direct comparison between a beam incident near the center and one incident near the edge of the same steel plate with the same acoustic conditions.

4.4 Negative Phase Velocities

The dispersion curves in Figure 53 for aluminum show that, in a very narrow frequency range near the onset of the S_1 Lamb mode, the individual modal curves can become double-valued. Both Tolstoy and Usdin [61] and Viktorov [49] speculated that this could be caused by the occurrence of a negative phase velocity. This would imply that the Lamb wave travels in the opposite direction in the plate from the previous examples in this chapter. This would

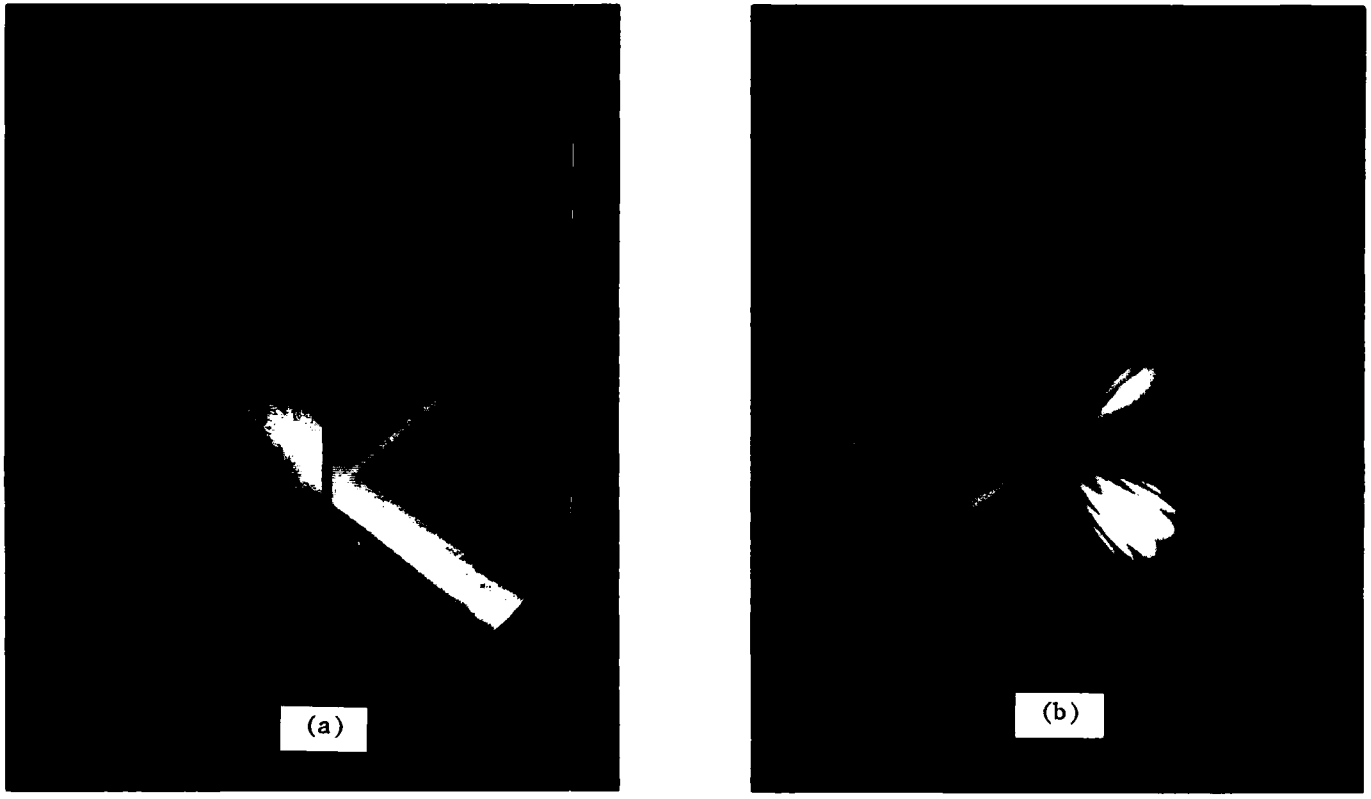

FIGURE 20. Transmission through a 0.023 in. thick steel plate at a frequency of 2.125 MHz, which is 5.26 times the classical coincidence frequency of the plate. The A_0 Lamb mode is excited at an angle of incidence of 38.5°. Transducer AL680B which has a beam width of 1.0 in. was used. (a) A continuous beam strikes near the plate edge. (b) A 10 μs pulse is shown 25 μs after first contacting the plate.

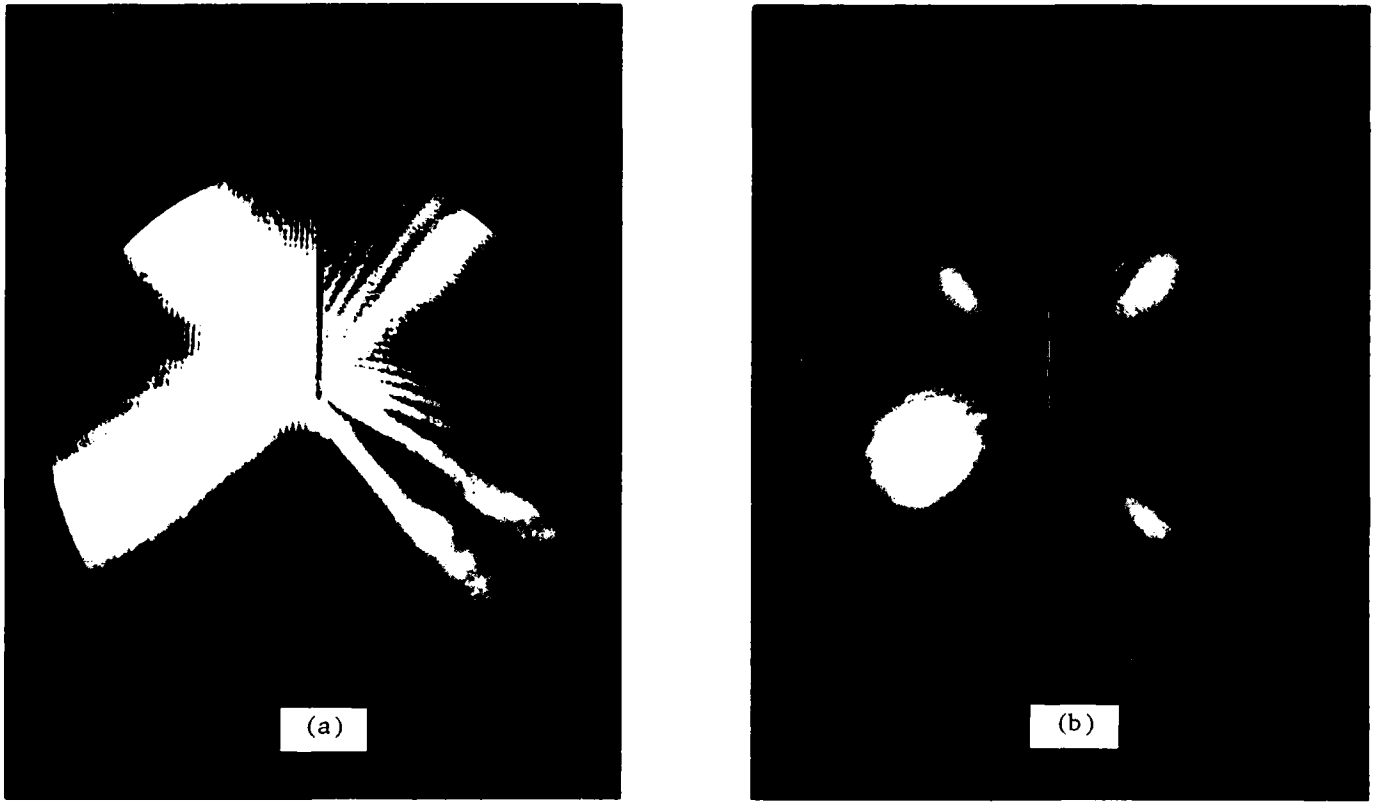

FIGURE 21. Transmission through a 0.056 in. thick steel plate at a frequency of 688.6 kHz, which is 4.17 times the classical coincidence frequency of the plate. The A_0 Lamb mode is excited at an angle of incidence of 40^{o}. Transducer AL680A which has a beam width of 1.0 in. was used. (a) A continuous beam strikes near the plate edge. (b) A 10 μs pulse is shown 25 μs after first contacting the plate.

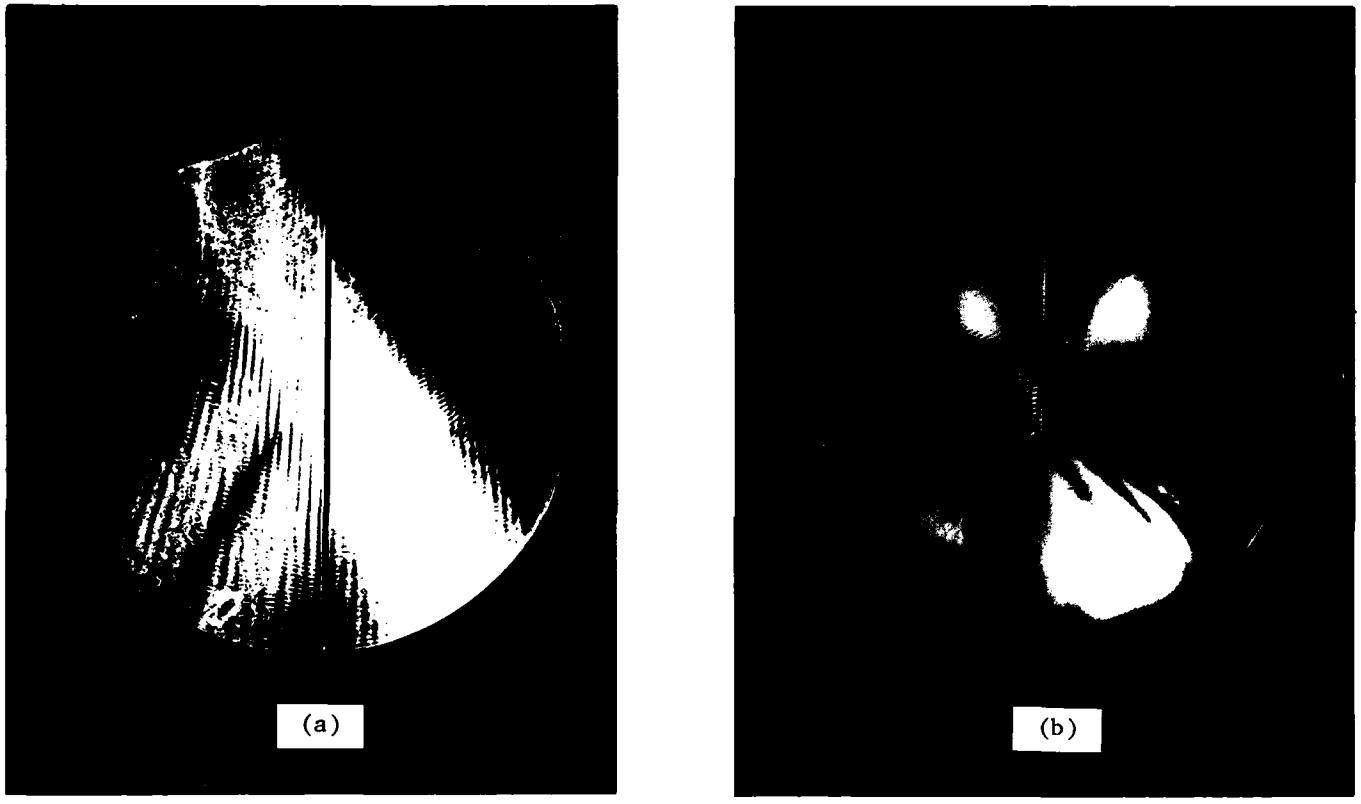

FIGURE 22. Transmission through a 0.023 in. thick steel plate at a frequency of 680.8 kHz, which is 1.685 times the classical coincidence frequency of the plate. The A_0 Lamb mode is excited at an angle of incidence of 60^{o}. Transducer AL680A which has a beam width of 1.0 in. was used. (a) A continuous beam strikes near the plate center. (b) A 10 μs pulse is shown 25 μs after first contacting the plate.

result in the reradiated pulse from the Lamb wave appearing on the opposite side of the plate-normal from the specularly reflected pulse. The time sequence of photographs in Figure 23 shows this. Note that, in Figure 23(c), the transmitted pulse is shifted upwards rather than downwards as before. In the remainder of the sequence one can see that the dark area representing the overlap of the specularly reflected pulse and the radiation from the Lamb wave is also angled in the opposite direction from the previous cases. Refer back to Figure 16, for example.

The sequence in Figure 24 shows a gradual increase in the angle of incidence. The phenomenon is quite obviously confined to a very narrow angular region as should be expected. It is also confined to a very narrow frequency range as is shown in the sequence in Figure 25.

4.5 Stroboscopic Observations

Under normal conditions, the schlieren system is operated in such a way that all data are collected using uniform, continuous acoustic beams as was shown in Figures 26. This is necessary to obtain accurate quantitative values for the magnitude of the peak of the resulting beam profile. It also possible to adjust the period of the flashing laser beam and the acoustic frequency so that a stroboscopic effect will result. A schlieren photograph showing this possiblity is shown in Figure 27. The photograph is, at first, somewhat misleading. The standing

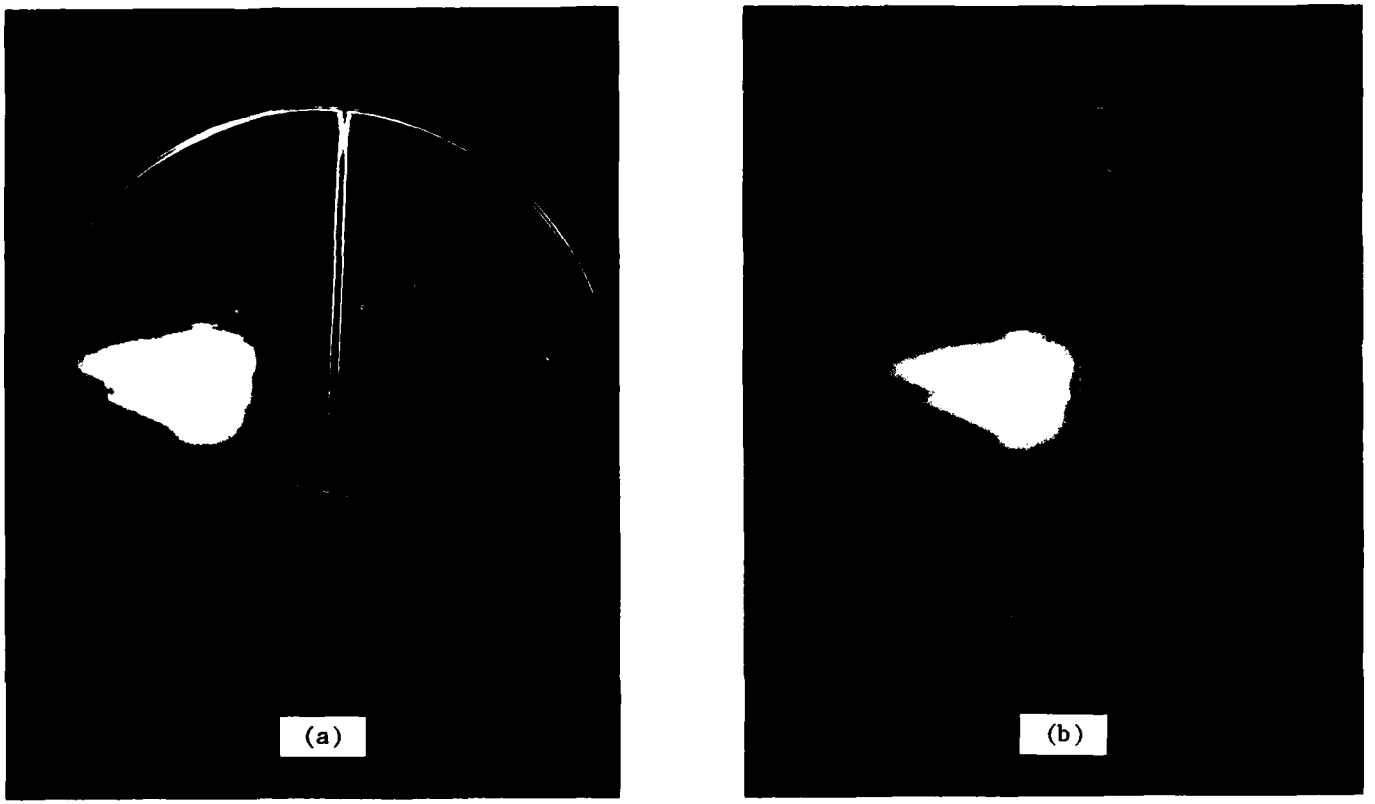

FIGURE 23. Transmission of a 10 μs acoustic pulse through a 0.032 in. thick aluminum plate at a frequency of 3.585 MHz, which is 12.96 times the classical coincidence frequency of the plate. The S_1 Lamb wave is excited at an angle of incidence of 4^o. Transducer AL680A which has a beam width of 1.0 in. was used. (a) At t_o = 0 μs. (b) At t_o + 10 μs.

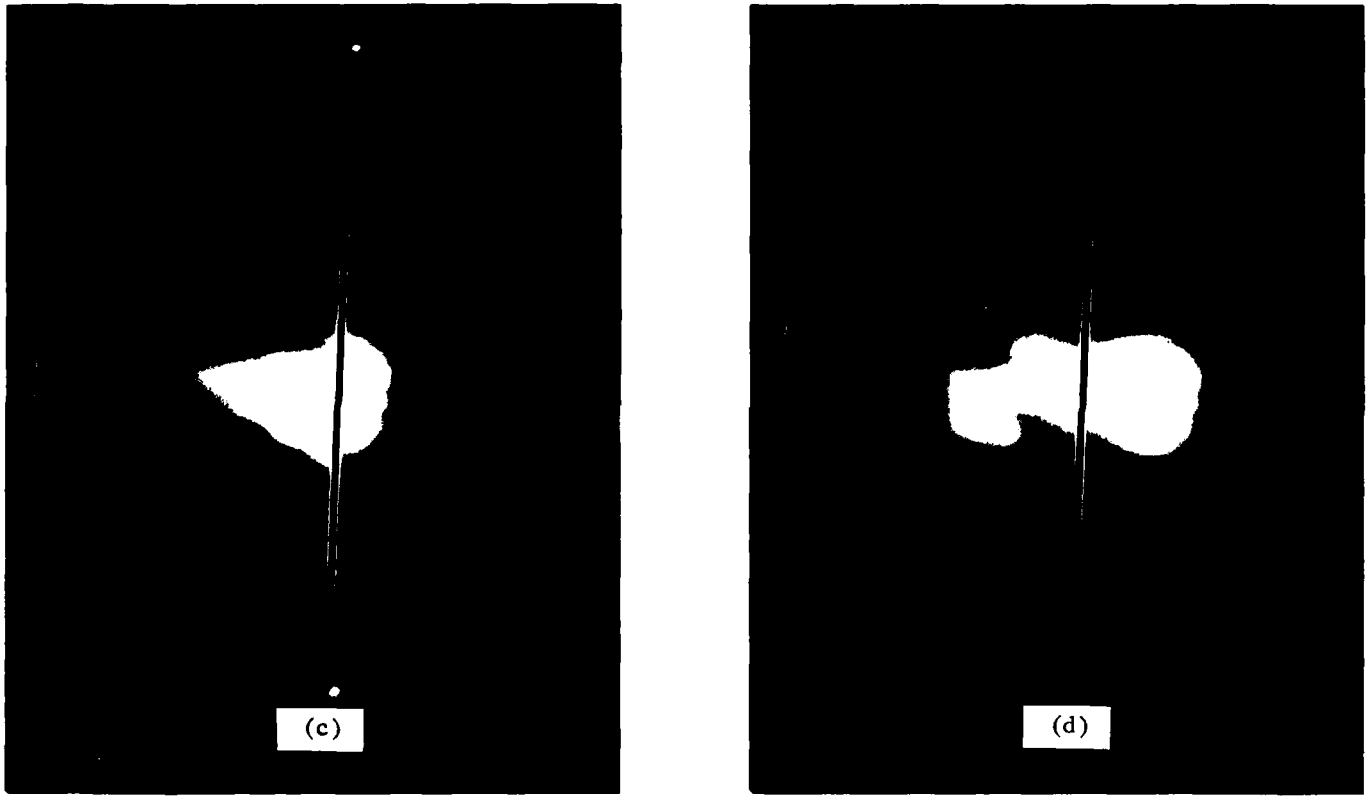

FIGURE 23. (cont.) (c) At t_o + 20 μs. (d) At t_o + 30 μs.

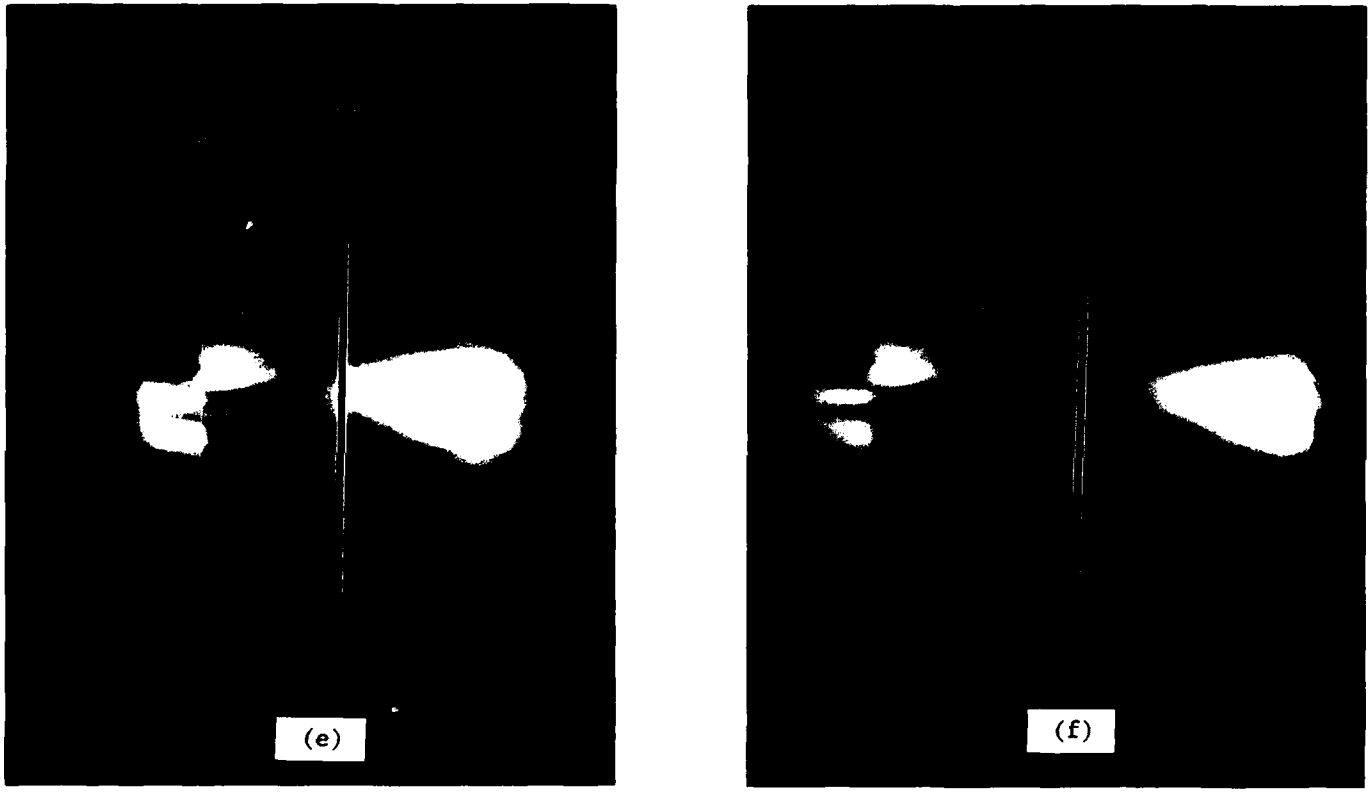

FIGURE 23. (cont.) (e) At t_o + 40 μs. (f) At t_o + 50 μs.

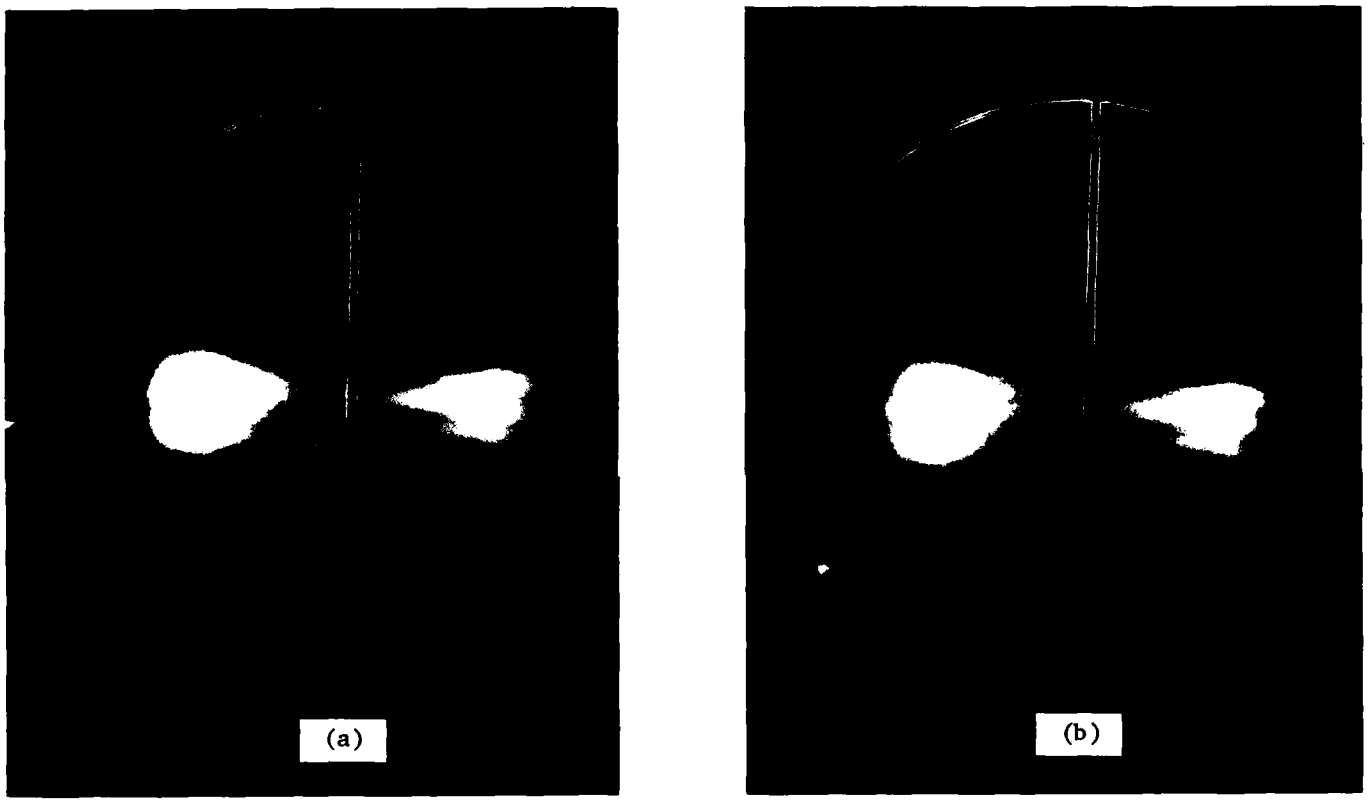

FIGURE 24. Transmission of a 10 μs acoustic pulse through a 0.032 in. thick aluminum plate at a frequency of 3.585 MHz, which is 12.96 times the classical coincidence frequency of the plate. Transducer AL680A which has a beam width of 1.0 in. was used. (a) At an angle of incidence of 0^{o}. (b) At 1^{o}.

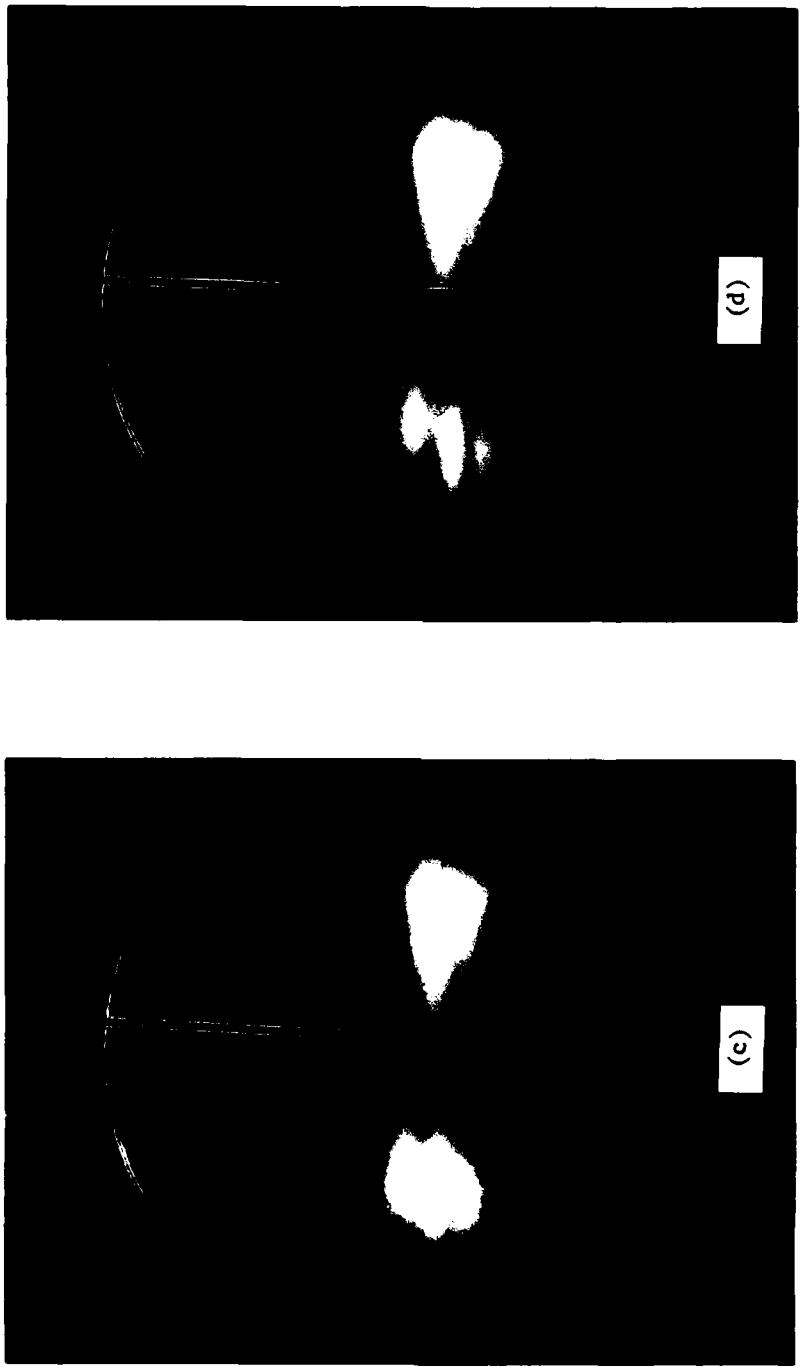

FIGURE 24. (cont.) (c) At 2°. (d) At 3°.

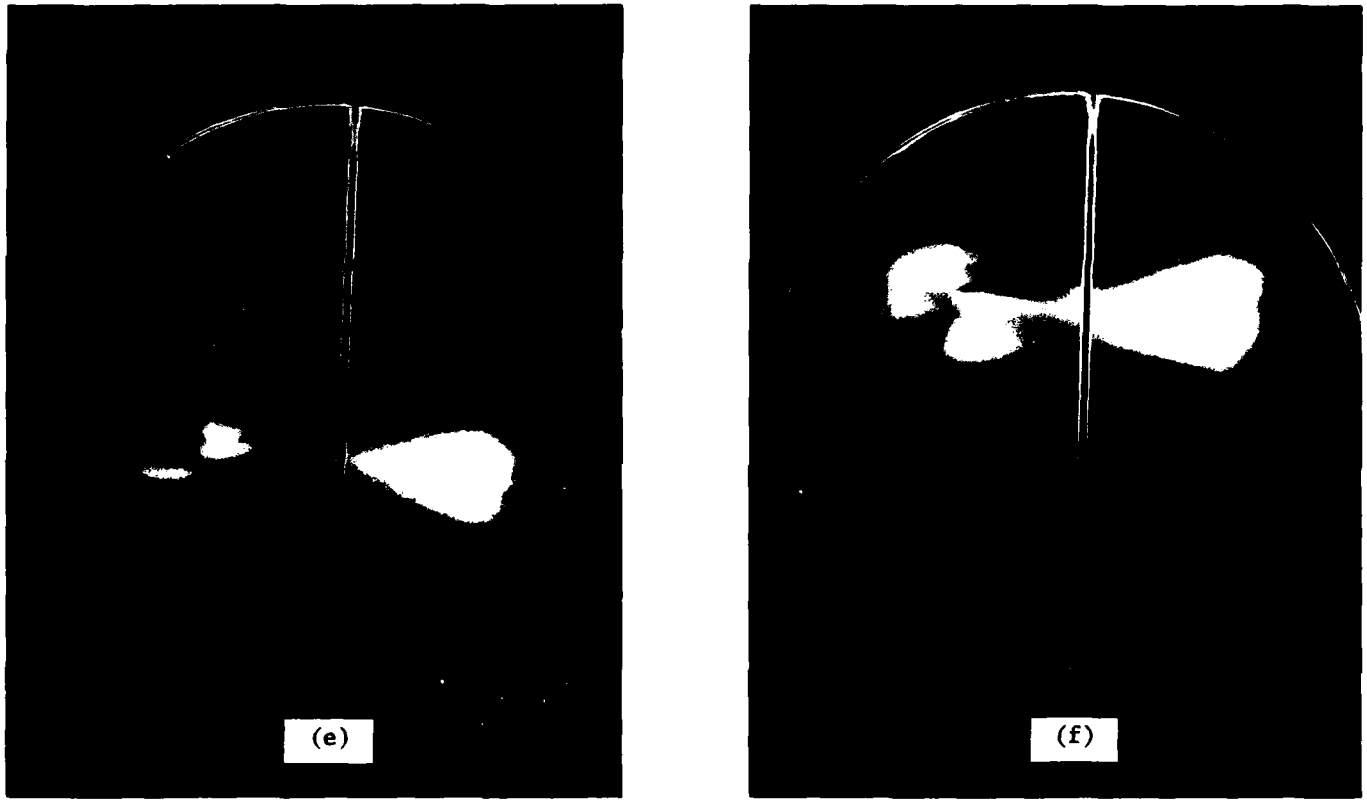

FIGURE 24. (cont.) (e) At 4^{o}. (f) At -4^{o}.

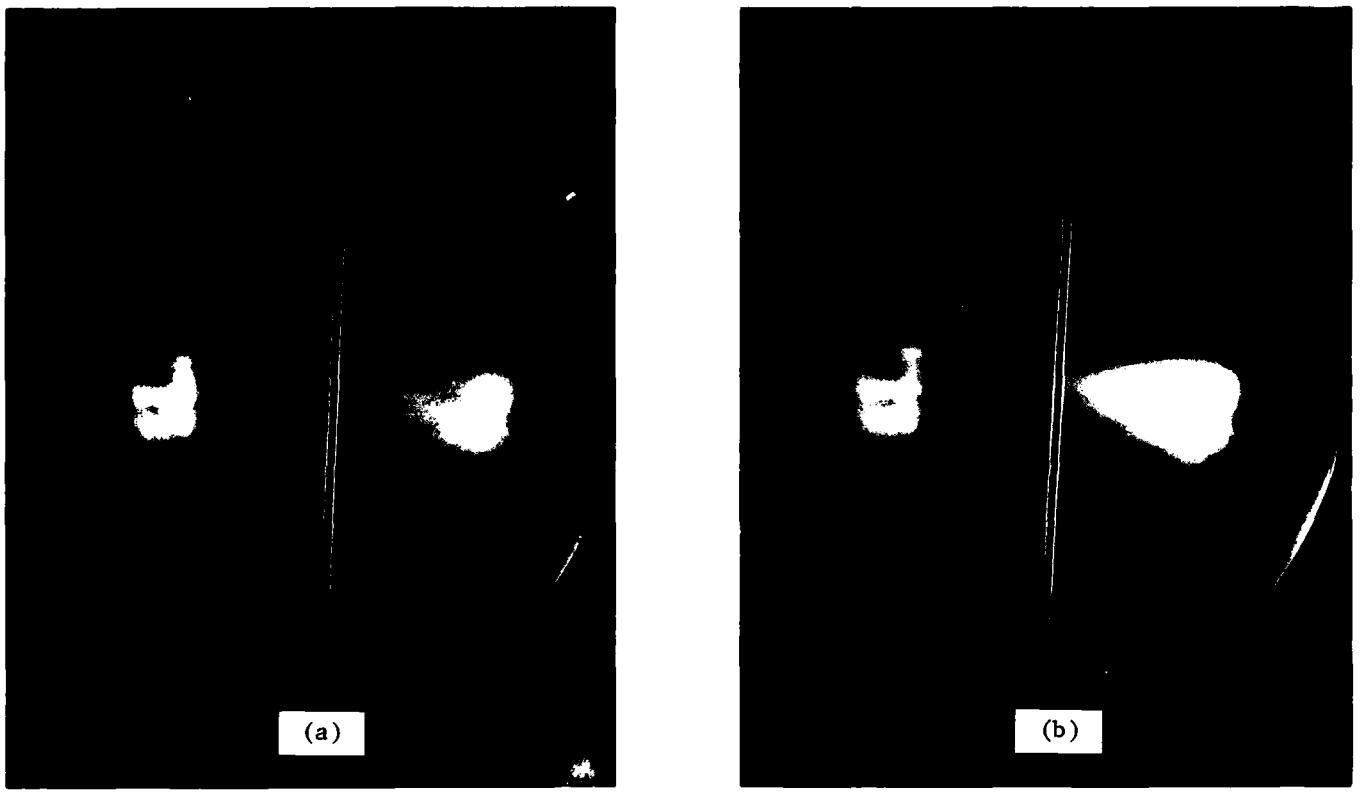

FIGURE 25. Transmission of a 10 μs acoustic pulse through a 0.032 in. thick aluminum plate at an angle of incidence of 4°. Transducer AL680A which has a beam width of 1.0 in. was used. (a) At a frequency of 3.504 MHz, which is 12.667 times the classical coincidence frequency of the plate. (b) At a frequency of 3.524 MHz, which is 12.739 times the classical coincidence frequency of the plate.

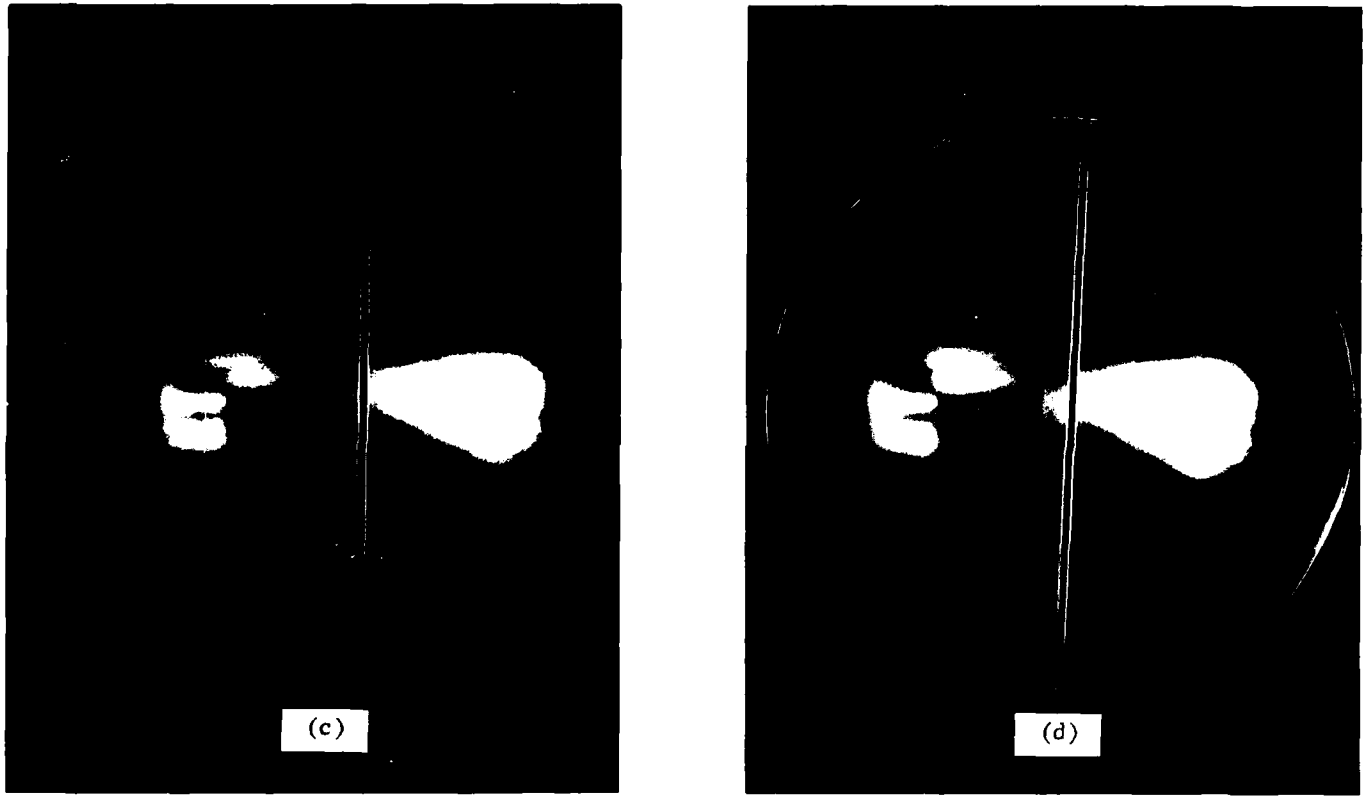

FIGURE 25. (cont.) (c) At a frequency of 3.544 MHz, which is 12.812 times the classical coincidence frequency of the plate. (d) At a frequency of 3.564 MHz, which is 12.884 times the classical coincidence frequency of the plate.

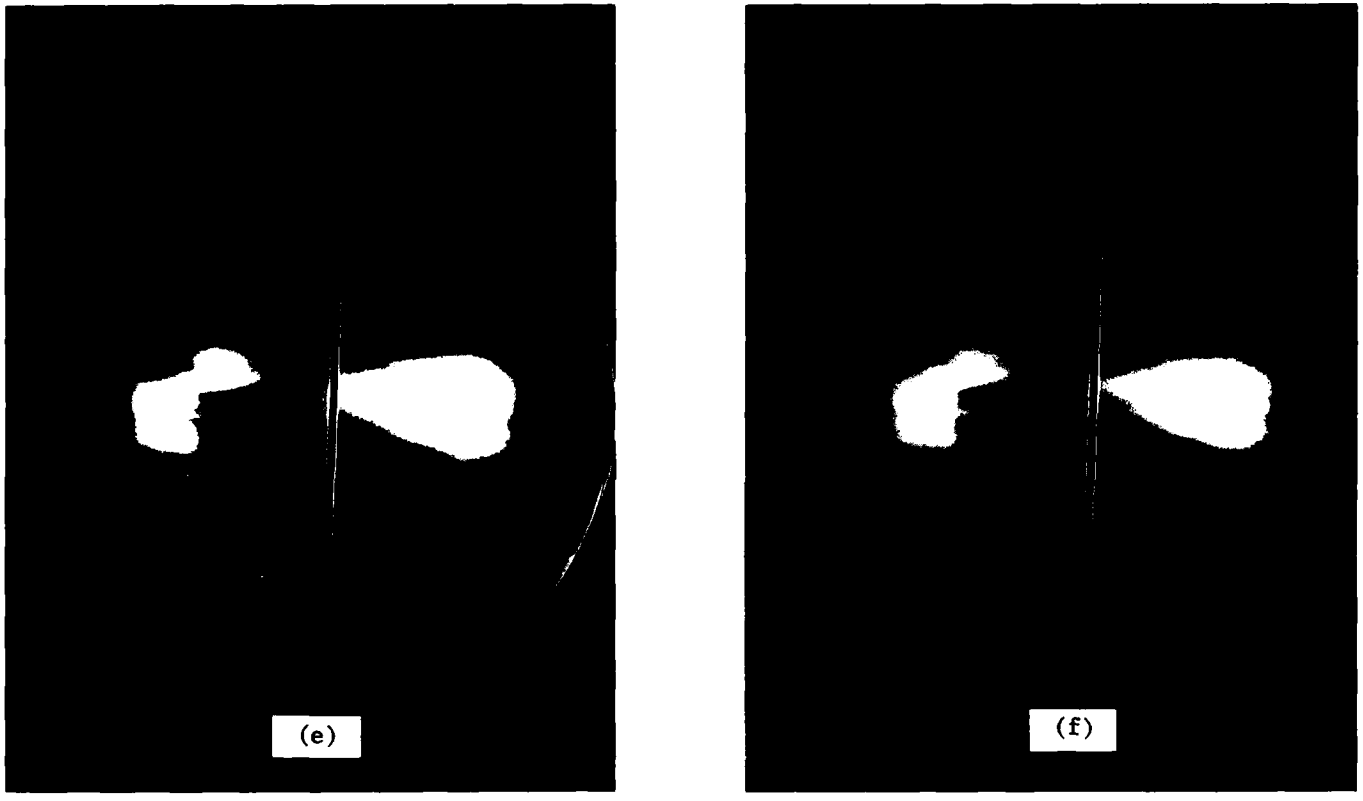

FIGURE 25. (cont.) (e) At a frequency of 3.604 MHz, which is 13.028 times the classical coincidence frequency of the plate. (f) At a frequency of 3.624 MHz, which is 13.101 times the classical coincidence frequency of the plate.

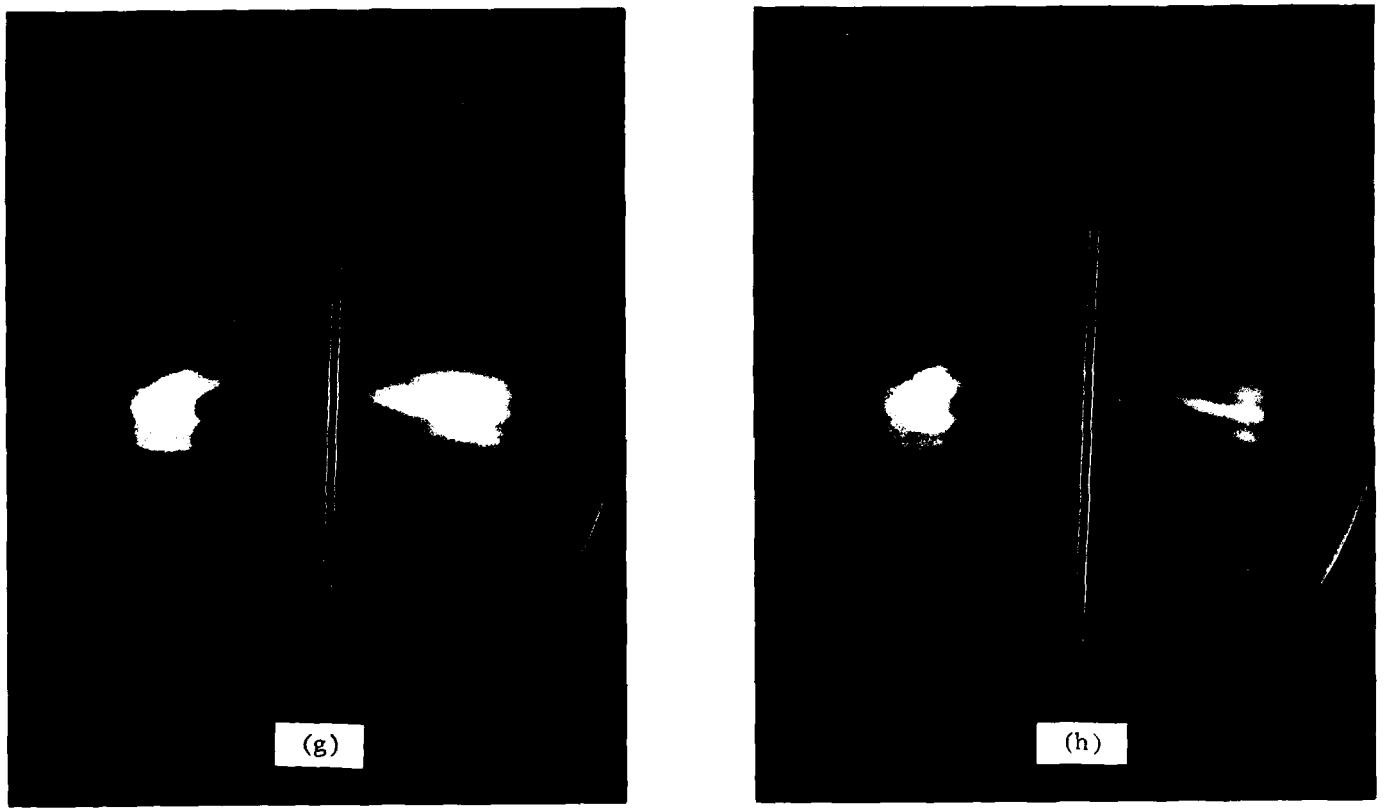

FIGURE 25. (cont.) (g) At a frequency of 3.644 MHz, which is 13.173 times the classical coincidence frequency of the plate. (h) At a frequency of 3.664 MHz, which is 13.245 times the classical coincidence frequency of the plate.

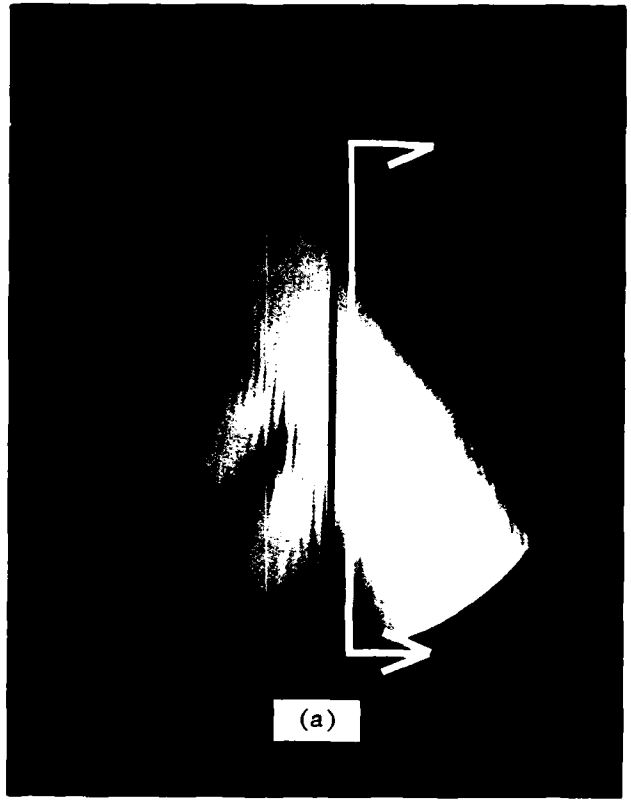

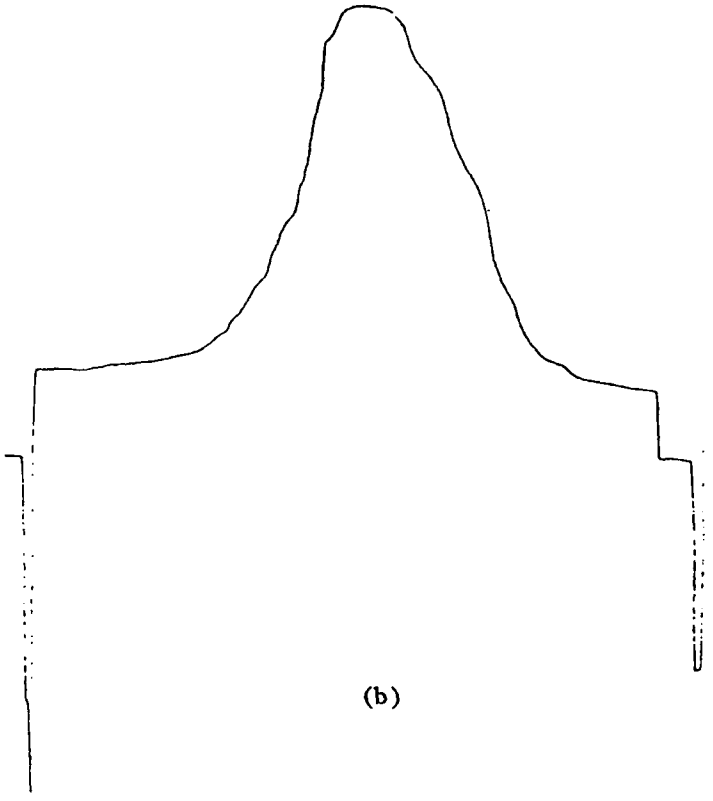

FIGURE 26. A 680.78 kHz acoustic beam incident on a 0.023 in. thick 304-stainless steel plate at an angle of 60^{o}. (a) Schlieren photograph showing the location of the quantitative data plot in white. (b) Profile of the transmitted beam.

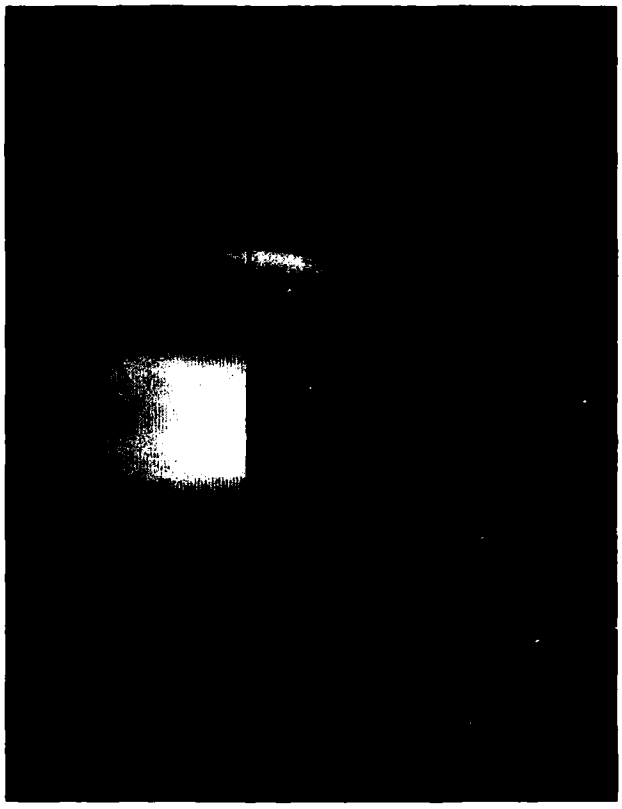

FIGURE 27. A 680 kHz acoustic beam is incident on a 0.023 in. thick 304-stainless steel plate at an angle of 10^{o}. The travelling wave fronts on the transmitted side of the plate are frozen by adjusting the stroboscopic repetition period to T_1 = 2 ms. The wave fronts appear stationary only at the discrete acoustic frequencies of 620.000 kHz, 620.250 kHz, 620.500 kHz, etc. Transducer AL680A was used which has a beam width of 1.0 in.

waves produced by the overlap of the incident and reflected beams are shown occurring parallel to the plate as would be expected and, in fact, has been observed in other photographs. There are also stationary wavefronts perpendicular to the plate, but these represent travelling waves in the plate which have been frozen by the stroboscopic effect. Proof that this is in fact the correct interpretation of the photograph is presented in Figure 28 and Table 3. For a fixed value of the strobe period, T_1 = 2 ms in this case, the wave fronts perpendicular to the plate appear to be stationary only at discrete acoustic frequencies. For the case shown, these discrete frequencies are spaced exactly 250 kHz apart, i.e., at $f = 1/2T_1$, which is to be expected since the distance between the fronts shown in the schlieren images is $\lambda/2$.

The stroboscopic schlieren effect lends itself to many applications. The distance between the travelling wave fronts that appear perpendicular to the plate is determined by the incidence angle and the wavelength in the surrounding medium. Thus, given the acoustic frequency and the angle of incidence, the velocity in the surrounding medium can be found from the distance between these wavefronts ($c = 2fd \sin\theta$). In some applications, the angle of incidence is difficult to determine; the stroboscopic schlieren method could prove useful in that case. A valuable application for the current schlieren system would be as a means to obtain a very accurate calibration of the linear

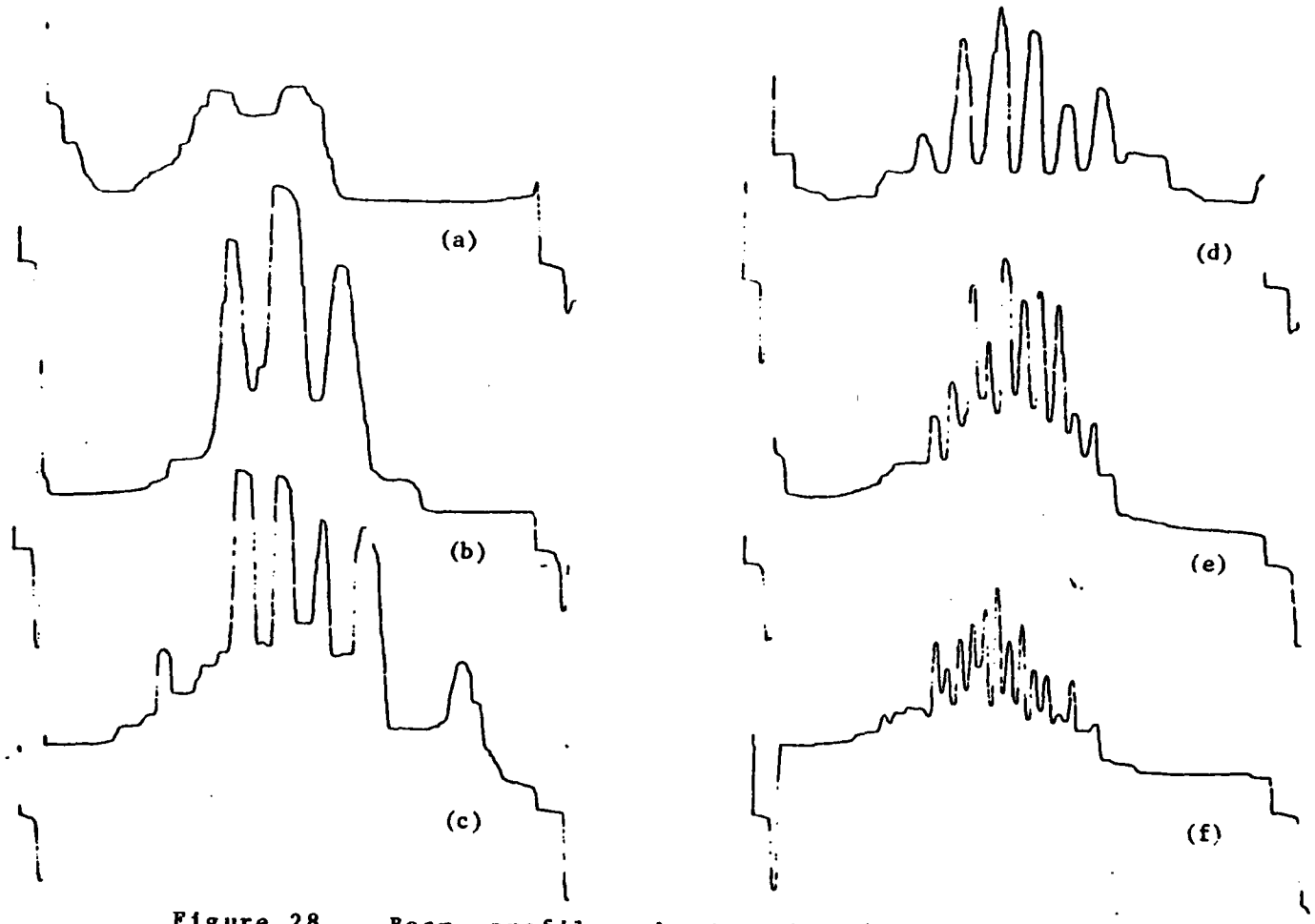

Figure 28. Beam profiles showing the $\lambda/2$ spacing of the travelling wave fronts which occur perpendicular to the plate as was shown in Figure 27. See Table 3 for comparison between the theoretical and experimental spacings. (a) 194 kHz at 10^{o}. (b) 194 kHz at 20^{o}. (c) 194 kHz at 30^{o}. (d) 620 kHz at 10^{o}. (e) 620 kHz at 20^{o}. (f) 620 kHz at 30^{o}.

TABLE 3

Acoustic Frequencies Producing the Stroboscopic Effect

Freq.	Ω	Angle	$\sin\theta_i$	λ	$\lambda/2\sin\theta_i$	Spacing
194kHz	0.48	10°	0.177	0.309"	0.891"	0.565"
194	0.48	20	0.342	0.309	0.459	0.436
194	0.48	30	0.500	0.309	0.314	0.320
620	1.53	10	0.177	0.097	0.279	0.280
620	1.53	20	0.342	0.097	0.142	0.141
620	1.53	30	0.500	0.097	0.097	0.099

distances depicted on the photographs and on the dataline plots such as were shown in Figures 26 and 28. This calibration is normally quite difficult to obtain accurately and is necessary for the investigation of the beam shift phenomenon, etc.

4.6 Examples

The standing wave pattern shown in Figure 19 was produced by the reflection of the S_0 Lamb wave from the free edge of the plate. The spacing between the wave fronts agrees quite well with the value of one-half the trace wave length at the plate surface. This can be checked in two ways. First, the diameter of the circular image corresponds to the aperture of the optical beam which is known to be 5 in. Thus, the scaling factor of the figure is 1:1.69 and the spacing is 0.0485 in. The theoretical spacing can be calculated from the measured angle of incidence, 17.5°, and frequency, 2.125 MHz. Hence,

$$\lambda/2 = \lambda_w/2 \sin\theta_i = c_w/2f \sin\theta_i$$
$$= 0.0469 \text{ in.} \qquad (62)$$

Similar analysis of more complex experimental geometries is also possible. Figure 29 shows an experimental model with a short 10 μs pulse of 900 kHz sound incident on it from the lower left. The pulse struck the flat bottom of the model just to the left of the field of view approximately 40 μs before the photograph was taken. The surface

FIGURE 29. Example of the detail of analysis possible with stroboscopic schlieren techniques. A 10 μs pulse of 900 kHz sound is shown incident on the bottom of a curved structure [83].

wave travelling along the curved bottom radiates out into the medium as is shown by the curved sound field below the model. When the plate wave strikes the prow, it radiates out into the medium in the forward direction, and also a portion of it reflects back in the plate creating a standing wave evidenced by the wave fronts which appear in the surrounding medium perpendicular to the surface of the model.

The distance between the wave fronts in the forward radiated field correspond closely to the expected 0.067 in. wavelength of the 900 kHz signal. The spacing between the wave front perpendicular to the surface, however, are considerably larger than what would be expected based on the measurements previously presented for flat plates. The actual velocity of compressional waves in the aluminum plate used for the bottom of the model was measured in the Applied Research Laboratory's Non-Destructive Testing Facility and was found to be 6861 m/s. This was considerably higher than the 5400 m/s velocity found for all of the aluminum alloys used in the investigations of flat plates. This would explain much of the discrepancy in the spacing of the perpendicular wave fronts.

4.7 Welded Plates

An important practical question in many engineering applications concerns the effect of structural welds on the reflected and transmitted sound fields. In order to gain

further insight into this question several models were constructed with different types of joints. A comparison of ribbed plates is shown in Figures 30 to 32. In Figure 30, two models are shown at identical experimental conditions. The model shown on the left was constructed by welding the rib into place; the model on the right was machined to the same dimensions from a single block of material. As can be seen, the structure of the transmitted sound field is quite similar, while that of the reflected field is not at all the same. The frequency and angle were chosen such that the A_0 Lamb mode was excited in the plate. The reflected field in Figure 30 (b) has the same characteristics as exhibited by beams reflected from plain flat plates near a Lamb mode; i.e., an overlap of a specular reflected field and a reradiated field with the dark band due to the 180° difference in phase between the two fields. The welded plate in Figure 30 (a), on the other hand, is quite dissimilar. It is evident that the weld bead has had a considerable effect on the flexural wave as it travelled down the plate. A similar comparison is shown in Figure 31. Although the same A_0 Lamb mode has been excited, the difference between the two reflected fields is not nearly as sharp.

Figure 32 has been obtained using a stroboscopic effect and can be analyzed in somewhat more detail. The diameter of the optical aperture, the thickness of the plate and the spacing between the wavefronts in the

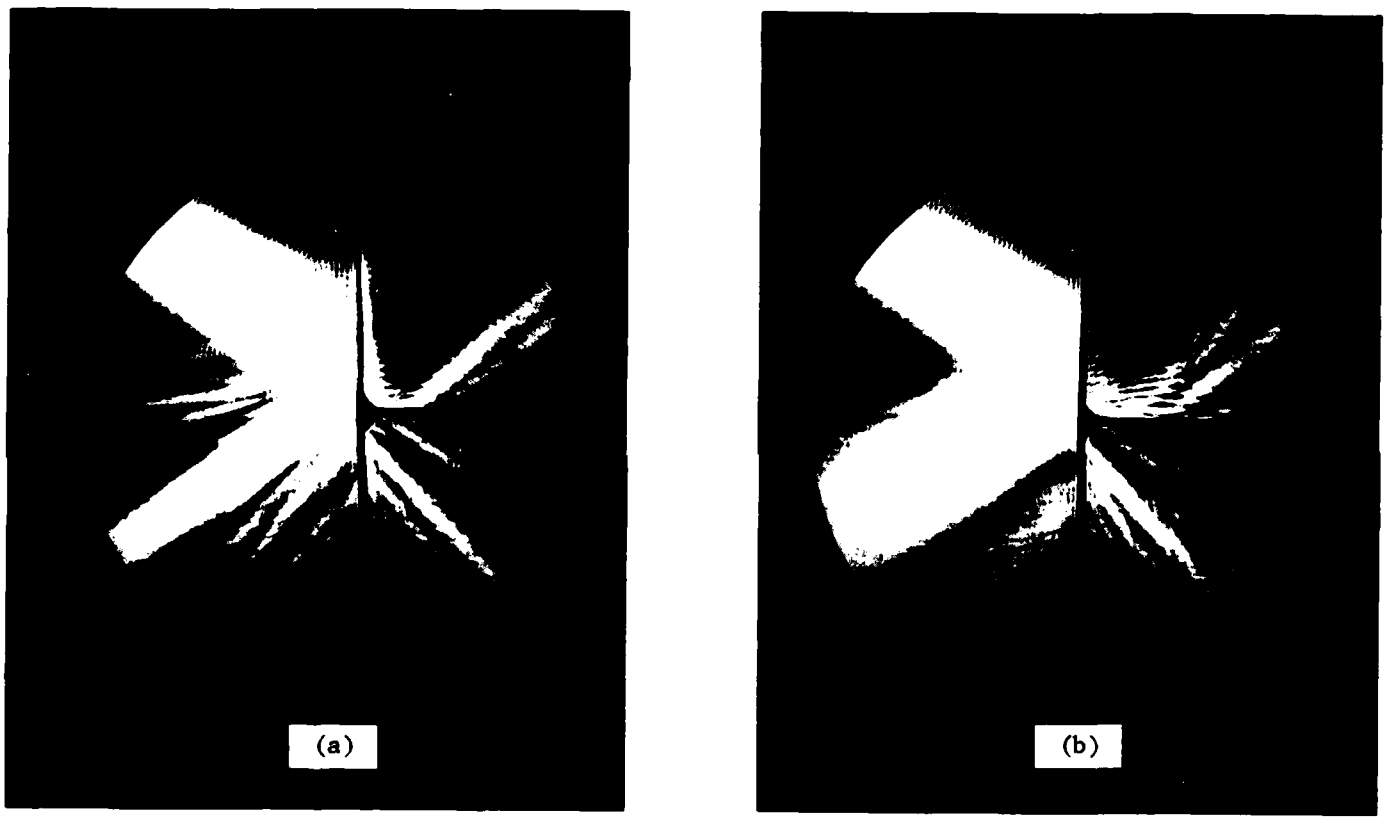

FIGURE 30. Acoustic beam incident on a 0.056 in. thick 304-stainless steel plate at an angle of 31.5°. The A_0 Lamb wave is excited. (a) Welded Plate. (b) Machined Plate.

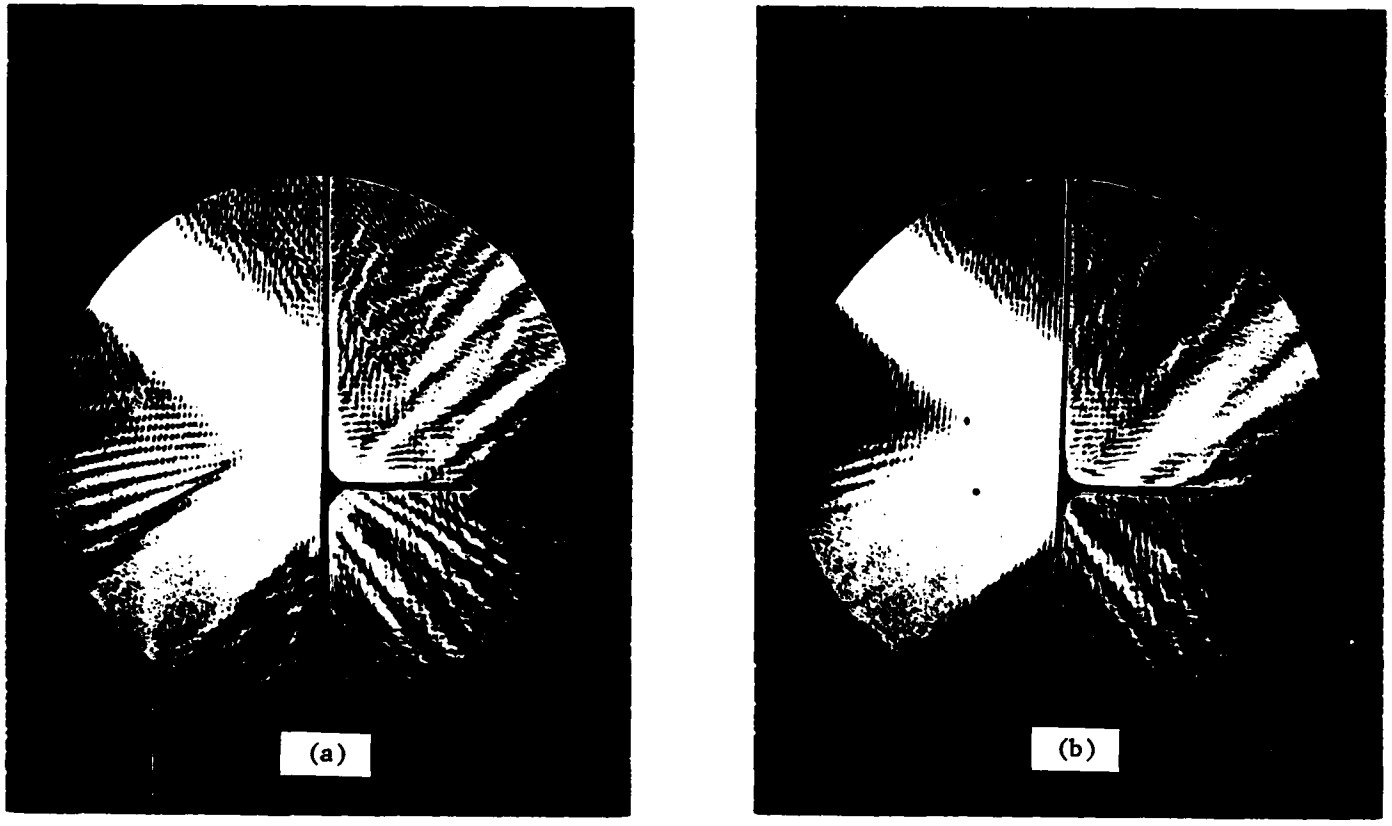

FIGURE 31. Acoustic beam incident on a 0.056 in. thick 304-stainless steel plate at an angle of 38°. The A_0 Lamb wave is excited. (a) Welded Plate. (b) Machined Plate.

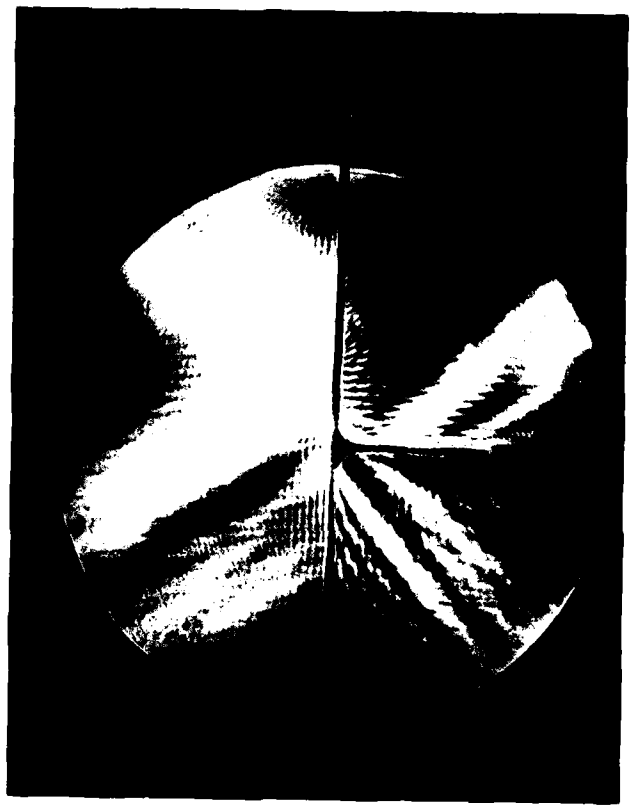

FIGURE 32. Acoustic beam incident of a 0.056 in. thick 304-stainless steel plate with a machined joint at an angle of 40^{o}. The A_0 Lamb wave is excited at a frequency of 622 kHz.

incident beam all provide means of determining the linear scaling factor of the figure and all agree to within 3 percent of each other. Thus, the actual spacing between other features of interest can be obtained quite reliably. The spacing between the wavefronts which occur parallel to the plate on the incident side are due to the standing waves formed by the superposition of the incident and reflected waves. At 622 kHz, the wavelength of the incident sound beam should be 2.39 mm and, at 40°, the spacing between these standing wavefronts should be 3.12 mm (i.e., $\lambda/\cos\theta$). The actual measured spacing is 3.1 mm. The A_0 Lamb mode radiates sound from the plate in such a way that wavefronts are formed perpendicular to the plate and have a spacing $\lambda/\sin\theta$. These are seen most clearly on the right side of the plate just above the rib. The measured spacing between these wavefronts is 3.6 mm which compares quite favorably with the computed spacing of 3.72 mm. The wavefronts evident below and perpendicular to the rib exhibit the same measured spacing, 3.6 mm; it is thus apparent that the same A_0 Lamb mode has been excited in the rib as was excited in the plate.

To investigate this more thoroughly, a set of models were constructed by butt-joining pieces of sheet steel edge-to-edge, by several different methods. Figure 33 shows a reference photograph of a solid plate having no joint together with three plates of the same material but joined by soft soldering, by silver soldering, and by

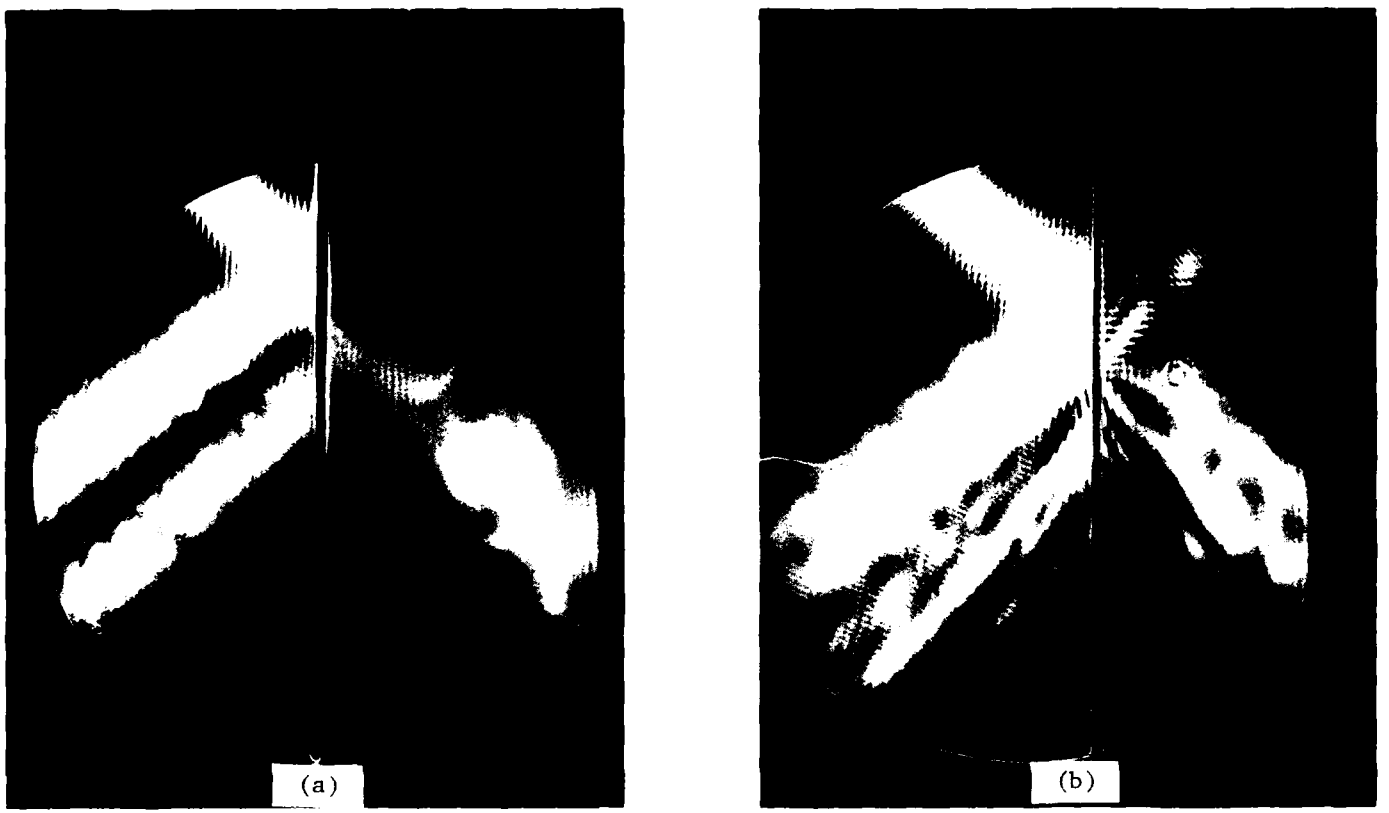

FIGURE 33. Transmission of an acoustic beam through a 0.056 in. thick steel plate at a frequency of 679 kHz, which is 4.12 times the classical coincidence frequency of the plate. (a) Solid Plate. (b) Soft Solder. In all cases the joint line is perpendicular to the plane of the photograph and at the center of the incident beam.

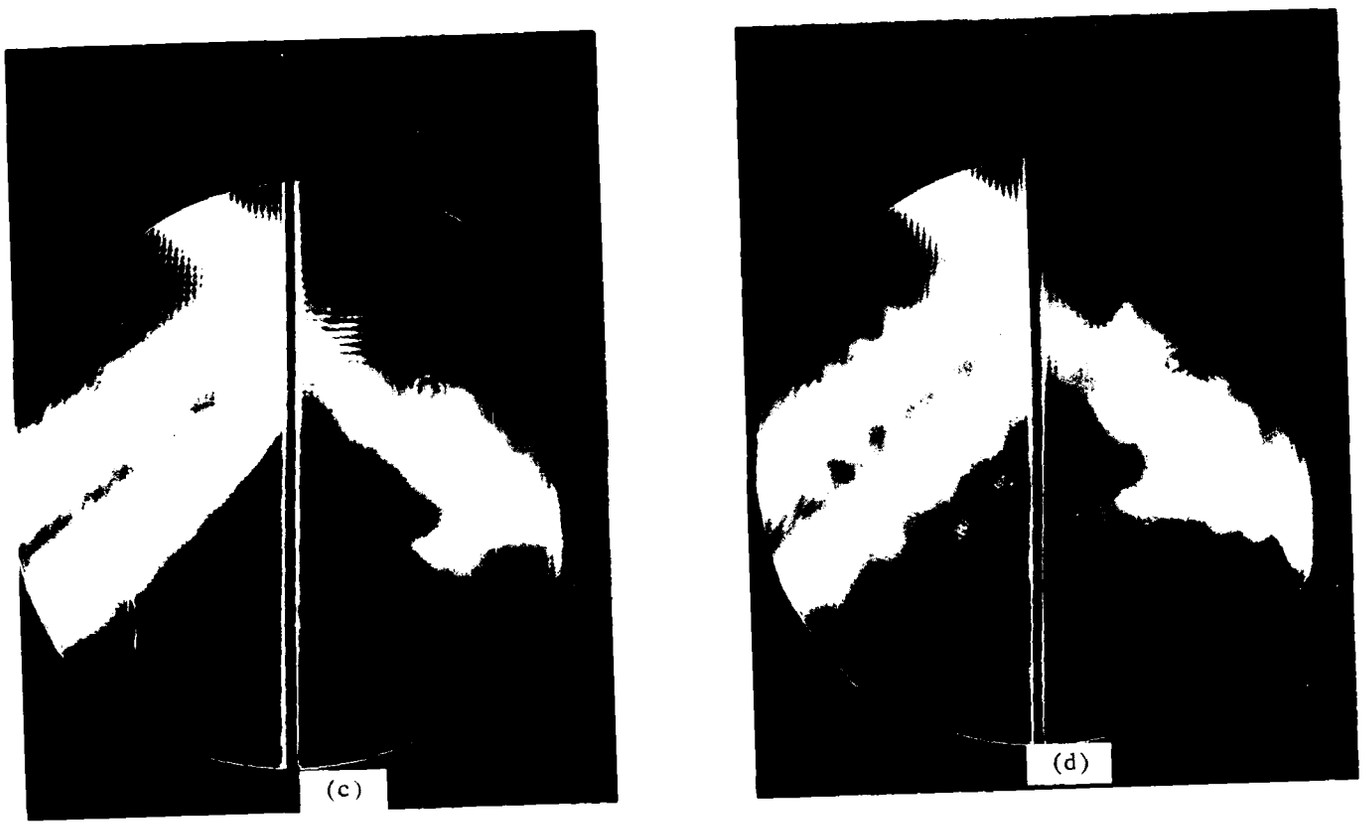

FIGURE 33. (continued) (c) Silver Solder. (d) Weld.

welding, respectively. The soft solder, Figure 33(b), shows a beam being radiated into the upper right quadrant of the photograph, just as one would expect from the free edge of a plate (see Figure 20, for example). The silver solder, which forms a stiffer joint, shows a reduction in the intensity of this particular beam, and the final photograph of Figure 33 shows that the welded plate, which has an even higher stiffness, exhibits no evidence of a beam in the upper right quadrant. The correlation of this sequence of photographs with the stiffness of the joint and the resulting similarities with the previous photographs showing the effects of free edges is quite remarkable.

CHAPTER 5

QUANTITATIVE RESULTS

5.1 Benchmarks

The two benchmarks against which the success of this experimental method must be judged are the previous quantitative schlieren techniques by Smirnov et al. [84] which used densitometry methods and by Stanic [81] which used video sampling methods. Densitometry requires careful preparation of photographic negatives and their accompanying calibration curves. This is a slow tedious task since the results are highly sensitive to the timing, temperature, etc., of the photographic development process. Spectroscopists, however, have raised densitometry to a high art form and the results of Smirnov et al. reflect this. They present a table of 25 data points for the transmission through plates which demonstrate an agreement with theory with an error of only 6 percent.

The video sampling method used by Stanic (and in this investigation) should be capable of the same degree of accuracy obtained by Smirnov, if not greater. The calibration procedures are nearly identical, except that it is a

vidicon tube which must be calibrated rather than a shipment of photographic supplies. This should be an advantage over the densitometry method. The results published by Stanic do not reflect this expectation. He gives no estimation of error, but one can easily be found by performing a regression analysis on the 85 data points he presents in Reference [81]. Data from Figure 36 of Reference [81] is replotted in Figure 34 with the classical and Mindlin theories added for comparison. Note that because no data is included near the region of 0^{o} to 30^{o} that the inclusion or omission of the longitudinal wave term developed in Section 2.3.3 is immaterial in the error calculation. These data can thus be regressed onto the Mindlin curve (known to be more accurate than the classical theory in this frequency range) and the RMS value of the residuals gives a value of 75 percent for the standard error of estimate, which does not compare favorably with the 6 percent error found by Smirnov. Even more disturbing is the fact that, when the data is regressed onto the classical curve, the standard error improves slightly, indicating that the data does not support the Mindlin theory as well as it does the classical.

The remainder of this chapter will be devoted to an attempt to vindicate both the video sampling method of quantizing schlieren data as well as the Mindlin plate theory. Additionally, data will be presented which demonstrate the effects of the longitudinal wave term. It will

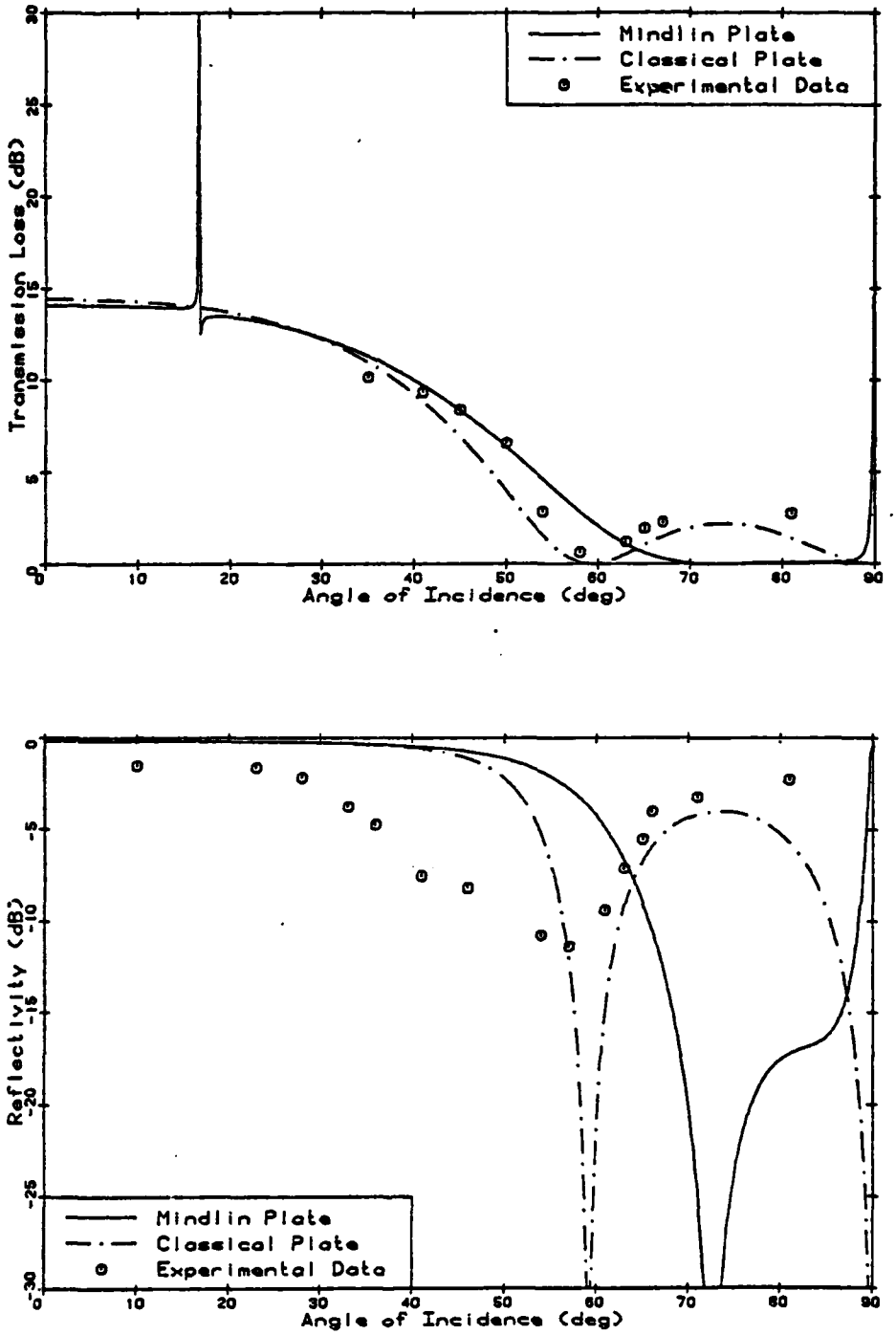

FIGURE 34. Data from Figure 36 of Stanic [81] with theoretical curves added. (a) Transmission Loss and (b) Reflectivity for a 3.38 MHz (Ω = 1.35) acoustic beam incident of a 0.004 in. thick steel plate.

also be shown that not only is the video method capable of the same 5-6 percent level of accuracy found by the densitometry method but that the schlieren system developed at the Applied Research Laboratory is able to maintain that level of accuracy at frequencies as low as 179 kHz.

5.2 Simple Plates

Extensive transmission data were collected on simple flat metal plates. Seven thicknesses of sheet aluminum and six transducers with different resonance frequencies and accompanying higher harmonics provided an effective frequency range from 0.5 to 110 times the classical coincidence frequency of the plate. Consequently, it was possible to plot transmission loss curves as a function of the angle of incidence for nearly 100 values of the frequency parameter, Ω. Each of these contained approximately 70 data points spaced at one-degree increments ranging from normal incidence, 0^{o}, to about 70^{o}, at which point the edge effects of the plate rendered interpretation of the data difficult. Although most of the data were obtained using aluminum plates, representative data were also obtained for 304-stainless steel plates. The angular locations of the peaks were then summarized in a single curve (for aluminum) which represents the dispersion of the sound velocity in the plate.

5.3 Transmission Loss Curves

Transmission loss curves were obtained by comparing the level of the transmitted sound to the level of the incident sound beam at the same physical location in the tank by simply removing the plate to obtain a reference level. This technique removed the necessity of obtaining calibration curves for a large network of points across the vidicon tube. This would normally have to be done since the response falls off near the edges of the tube. Angular data were then obtained by rotating the sample about its vertical axis, which can be visualized most easily by referring to Figure 6.

Figures 35 and 36 show representative curves for aluminum and stainless steel, respectively, at frequencies below coincidence. Also included are the theoretical predictions based on the classical plate theory and on the augmented Mindlin theory developed in Section 2.3.3. At a frequency as low as this, the two theories agree very closely, as would be expected, with the exception of the spike at 16° produced by the longitudinal wave component. This phenomenon occurs at such a narrow angular range that the experimental data do not follow the sharp rise. Still it is interesting to note that the data do reflect the existence of some anomaly occurring at this point. Since the existence of the longitudinal wave is almost universally ignored, the appearance of it at this low

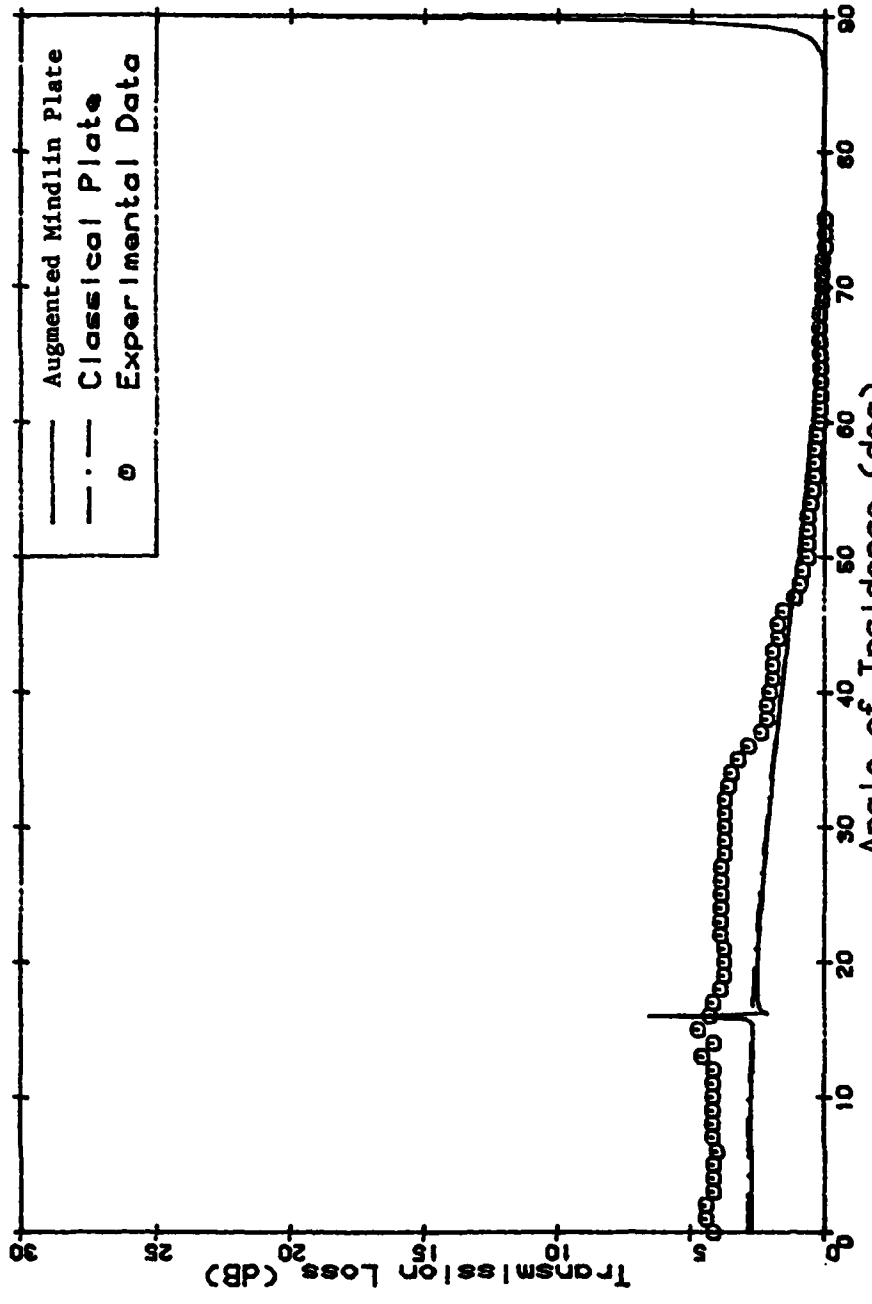

FIGURE 35. Transmission loss as a function of angle of incidence for a 0.020 in. thick aluminum plate at a frequency of 335 kHz, which is 0.75 times the classical coincidence frequency of the plate.

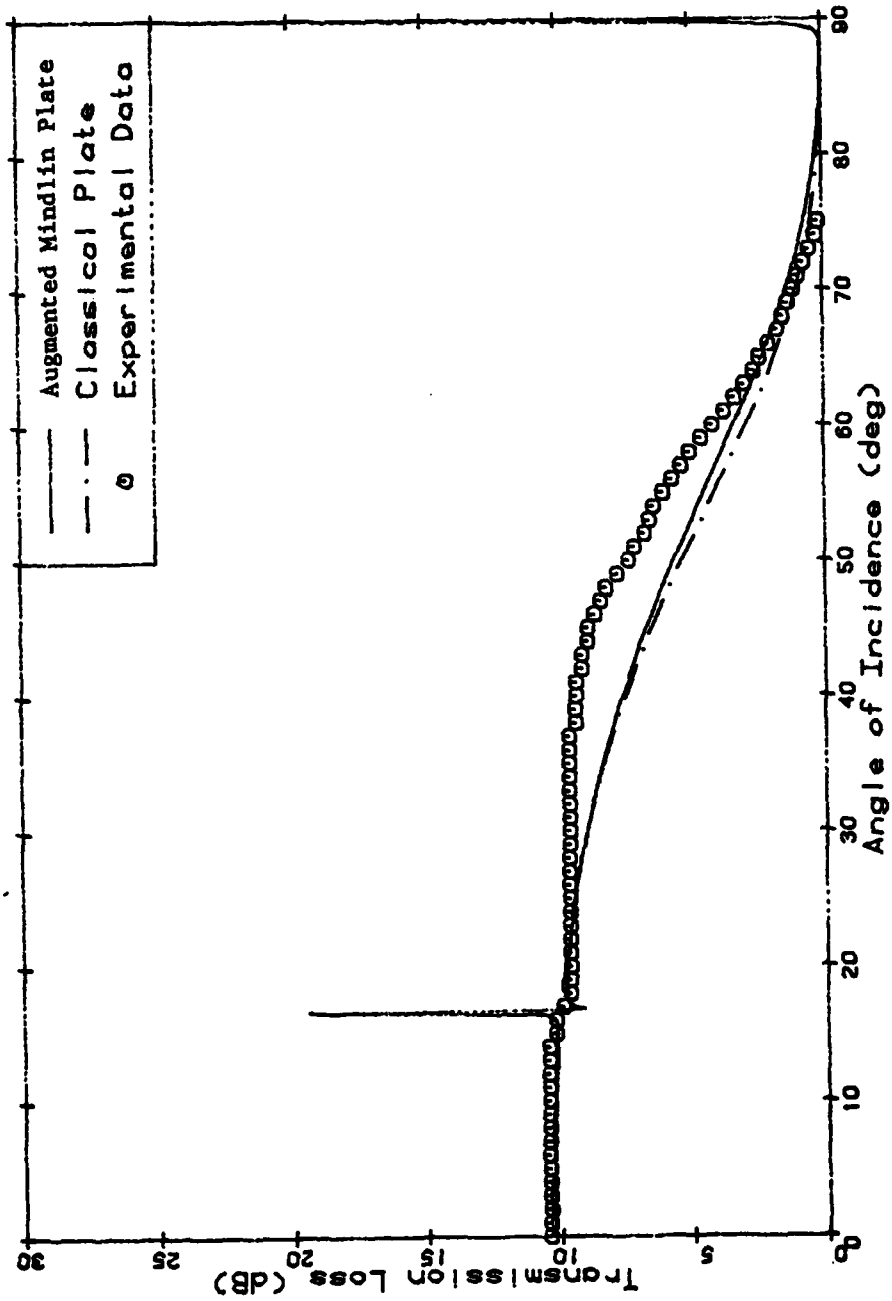

FIGURE 36. Transmission loss as a function of angle of incidence for a 0.023 in. thick aluminum plate at a frequency of 335 kHz, which is 0.83 times the classical coincidence frequency of the plate.

frequency would be an important result. A system with a more narrow angular resolution could well demonstrate the full effect of this phenomenon.

The presence of the peak in question becomes quite clear at $\Omega = 1.5$ as is shown in Figure 37 for aluminum and at $\Omega = 2.5$ as is shown in Figure 38. As the frequency increases, the peak broadens and the data is more able to accurately reflect the amplitude as is shown in Figure 39 for $\Omega = 4.73$. Here, the limited dynamic range of the experimental system becomes more noticeable. The background light level appears on the figure as an upper cutoff at about 15 dB. This level is dependent on the power level which the transducer is capable of delivering into the water, as well as the alignment of the schlieren apparatus; the best dynamic range ever achieved was 20 dB. Figure 40 for steel at $\Omega = 5.28$ shows the problem even more clearly. This truncation effect will appear in most of the remaining data curves which will be presented herein. It should also be noted that the addition of the longitudinal wave term, even though it accurately predicts the shape of the peak at 16°, is beginning to have a detrimental effect on the theoretical predictions near the grazing angle. This will also become more noticeable as the frequency parameter is increased.

At $\Omega = 6$, a third peak produced by the A_1 Lamb mode appears at normal incidence and slowly moves outward as the frequency parameter is increased. Simultaneously, the

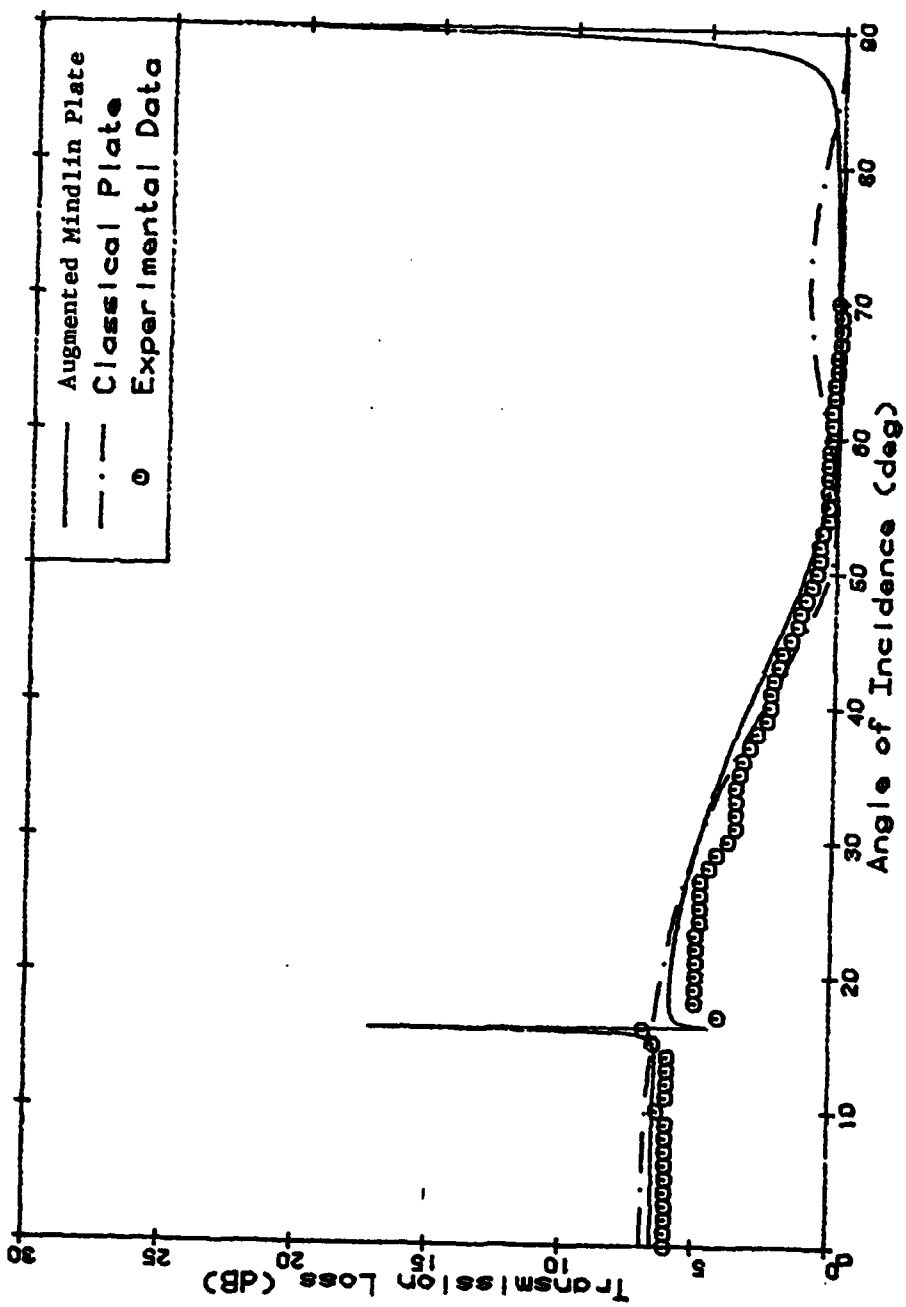

FIGURE 37. Transmission loss as a function of angle of incidence for a 0.020 in. thick aluminum plate at a frequency of 687 kHz, which is 1.53 times the classical coincidence frequency of the plate.

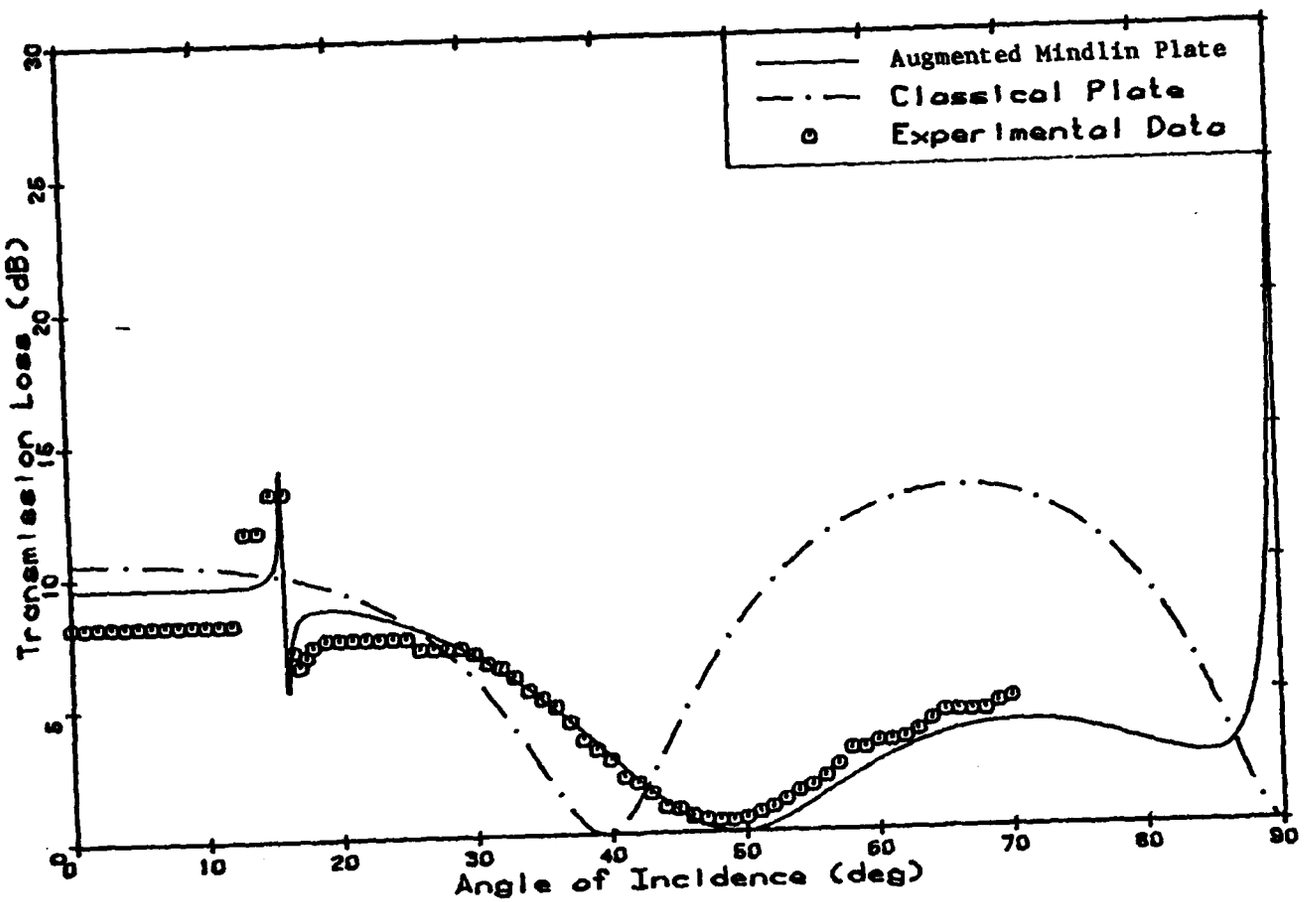

FIGURE 38. Transmission loss as a function of angle of incidence for a 0.032 in. thick aluminum plate at a frequency of 688 kHz, which is 2.49 times the classical coincidence frequency of the plate.

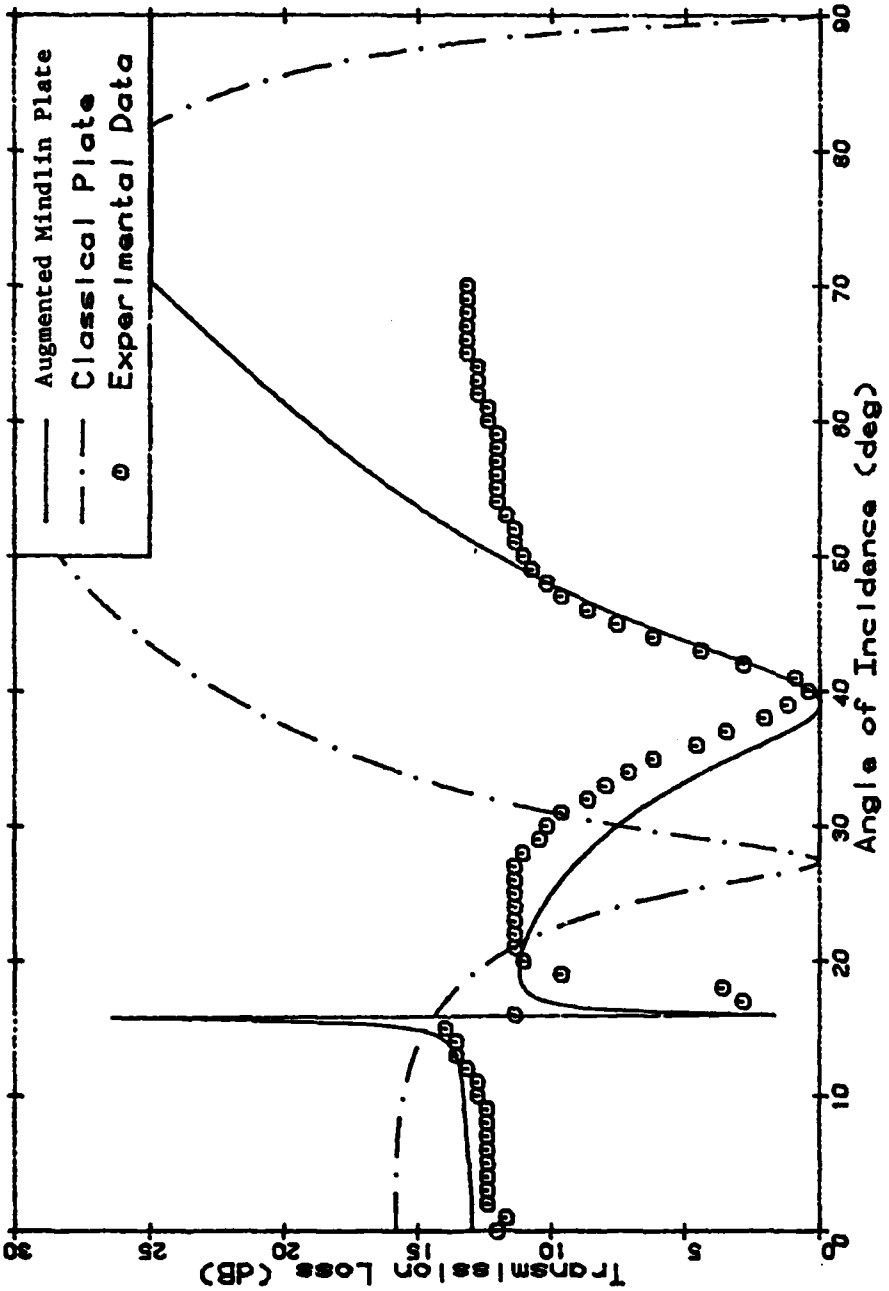

FIGURE 39. Transmission loss as a function of angle of incidence for a 0.020 in. thick aluminum plate at a frequency of 2.127 MHz, which is 4.73 times the classical coincidence frequency of the plate.

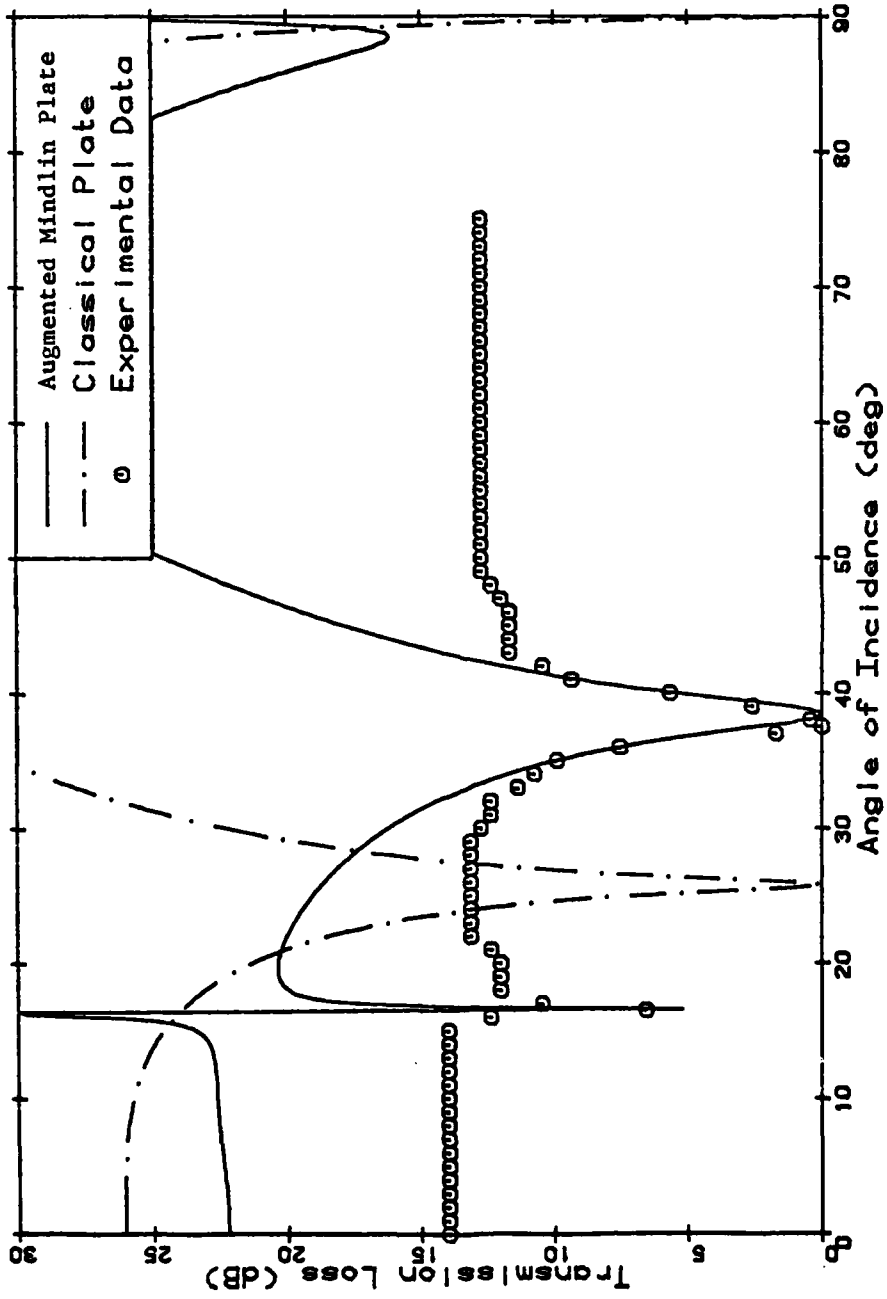

FIGURE 40. Transmission loss as a function of angle of incidence for a 0.023 in. thick aluminum plate at a frequency of 2.138 MHz, which is 5.28 times the classical coincidence frequency of the plate.

location of the "longitudinal" peak, actually the S_o Lamb wave, which up until now has remained consistently at 16°, begins moving farther out in the direction of the grazing angle. This is shown in Figure 41 for $\Omega = 7.71$. The augmented Mindlin theory is, however, still able to track the main lobe, which is produced by the A_o Lamb mode, remarkably well. This mode, as the previous sequence of figures has shown, first appears at the grazing angle at a frequency slightly above coincidence and moves in the direction towards the plate normal, i.e., in the opposite direction of all the other peaks. Figure 41 represents the first accurate comparison between experimental data and theory which includes all three of these Lamb modes. Previously, only the locations, not the shapes of the peaks, have been correctly reproduced.

As the frequency is increased further, the deviation between the theory and experimental data becomes more pronounced. This is as expected. An interesting point is that the breakdown in the theoretical description of the longitudinal wave did not occur at a much lower frequency. At $\Omega = 14.94$ (Figure 42), this becomes quite apparent. A fourth mode, S_2, has now appeared at normal incidence and the A_0 and S_0 modes have coalesced into a broad peak at 30°. Theoretically, 30° is the predicted lower limit for the A_0 mode. Also, note that the longitudinal wave model is still predicting the same angle of 16°, which is obviously incorrect at this frequency.

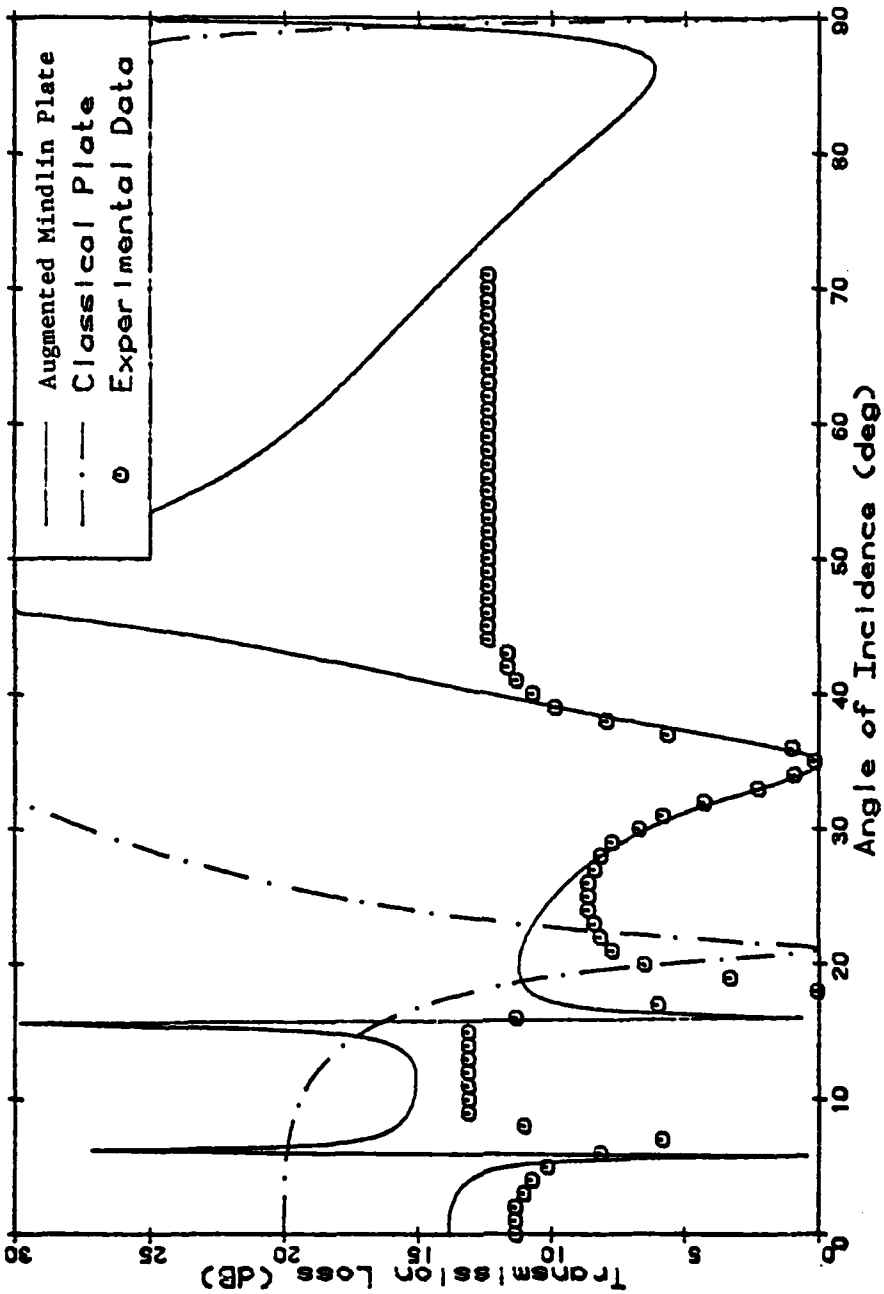

FIGURE 41. Transmission loss as a function of angle of incidence for a 0.032 in. thick aluminum plate at a frequency of 2.132 MHz, which is 7.71 times the classical coincidence frequency of the plate.

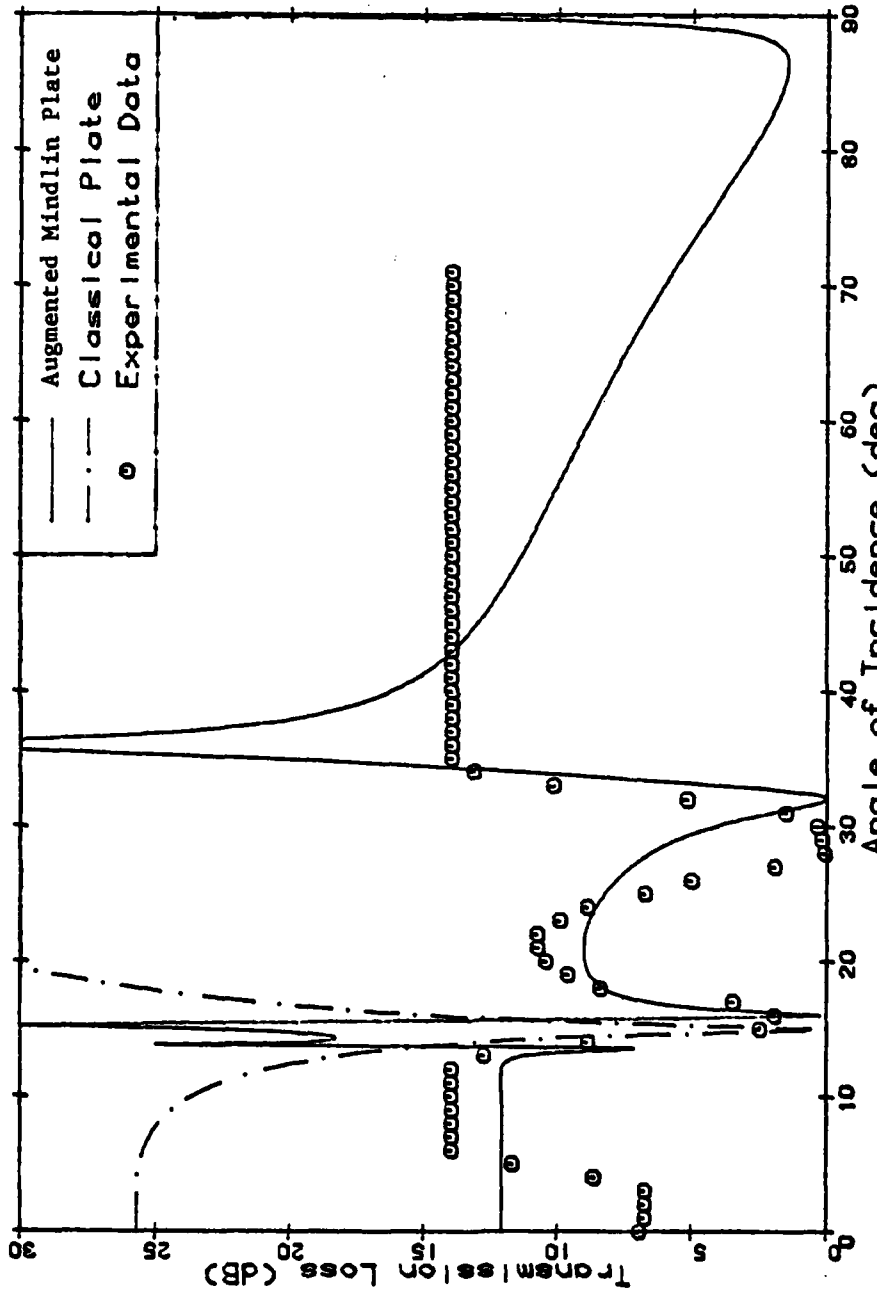

FIGURE 42. Transmission loss as a function of angle of incidence for a 0.195 in. thick aluminum plate at a frequency of 689 kHz, which is 14.94 times the classical coincidence frequency of the plate.

As the frequency is further increased through the range between Ω = 15 and 35 as is shown in Figures 43 and 49, the amplitude of the lobe at 30° gradually reduces and eventually vanishes at Ω = 35. This phenomenon has apparently not received previous attention in the literature. None of the theoretical treatments to date predict such an occurrence; yet, on inspection it appears to be real. The peak in question is composed of both the A_0 and S_0 modes, which are, respectively, the lowest antisymmetrical and the lowest symmetrical modes of the plate. When they both reach 30°, the phase velocities become nearly equal; thus, the wavelengths approach the same value and phase. Consequently, when the incident sound beam drives the back of the plate, the symmetrical motion on the front of the plate will be exactly matched and out of phase with the antisymmetrical motion produced by the A_0 mode. As this cancellation becomes exact, the amplitude of the transmitted wave is reduced until it eventually reaches zero. This is shown schematically in Figure 50. If the hypothesis is correct, the same reasoning should apply to each A_n-S_n pair, and this appears to be the case. The same effect can be seen clearly for the A_1-S_1 pair as well as the A_2-S_2 pair, but as the frequency is increased further into the Ω = 100 range, the proliferation of new modes is such that it is no longer possible to identify modes with absolute certainty. An improvement in the angular resolution of the system would be necessary. Figures 51 to 56 show the gradual

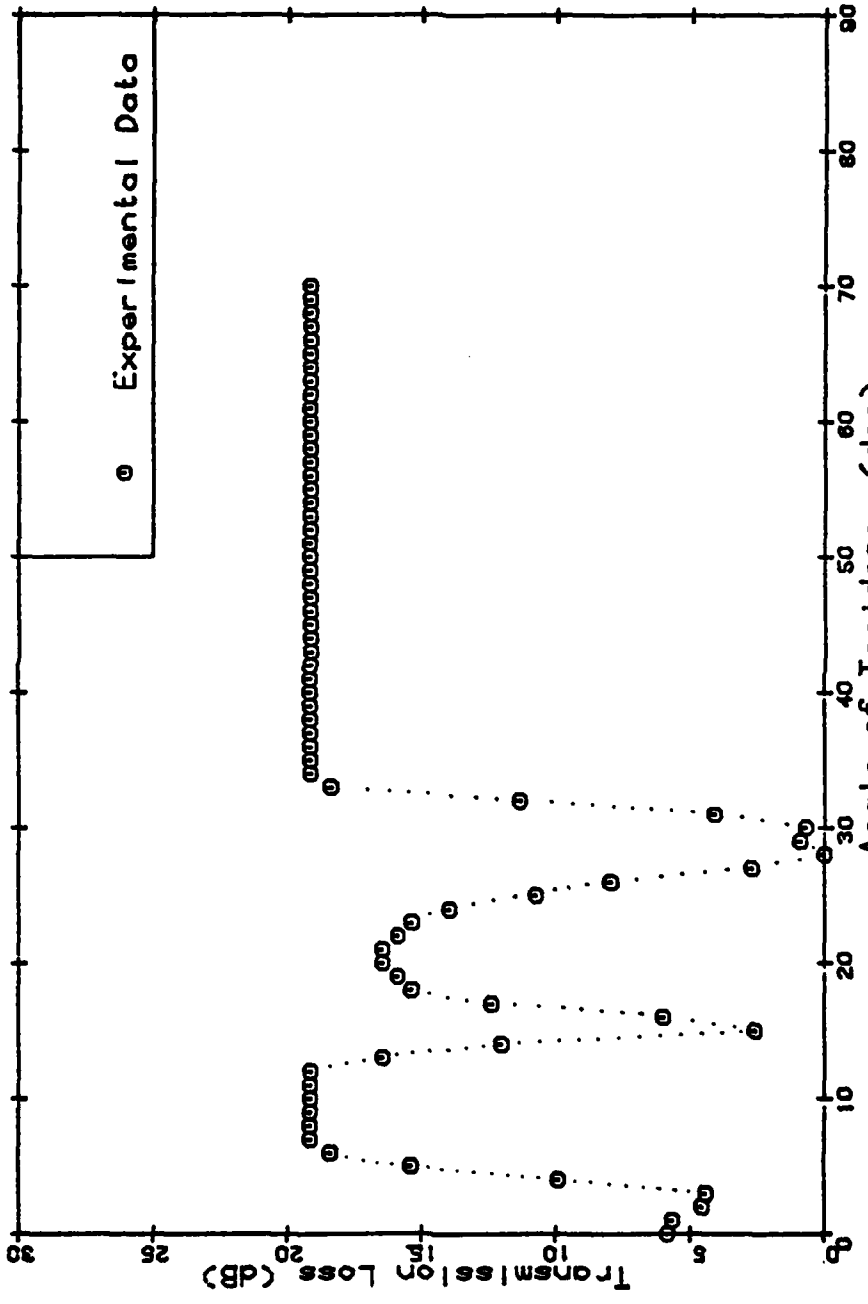

FIGURE 43. Transmission loss as a function of angle of incidence for a 0.127 in. thick aluminum plate at a frequency of 1.084 MHz, which is 15.3 times the classical coincidence frequency of the plate.

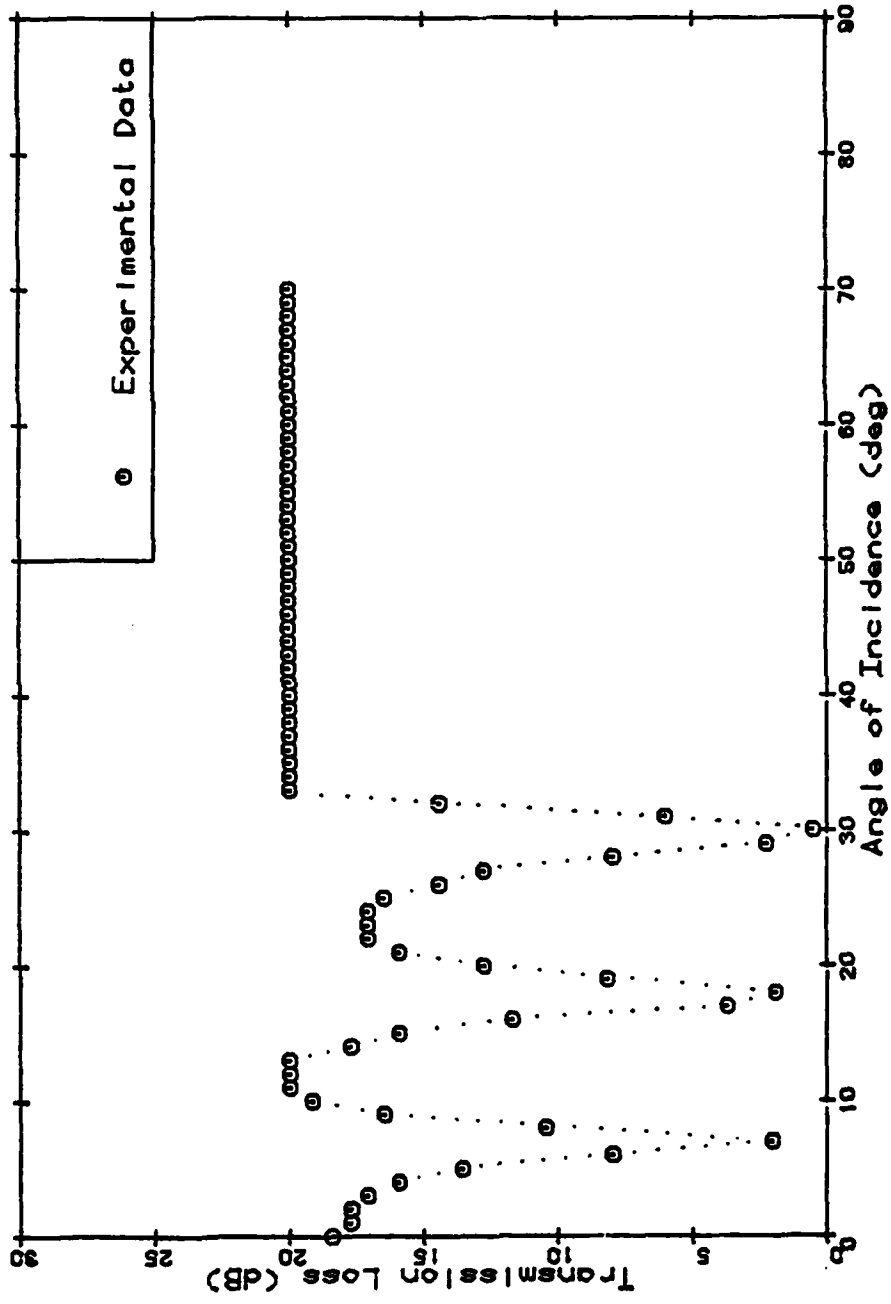

FIGURE 44. Transmission loss as a function of angle of incidence for a 0.127 in. thick aluminum plate at a frequency of 1.270 MHz, which is 17.9 times the classical coincidence frequency of the plate.

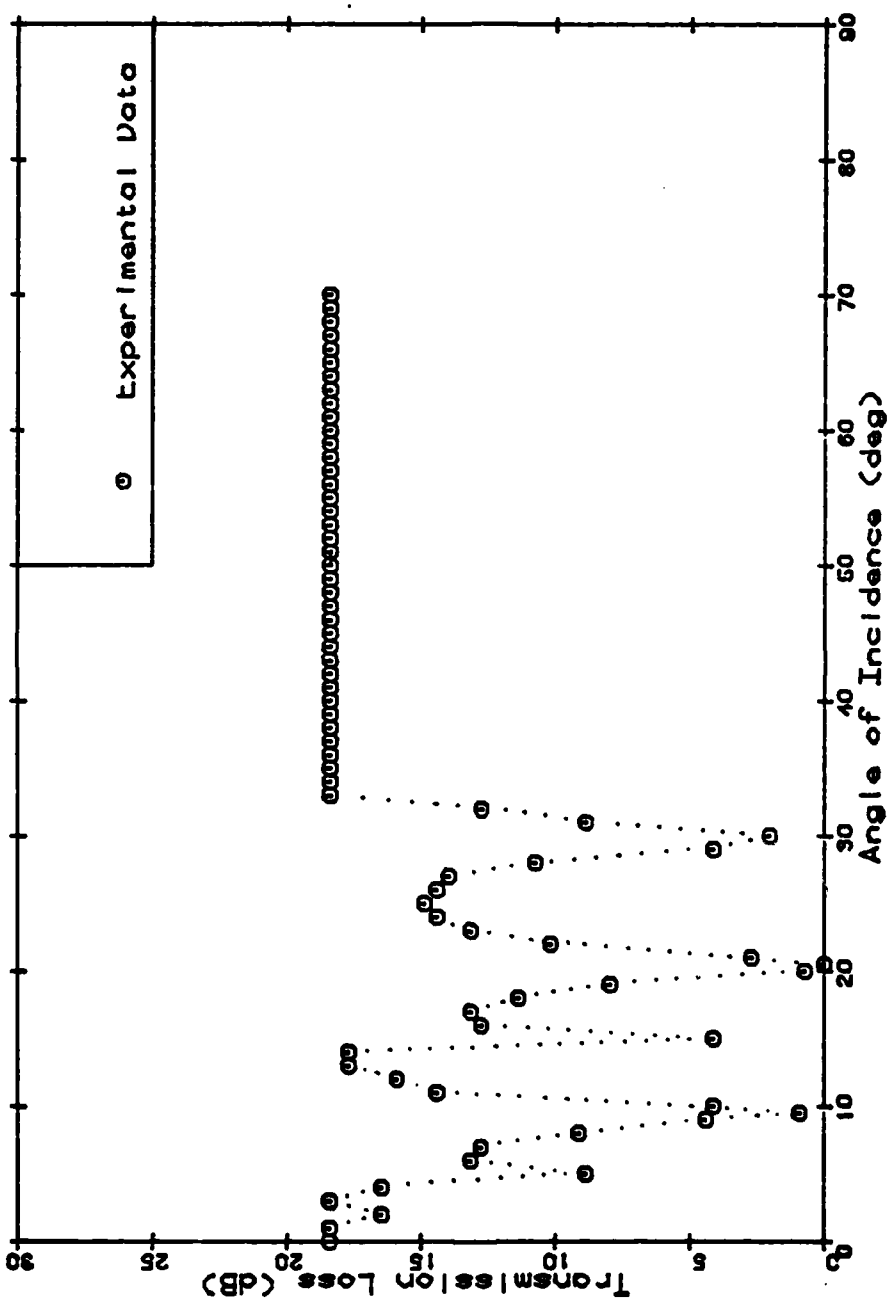

FIGURE 45. Transmission loss as a function of angle of incidence for a 0.127 in. thick aluminum plate at a frequency of 1.471 MHz, which is 20.9 times the classical coincidence frequency of the plate.

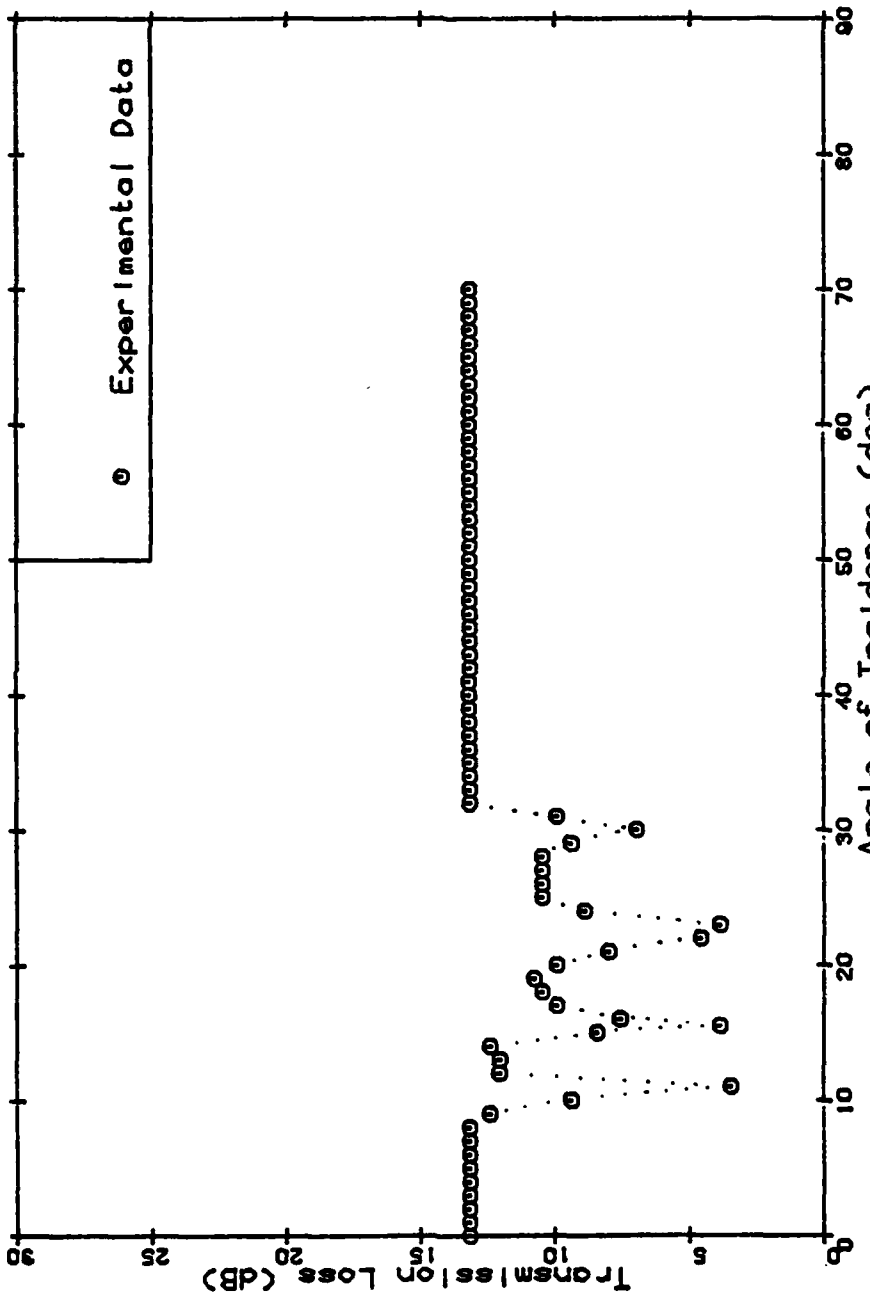

FIGURE 46. Transmission loss as a function of angle of incidence for a 0.127 in. thick aluminum plate at a frequency of 1.630 MHz, which is 23.0 times the classical coincidence frequency of the plate.

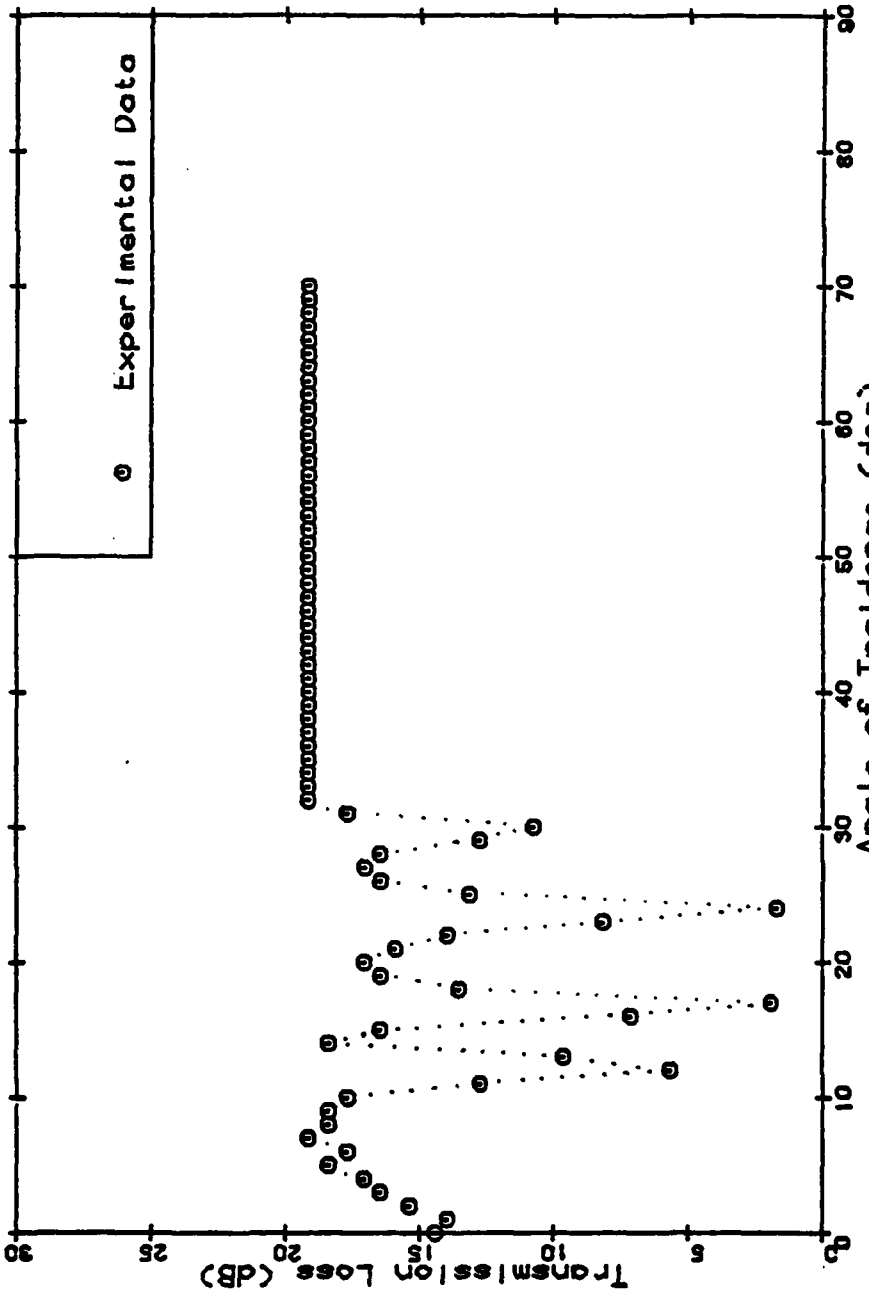

FIGURE 47. Transmission loss as a function of angle of incidence for a 0.127 in. thick aluminum plate at a frequency of 1.815 MHz, which is 25.6 times the classical coincidence frequency of the plate.

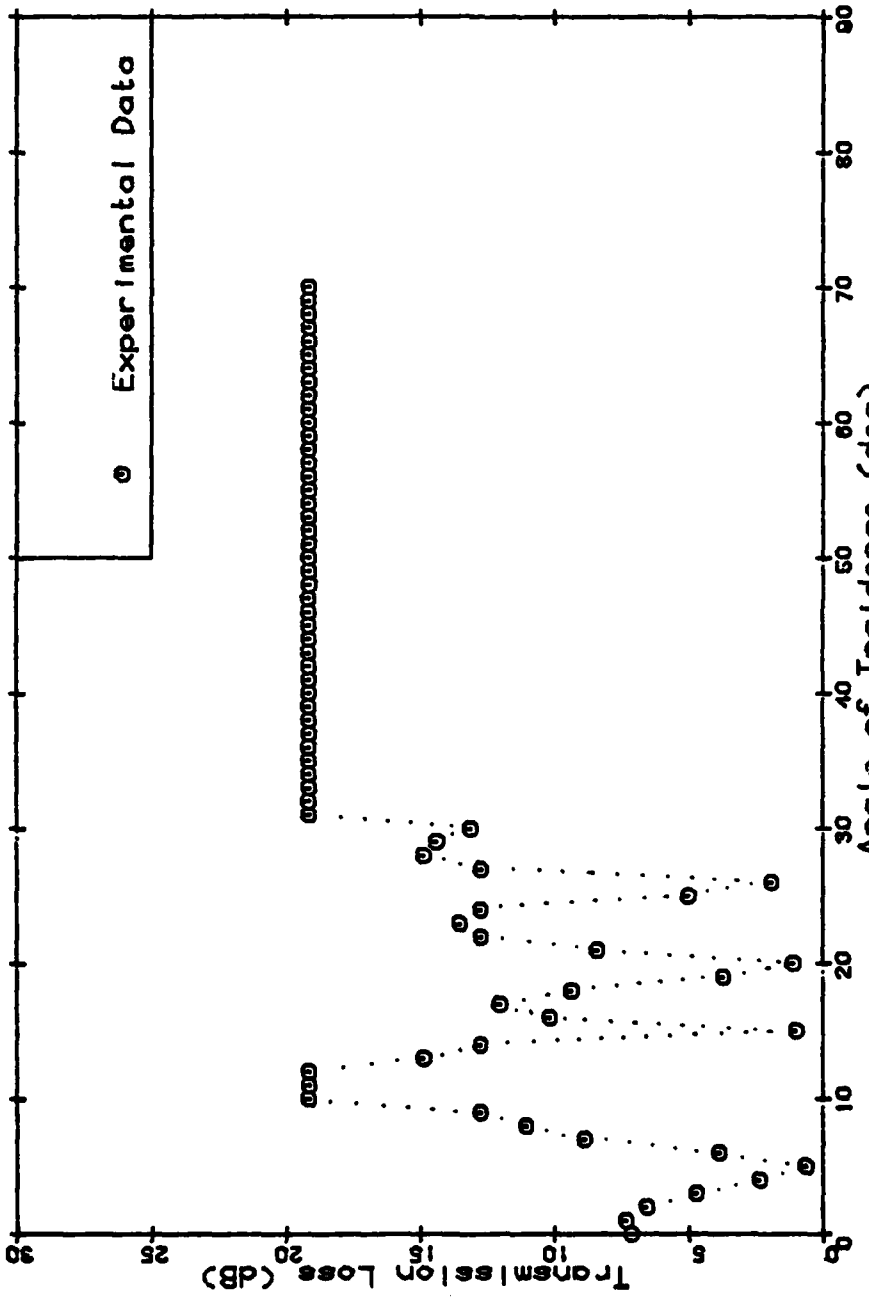

FIGURE 48. Transmission loss as a function of angle of incidence for a 0.127 in. thick aluminum plate at a frequency of 2.125 MHz, which is 30.0 times the classical coincidence frequency of the plate.

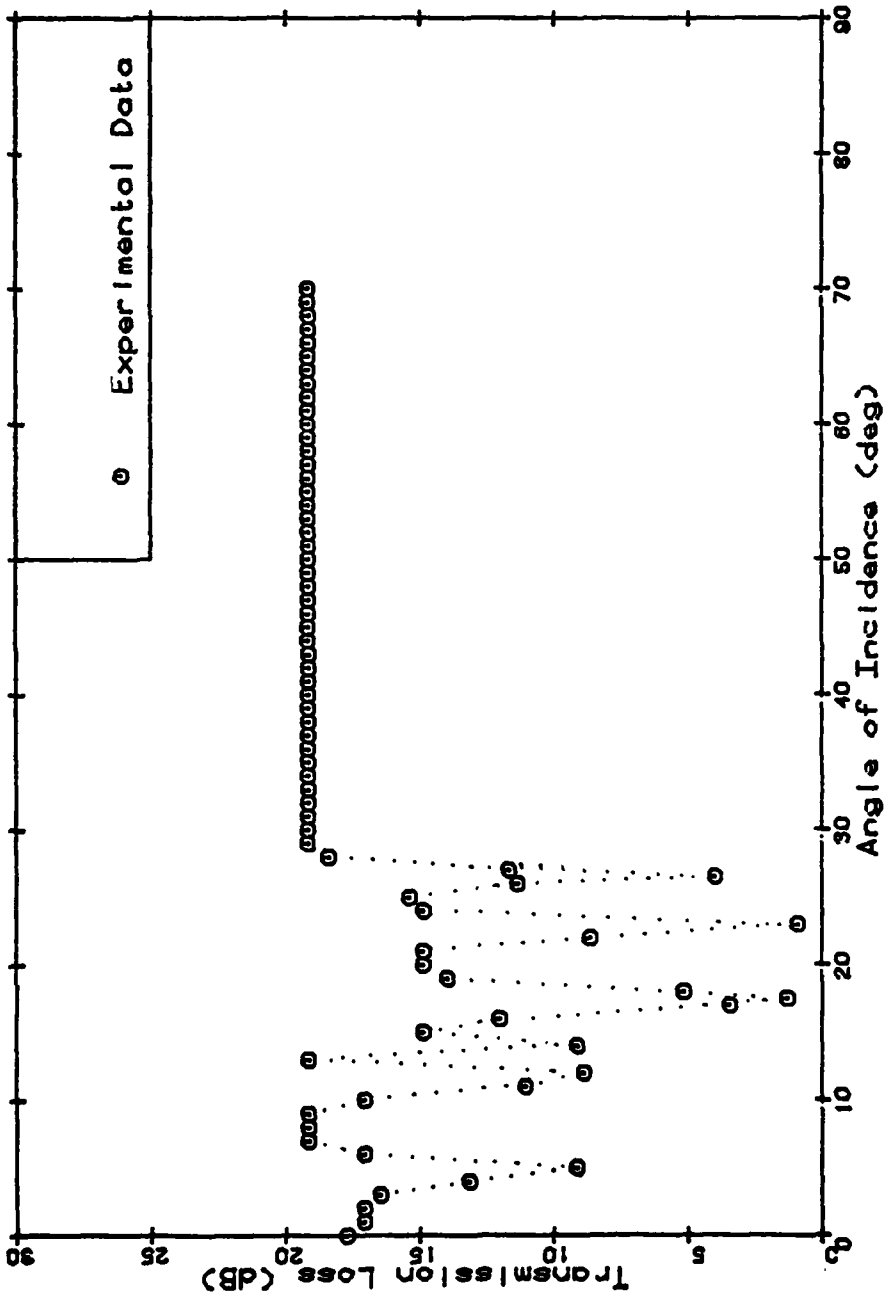

FIGURE 49. Transmission loss as a function of angle of incidence for a 0.127 in. thick aluminum plate at a frequency of 2.538 MHz, which is 35.9 times the classical coincidence frequency of the plate.

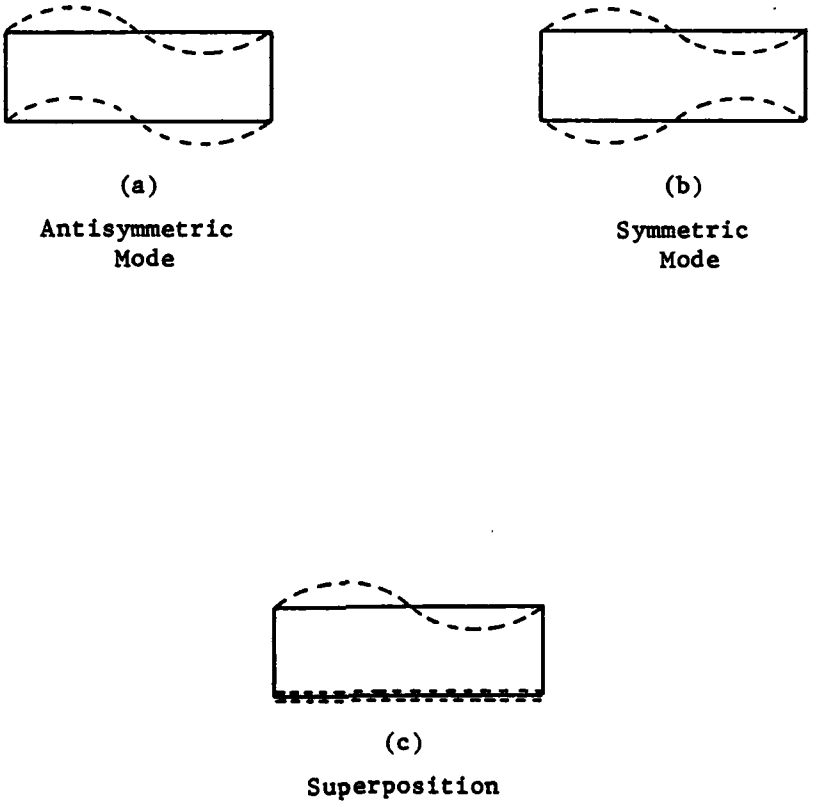

FIGURE 50. Cancellation of modal pairs.

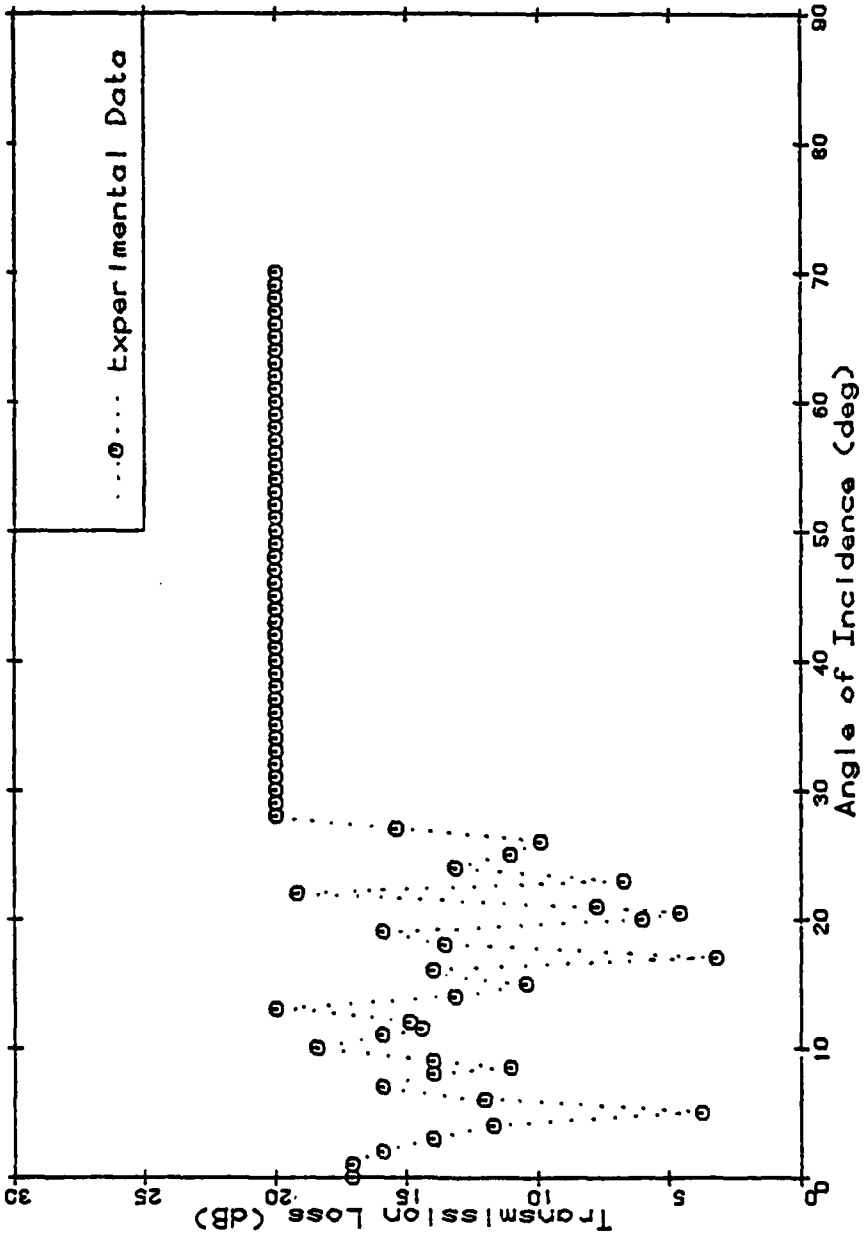

FIGURE 51. Transmission loss as a function of angle of incidence for a 0.501 in. thick aluminum plate at a frequency of 1.081 MHz, which is 60.4 times the classical coincidence frequency of the plate.

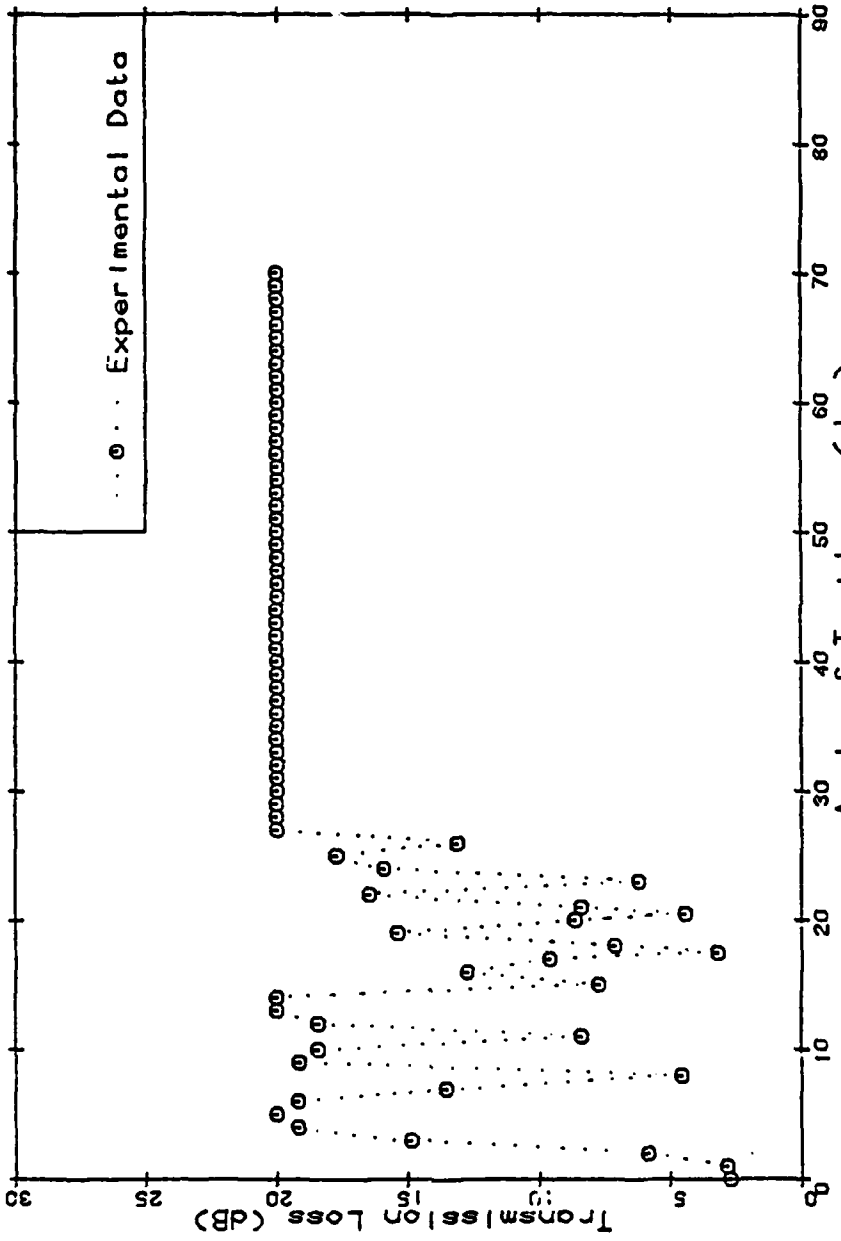

FIGURE 52. Transmission loss as a function of angle of incidence for a 0.501 in. thick aluminum plate at a frequency of 1.263 MHz, which is 70.4 times the classical coincidence frequency of the plate.

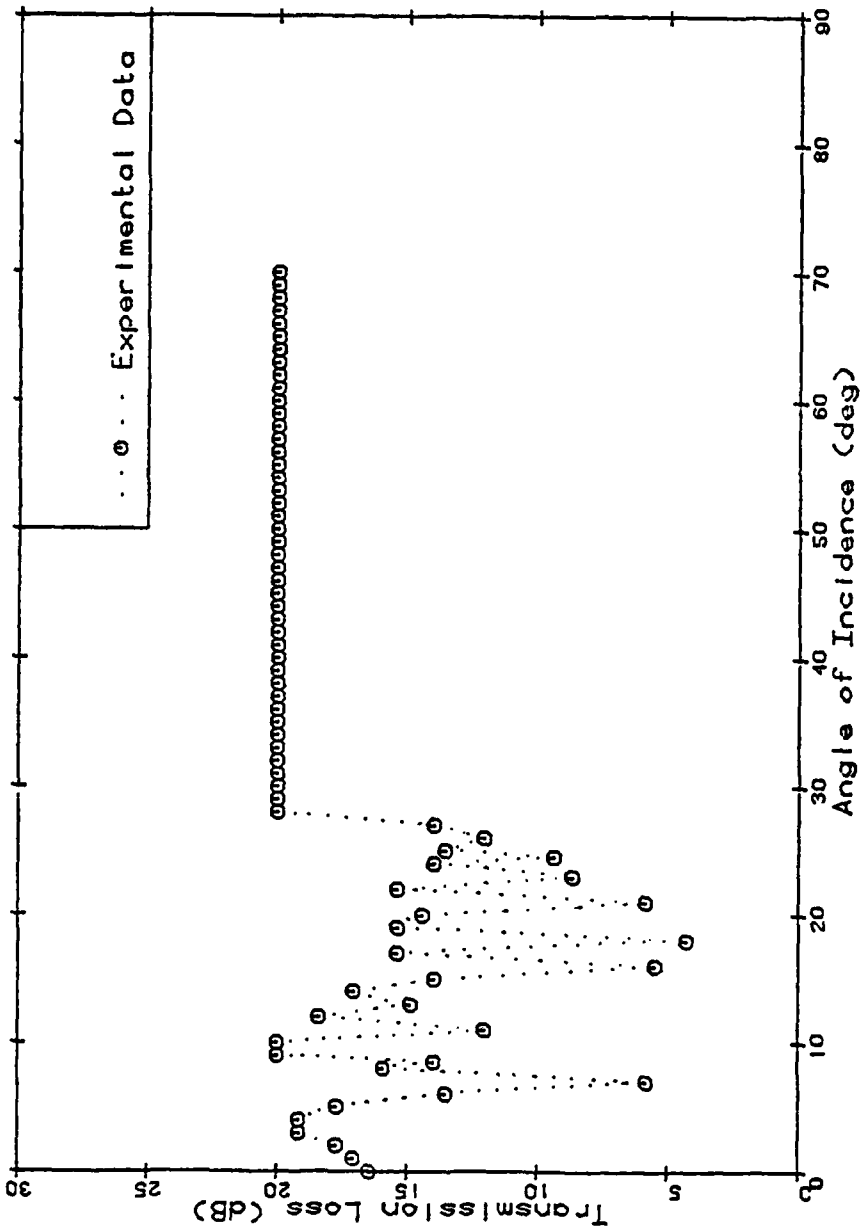

FIGURE 53. Transmission loss as a function of angle of incidence for a 0.501 in. thick aluminum plate at a frequency of 1.447 MHz, which is 80.6 times the classical coincidence frequency of the plate.

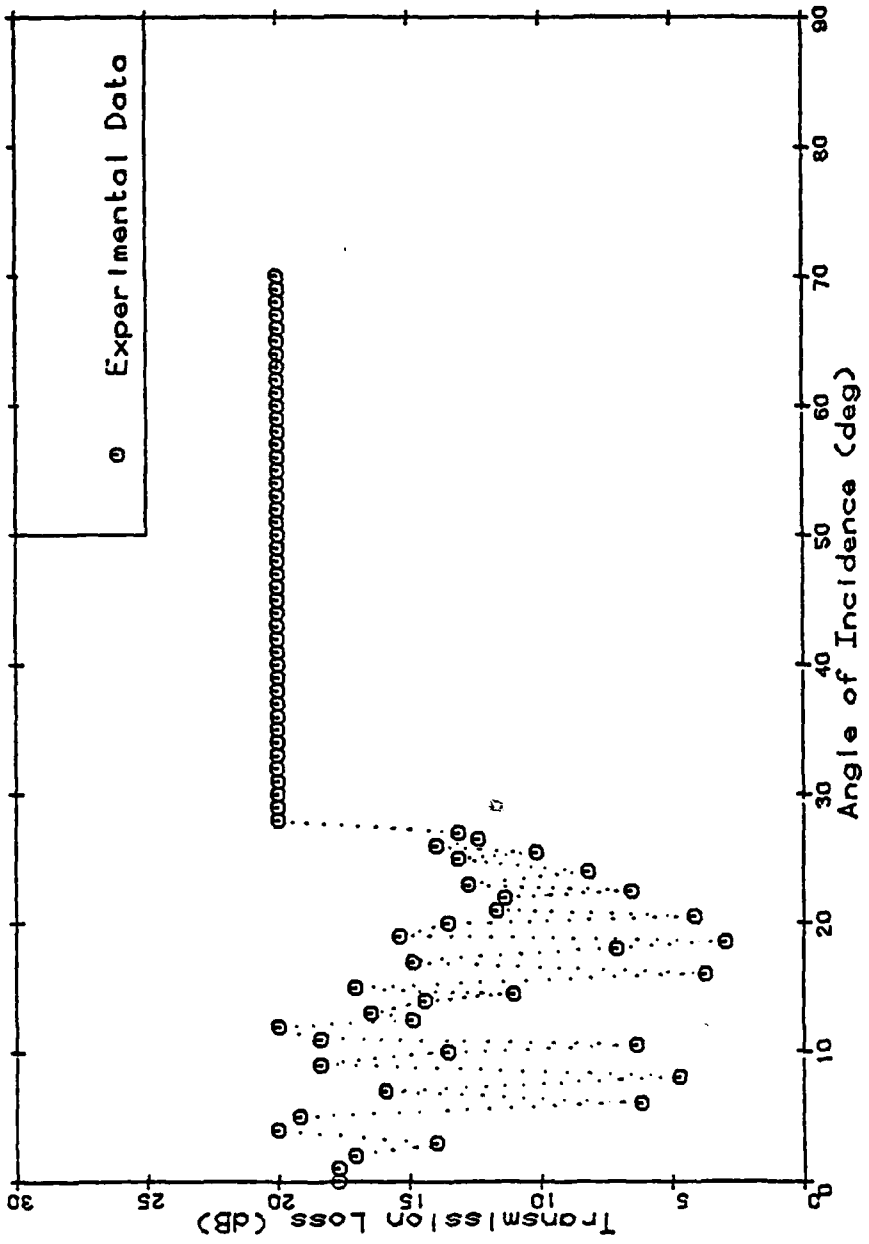

FIGURE 54. Transmission loss as a function of angle of incidence for a 0.501 in. thick aluminum plate at a frequency of 1.627 MHz, which is 90.7 times the classical coincidence frequency of the plate.

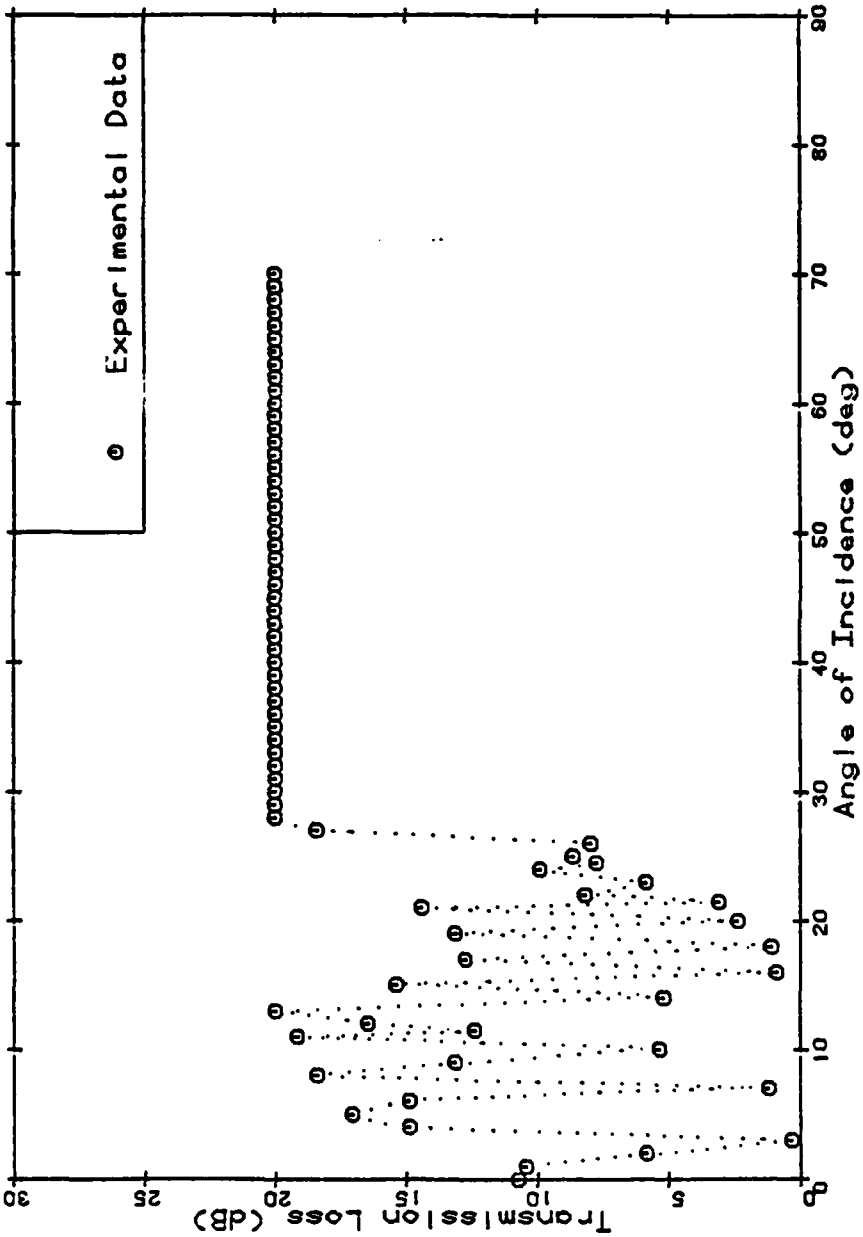

FIGURE 55. Transmission loss as a function of angle of incidence for a 0.501 in. thick aluminum plate at a frequency of 1.806 MHz, which is 101 times the classical coincidence frequency of the plate.

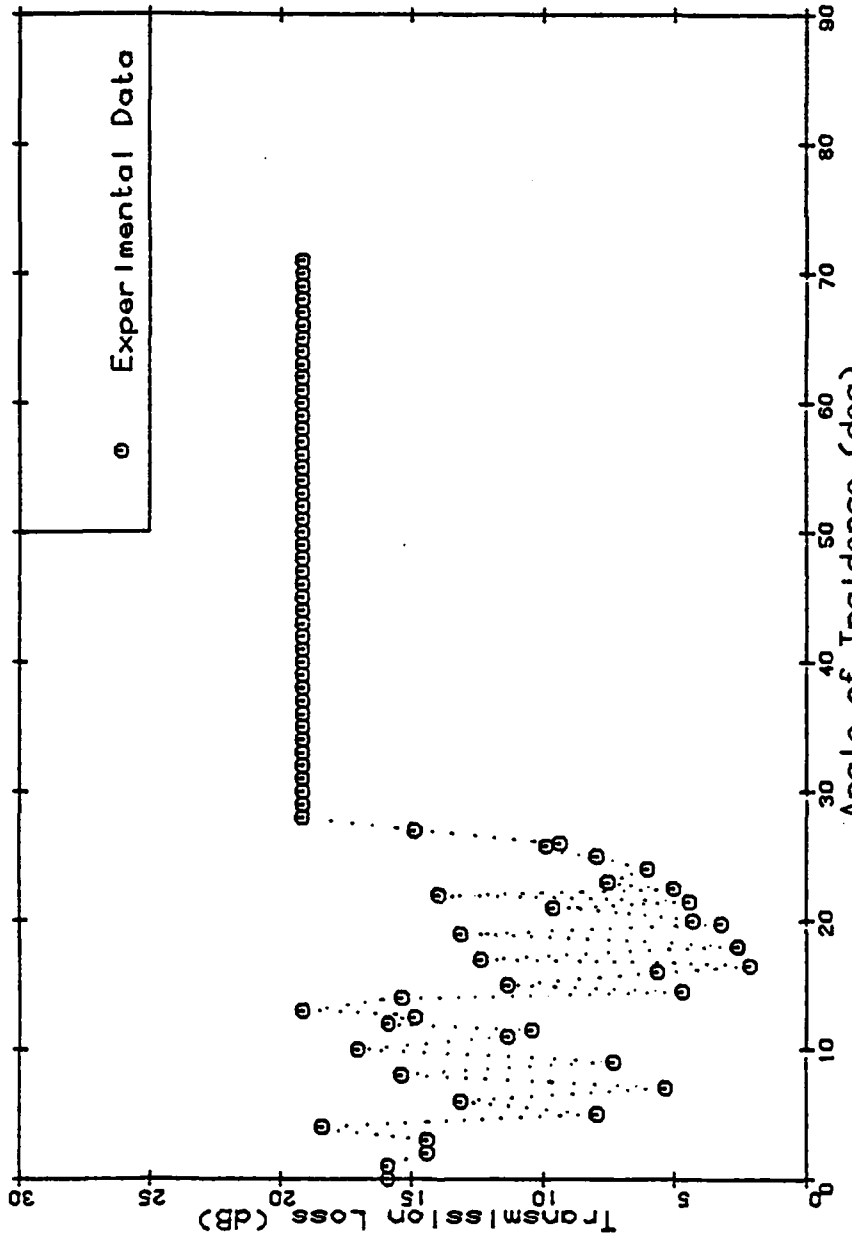

FIGURE 56. Transmission loss as a function of angle of incidence for a 0.501 in. thick aluminum plate at a frequency of 2.124 MHz, which is 119 times the classical coincidence frequency of the plate.

movement of the peaks as the frequency is further increased. The disappearance of each pair of peaks after they have settled at their upper limit does appear to be true for the lower peaks. Each A_n-S_n pair has a slightly lower limit than the previous pair; thus, as these peaks vanish, the transmission is tightly confined to the region near the normal of the plate. This same observation should also apply to the radiation pattern of a vibrating plate; i.e., as the frequency is increased above the coincidence frequency of the plate, the radiation should be concentrated more and more into the angular region near the plate normal.

5.4 Dispersion Curves

Although the shape of the peaks in the transmission curves has proven to be very difficult to predict, the angular locations of the peaks have been well known for many years. In order to compare the results presented in the last section with the theoretical results derived by Rayleigh [1] and Lamb [3], the locations of each of the peaks for aluminum have been summarized in Figure 57. The theoretical curves have been replotted from Viktorov [49] and apply for a Poisson's ratio of 0.34, which provides a fairly accurate representation for aluminum. The coalescing and subsequent disappearance of the A_n-S_n pairs is clear in the experimental data, but, as noted previously, the theoretical curves do not reflect this phenomenon. The

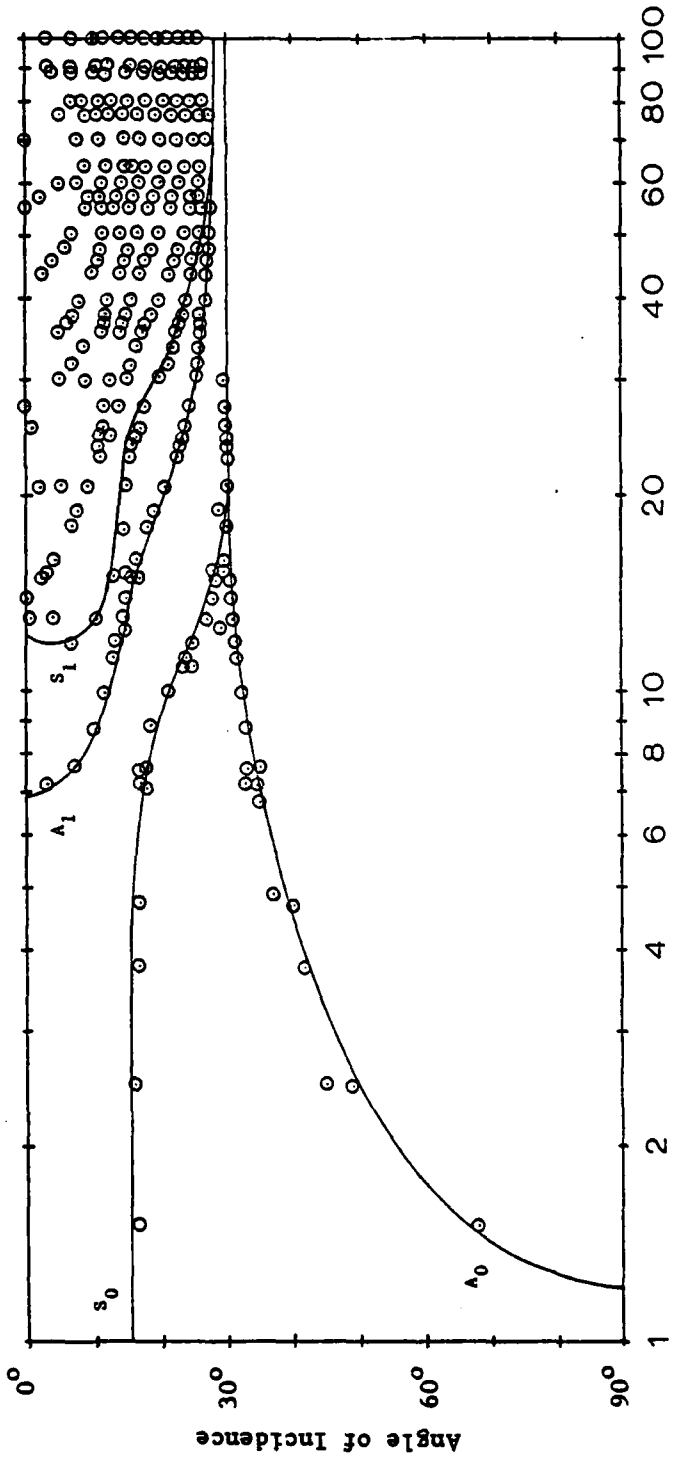

FIGURE 57. Dispersion curves for an aluminum plate in water.

Mindlin plate theory has been verified by many different experiments and the sound transmission for specific Lamb modes has been verified by many others, but always for much more limited frequency ranges than the current investigation. The schlieren method makes it possible to study the transmission of sound through plates, and thus to study the effects of the Lamb modes in a very wide frequency range because of the advanced equipment and the basic unintrusiveness of the method.

Figure 57 shows the overall study of Lamb waves for aluminum plates submerged in water. The frequencies are normalized to the classical coincidence frequency of the plate and cover the range from 1 to 100. The figure represents a summary of approximately 7000 schlieren recordings of incident and transmitted sound waves. The theoretical curves included were obtained by numerical solution of the Rayleigh-Lamb relation derived in Section 2.3.1.

Many of the individual sound transmission curves from which Figure 57 was obtained are shown in Figures 35 - 56 plotted as functions of the incident angle. Experimental evidence for the existence of the peak caused by the longitudinal term not included in the original Mindlin theory is quite apparent in many of these curves, and the agreement with the theory presented in Section 2.3.3 is quite good for frequencies up to nearly 10 times the coincidence frequency.

CHAPTER 6

SUMMARY AND CONCLUSIONS

6.1 The Schlieren Method in the Range 27 kHz to 5 MHz

The video method of quantizing schlieren data was shown to be a viable and accurate laboratory technique. By using a periodically-interrupted, laser beam stroboscopic illumination could be used to determine the characteristics of complex acoustic fields, e.g., accurately measuring the Lamb wave lengths associated with plate vibrations and the surface wave lengths in the investigation of curved and ribbed structures. Although previous investigators could obtain data which had no better than a 75 percent accuracy, the data presented herein consistently reflects a probable error of 1/2 dB, i.e., 6 percent, in amplitude and 1/4 degree in angular resolution. (Figure 58 shows the typical repeatability between experimental runs taken several months apart.) This level of accuracy, together with the speed and convenience of the video method over alternate means of quantizing schlieren data, should offer great encouragement for its future use. The schlieren technique

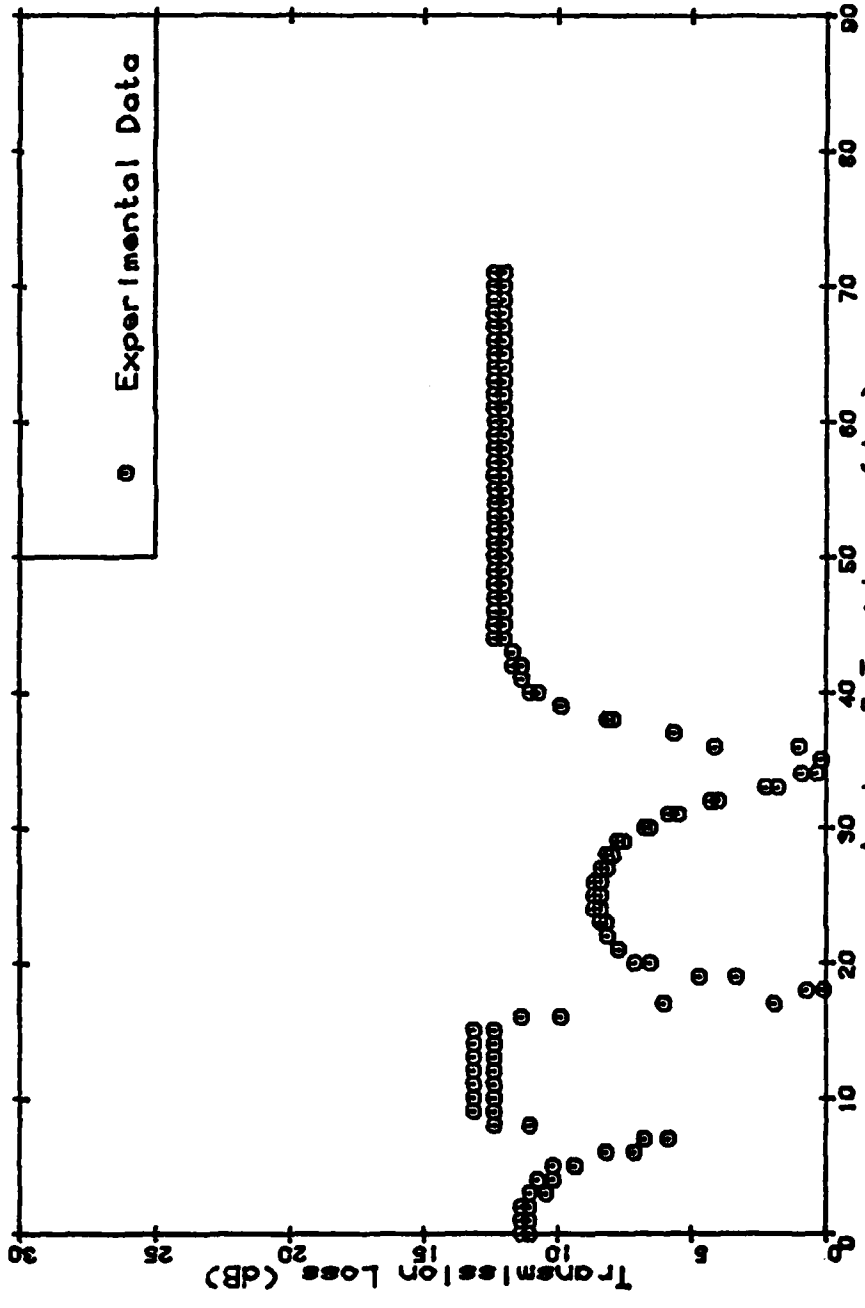

FIGURE 58. A comparison of two experimental data sets for a 0.032 in. thick aluminum plate at a frequency of 2.132 MHz, which is 7.71 times the classical coincidence frequency of the plate, shows that the repeatability using the current experimental method is consistantly within 1/2 dB.

has long been recognized as a valuable laboratory tool. The added ability to produce extremely accurate quantitative data will greatly enhance this value.

6.2 Results

By making use of stroboscopic illumination to investigate progressive waves and constant illumination to investigate standing wave fields, an exact analysis of complex wave fields could be performed that was heretofore impossible. The various field components such as radiation due to progressive Lamb waves, due to Rayleigh surface waves, or due to forced excitation of steady-state vibrations could be uniquely analyzed with very high accuracy. It was thus possible, for instance, to examine accurately the vibration of complex structures such as joints, ribbed joints, and curved bodies.

Much work was also done in the investigation of the transmission and reflection of bounded acoustic beams. The acoustic transfer function derived by Stuart [40] and the corresponding transmission coefficient presented in Section 2.3.2 have been confirmed for frequencies up to approximately 15 times the classical coincidence frequency of the plate. Furthermore, the additional longitudinal term included in Section 2.3.3 has been confirmed for frequencies up to approximately 8 times the coincidence frequency. These results show that current theoretical treatments are now able to predict accurately the shape of the lobes in

the transmission and radiation curves produced by the lowest three Lamb modes. Previously, only the angular locations of these peaks were known from the dispersion relations obtained by Rayleigh [1] and Lamb [3]. This research has also produced data which extends the confirmed range of validity of those dispersion curves to frequencies greater than 100 times the coincidence frequency. The dispersion curves predict that the angular locations of the two lobes produced by each A_n-S_n pair of Lamb modes will approach the same asymptotic value at high frequencies. This was found to be correct, as previous research has also shown, but more significantly, it was discovered that as each pair of lobes coalesce, they also cancel and the transmission at that location goes to zero as the frequency increased further.

6.3 Future Work

The most obvious point which needs to be improved is the thin-plate model used to derive the longitudinal wave term in Section 2.3.3. At frequencies above coincidence, the plate cannot be accurately regarded as "thin" (i.e., with respect to a wavelength) and it is surprising that the results are as accurate as they appear to be. A model based on a "thick" plate should greatly extend the range of validity.

The schlieren system, as it was configured, can be improved in many ways. The errors in each resulting data

set are not random; the experimental data drifts back and forth across the theoretical curves. However, as viewed over many data sets, the errors do appear to be more random. This implies that short term systematic errors are occurring in the experimental system. The most obvious source is the drift in the output level of the transducer, which is caused by the slow drifting of the frequency and output level of the oscillator. Another obvious point which needs to be corrected is the stability of the optical bench; the bench was moved from the first floor to the fourth floor of the Applied Science Building for use by this project. Not only is an upper floor more susceptible to structural vibrations, but the granite table it was originally situated on had to be left behind due to its weight. The quantitative data scan across the video image is confined to a single vertical slice. This greatly limits the types of experimental geometries which can be reasonably investigated. There are several commercial video image digitizers available that are far more flexible. One obvious additional convience would be the procurement of a small microcomputer in order to process the large volume of digital data which can be produced with the current system. The main benefits of such a system would be the ability to base transmission and reflection coefficients on the integral over the beam width rather than on just a comparison of on-axis intensities. Unfortunately, most of the power inherent in that approach would

be lost with the current image digitizer since it is frequently impossible to align the experiment in such a way that the acoustic beam is perpendicular to the data sampling line.

REFERENCES

1. Lord Rayleigh (J. W. Strutt), "On the Free Vibrations of an Infinite Plate of Homogeneous Isotropic Elastic Matter," Proc. of the Math. Soc., London 20, 225-234 (1889).

2. H. Lamb, "On the Flexure of an Elastic Plate," Proc. Math. Soc., London 21, 85 (1889-90).

3. H. Lamb, "On Waves in an Elastic Plate," Proc. R. Soc. London 93A, 114-128 (1917).

4. C. G. Knott, "Reflection and Refraction of Elastic Waves," Philos. Mag., Series 5, 48, 64 (1899).

5. R. B. Lindsay, C. R. Lewis, and R. D. Albright, "Acoustic Filtration in Non-Homogeneous Media," J. Acoust. Soc. Am. 5, 202 (1934).

6. R. B. Lindsay, J. Appl. Phys. 9, 612 (1938).

7. R. B. Lindsay, "Filtration of Oblique Elastic Waves in Stratified Fluid-Solid Media," J. Acoust. Soc. Am. 11, 165(A) (1939).

8. J. B. Smyth and R. B. Lindsay, "Supersonic Transmission at Oblique Incidence Through a Solid Plate in Water," J. Acoust. Soc. Am. 16, 20-25 (1944).

9. C. Schaefer and L. Bergmann, Sitz. Ber. Berliner Akad. 1934, 155.

10. C. Schaefer and L. Bergmann, Z. Tech. Phys. 17, 441 (1936).

11. C. Schaefer, L. Bergmann, and H. J. Goehlich, Glastechn. Ber. 15, 447 (1937).

12. R. Bär and A. Walti, "Uber die Bestimmung der Poisson'schen Elastizitätzkonstante mit Hilfe von Ultraschallwellen," Helv. Phys. Acta 7, 658-661 (1934).

13. A. Walti, "Uber die Bestimmun der elastischen Konstanten isotroper fester Köper mit Hilfe von Ultraschallwellen," Helv. Phys. Acta 11, 113-139 (1938).

14. F. H. Sanders, "Transmission of Sound through Thin Plates," Can. J. Phys. 17A, 179-193 (1939).

15. M. F. M. Osborne and S. D. Hart, "Transmission, Reflection, and Guiding of an Exponential Pulse by a Steel Plate in Water, I. Theory," J. Acoust. Soc. Am. 17, 1-18 (1945).

16. M. F. M. Osborne and S. D. Hart, "Transmission, Reflection, and Guiding of an Exponential Pulse by a Steel Plate in Water, II. Experiment," J. Acoust. Soc. Am. 18, 170-184 (1946).

17. E. Reissner, "The Effect of Transverse Shear Deformation on the Bending of Elastic Plates," J. Appl. Mech. 12, 69 (1945).

18. E. Reissner, "On Bending of Elastic Plates," Quarterly of Appl. Math. 5, 55-68 (1947).

19. F. A. Firestone, Non-Distru. Test 7, 2 (1948).

20. R. D. Fay, "Interactions Between a Plate and a Sound Field," J. Acoust. Soc. Am. 20, 620-625 (1948).

21. W. J. Finney, "Reflection of Sound from Submerged Plates," J. Acoust. Soc. Am. 20, 626-637 (1948).

22. R. D. Fay and O. V. Fortier, "Transmission of Sound through Steel Plates Immersed in Water," J. Acoust. Soc. Am. 23, 339-346 (1951).

23. W. C. Schneider and C. J. Burton, "Determination of the Elastic Constants of Solids by Ultrasonic Methods," J. Appl. Phys. 20, 48-58 (1949).

24. C. J. Burton and R. B. Barnes, "A Visual Method for Demonstrating the Path of Ultrasonic Waves through Thin Plates of Material," J. Appl. Phys. 20, 462-467 (1948).

25. A. Schoch, "Schallreflexion, Schallbrechung, und Schallbeugung," Erg. der Exakten Naturwiss. 23, 127-234 (1950).

26. R. D. Mindlin, "Influence of Rotary Inertia and Shear on Flexural Motions of Isotropic Elastic Plates," J. Appl. Phys. 18, 31-38 (1951).

27. T. R. Kane and R. D. Mindlin, "High-Frequency Extensional Vibrations of Plates," J. Appl. Phys. 23, 277-283 (1956).

28. R. D. Mindlin and M. A. Medick, "Extensional Vibrations of Elastic Plates," J. Appl. Phys. 26, 561-569 (1959).

29. R. D. Mindlin, "Waves and Vibrations in Isotropic, Elastic Plates," in Structural Mechanics, edited by J. N. Goodier and N. J. Hoff (Pergman Press, London, 1960), pp. 199-232.

30. K. R. Makinson, "Transmission of Ultrasonic Waves through a Thin Solid Plate at the Critical Angle for the Dilatational Wave," J. Acoust. Soc. Am. 24, 202-206 (1952).

31. L. P. Liamshev and S. N. Rudakov, "Reflection of Sound by Thick Bounded Plates in a Liquid," Sov. Phys. Acoust. 2, 242-244 (1956).

32. L. M. Liamshev and S. N. Rudakov, "Sound Radiation from Plates and Shells in Water," Sov. Phys. Acoust. 7, 302-304 (1961).

33. D. C. Worlton, "Experimental Confirmation of Lamb Waves at Megacycle Frequencies," A. Appl. Phys. 32, 967-971 (1961).

34. K. Tamm and O. Weis, "Untersuchungen Über periodishe Wellen, Exponentielle und Komplexe Nahfelder im Begrenzten Festkörper," Acustica 9, 275-288 (1959).

35. D. Feit, "Pressure Radiated by a Point-Exited Elastic Plate," J. Acoust. Soc. Am. 40, 1489-1494 (1966).

36. D. Feit, "Sound Radiation from Orthotropic Plates," J. Acoust, Soc. Am. 47, 388-389 (1970).

37. P. R. Stepanishen, "Influence of Rotary Inertia and Shear Deformation on Acoustic Transmission through a Plate," J. Acoust. Soc. Am. 58, 741-745(L) (1975).

38. J. W. Young, "Comments on `Influence of Rotary Inertia and Shear Deformation on Acoustic Transmission through a Plate,'" J. Acoust. Soc. Am. 59, 1500-1501(L) (1976).

39. P. R. Stepanishen, "Reply to `Comments on `Influence of Rotary Inertia and Shear Deformation on Acoustic Transmission through a Plate,''" J. Acoust. Soc. Am. 59, 1501-1502(L) (1976).

40. A. D. Stuart, "Acoustic Radiation from Submerged Plates. I. Influence of Leaky Wave Poles," J. Acoust. Soc. Am. 59, 1160-1169 (1976).

41. A. D. Stuart, "Acoustic Radiation from Submerged Plates. II. Radiated Power and Damping," J. Acoust, Soc. Am. 59, 1170-1174 (1976).

42. D. G. Crighton, "The Free and Forced Waves on a Fluid-Loaded Elastic Plate," J. Sound Vib. 63, 225-235 (1979).

43. W. A. Strawderman, S.-H. Ko, and A. H. Nuttal, "The Real Roots of the Fluid-Loaded Plate," J. Acoust. Soc. Am. 66, 579-585 (1979).

44. M. Pierucci and T. S. Graham, "A Study of Bending Waves in Fluid-Loaded Thick Plates," J. Acoust. Soc. Am. 65, 1190-1197 (1979).

45. A. J. Rudgers, "Acoustic Reflection and Radiation by Thick Fluid-Loaded Composite Plates," J. Acoust. Soc. Am. 66, 571-578 (1979).

46. M. L. Rumerman, "Nonspecular Acoustic Backscattering from Finite Plates," J. Acoust. Soc. Am. 65, 1121-1126 (1979).

47. W. M. Ewing, W. S. Jardetzky, and F. Press, Elastic Waves in Layered Media, (McGraw-Hill, New York, 1957).

48. L. M. Brekhovskikh, Waves in Layered Media, (Academic Press, New York, 1960).

49. I. A. Viktorov, Rayleigh and Lamb Waves, (Plenum Press, New York, 1967).

50. M. C. Junger and D. Feit, Sound, Structures and their Interaction, (MIT Press, Cambridge, 1972).

51. K. F. Graff, Wave Motion in Elastic Solids, (Ohio State University Press, Columbus, 1975).

52. J. Götz, "Uber den Schalldurchgang durch Metallplatten in Flüssigkeiten bei schrägem Einfall einer eben Welle," Akust. Z. 8, 145-168 (1943).

53. A. Schoch, "Der Schalldurchgang durch Platten," Acustica 2, 1-19 (1952).

54. W. G. Neubauer, "Ultasonic Reflection of a Bounded Beam at Rayleigh and Critical Angles for a Plane Liquid-Solid Interface," J. Appl. Phys. 44, 48-55 (1973).

55. H. L. Bertoni and T. Tamir, "Unified Theory of Rayleigh-Angle Phenomona for Acoustic Beams at Liquid-Solid Interfaces," Appl. Phys. 2, 157-172 (1973).

56. T. J. Plona, M. Behravesh, and W. G. Mayer, "Ultrasonic Bounded Beam Reflection Effects at a Liquid-Solid Interface," J. Acoust. Soc. Am. 56, 1773-1775 (1974).

57. T. J. Plona, L. E. Pitts, and W. G. Mayer, "Ultrasonic Bounded Beam Reflection and Tranmsission Effects at a Liquid/Solid Plate/Liquid Interface," J. Acoust. Soc. Am. 59, 1324-1328 (1976).

58. L. E. Pitts, T. J. Plona, and W. G. Mayer, "Theoretical Similarities of Rayleigh and Lamb Modes of Vibration," J. Acoust. Soc. Am. 60, 374-377 (1976).

59. L. E. Pitts and W. G. Mayer, "Non-Specular Reflection from Solid Plates and Half-Spaces," Ultrasonics, 201-204 (1977).

60. L. E. Pitts, T. J. Plona, and W. G. Mayer, "Theory of Non-Specular Reflection Effects for an Ultrasonic Beam Incident of a Solid Plate in a Liquid," IEEE Trans. Sonics Ultrason. SU-24, 101-109 (1977).

61. I. Tolstoy and E. Usdin, "Wave Propagation in Elastic Plates: Low and High Mode Dispersion," J. Acoust. Soc. Am. 29, 37-42 (1957).

62. K. Negishi, "Negative Group Velocities of Lamb Waves," J. Acoust. Soc. Am. 64, S63(A) (1978).

63. Lord Rayleigh (J. W. Strutt), Nature, 95, 66 (1915).

64. P. W. Bridgman, Dimensional Analysis, (Yale University Press, New Haven, 1922).

65. L. E. Kinsler and A. R. Frey, Fundamentals of Acoustics, 2nd Ed., (John Wiley and Sons, New York, 1962).

66. C. A. Jensen, "Acoustic Transmission and Radiation by an Infinite Elastic Plate," Department of Engineering Science Honors Thesis, (The Pennsylvania State University, Aug. 1977).

67. C. L. Dym, C. S. Ventres and M. A. Lang, "Transmission of sound through sandwich panels: A reconsideration," J. Acoust. Soc. Am. 59, 364-367 (1976).

68. A. Toepler, "Beobachtungen nach einer neuen optischen Methode," (Max Cohen and Son, Bonn 1864).

69. A. Toepler, Ann. Phys. (Leipzig) 127, 556-580 (1866).

70. A. Toepler, Ann. Phys. (Leipzig) 131, 33-55 (1867).

71. A. Toepler, Ann. Phys. (Leipzig) 131, 180-215 (1867).

72. A. Toepler, Ann. Phys. (Leipzig) 134, 194-217 (1868).

73. C. V. Raman and N. S. Nagendra Nath, "The Diffraction of Light by High Frequency Sound Waves: Part I," Proc. Ind. Acad. Sci. (A) 2, 406-412 (1935).

74. C. V. Raman and N. S. Nagendra Nath, "The Diffraction of Light by High Frequency Sound Waves: Part II," Proc. Ind. Acad. Sci. (A) 2, 413-420 (1935).

75. C. V. Raman and N. S. Nagendra Nath, "The Diffraction of Light by High Frequency Sound Waves: Part III, Doppler Effect and Coherence Phenomena," Proc. Ind. Acad. Sci. (A) 3, 75-84 (1936).

76. C. V. Raman and N. S. Nagendra Nath, "The Diffraction of Light by High Frequency Sound Waves: Part IV Generalized Theory," Proc. Ind. Acad. Sci. (A) 3, 119-125 (1936).

77. C. V. Raman and N. S. Nagendra Nath, "The Diffraction of Light by High Frequency Sound Waves: Part V General Considerations - Oblique Incidence and Amplitude Changes," Proc. Ind. Acad. Sci. (A) 3, 459-465 (1936).

78. N. S. Nagendra Nath, "The Diffraction of Light by High Frequency Sound Waves: Generalized Theory," Proc. Ind. Acad. Sci. (A) 4, 222-242 (1937).

79. N. S. Nagendra Nath, "The Visiblity of Ultrasonic Waves and Its Periodic Variations," Proc. Ind. Acad. Sci. (A) 4, 262-274 (1937).

80. W. E. Moore and J. A. Bucaro, "Measurement of Acoustic Fields Using Schlieren and Holographic Techniques," J. Acous. Soc. Am. 63 (1978).

81. S. Stanic, "Quantitative Schlieren Visualization," Ph.D. Thesis, (The Pensylvania State University, 1977).

82. J. A. Bucaro and H. D. Dardy, "Low-Frequency Acousto-Optical Schlieren," J. Acoust. Soc. Am. 61, S81(A) (1977).

83. S. Stanic, Personal Communication (1980).

84. E. P. Smirnov, E. I. Kheifets, and E. L. Shenderov, "Quantitative Analysis of Sound Fields Visualized by the Shadow-Optical Method," Sov. Phys. Acoust. 19, 159-164 (1973).

VITA

Roger Thomas Richards was born on June 19, 1942, in Akron, Ohio. He received a B.S. degree in Physics from Westminster College, New Wilmington, PA, in June, 1964, and an M.S. degree in Physics from the Ohio University, Athens, Ohio, in August, 1969. From 1969 to 1971, he was employed as an Engineer in the Antisubmarine Warfare group at General Dynamics/Electronics Division, Rochester, New York. Since 1971, he has been at the Pennsylvania State University, University Park, PA, first as a NASA Trainee, and most recently as a Graduate Assistant in the Applied Research Laboratory. While there, he served on numerous university wide committees, including the Graduate Council, the Bicentenial Commission, the Executive Board of the Alumni Council, and the Educational Policy Committee of the Board of Trustees. During 1973 - 1974, he served as the President of the graduate student body.

He holds full membership in the Acoustical Society of America, the American Institute of Aeronautics and Astronautics, and the National Speleological Society of which he has served as the Nittany Grotto Vice-Chairman. He is also a member of Kappa Mu Epsilon, Sigma Pi Sigma, and Sigma Xi. He has been listed in eleven biographical reference works including, Who's Who in the East, American Men and Women of Science, Who's Who Among Students in American Universities and Colleges, as well as the British volumes Men of Achievement and the International Dictionary of Biography.

DISTRIBUTION

Commander (NSEA 09G32)
Naval Sea Systems Command
Department of the Navy
Washington, DC 20362 — Copies 1 and 2

Commander (NSEA 0342)
Naval Sea Systems Command
Department of the Navy
Washington, DC 20362 — Copies 3 and 4

Defense Technical Information Center
5010 Duke Street
Cameron Station
Alexandria, VA 22314 — Copies 5 through 16